Estrogen Deficiency-Induced Phosphoproteomic alterations in Skeletal Muscle of Female Mice

A DISSERTATION SUBMITTED TO THE FALCULTY OF
THE UNIVERSITY OF MINNESOTA

BY

MINA PANGDRA PEYTON

IN PARTIAL FULFILLMENT OF THE REQUIREMENTS FOR THE DEGREE
OF DOCTOR OF PHILOSOPHY

ADVISOR: DAWN A. LOWE, PH.D.

AUGUST 2022

ACKNOWLEDGEMENTS

First, I would like to thank my advisor, Dr. Dawn Lowe, for her guidance, support, and training. I remember visiting her lab in 2017 as a postbaccalaureate research fellow to discuss research interests. Back then, I could not have imagined the research projects I would accomplish during my graduate training in your lab. Your willingness and trust to let me venture into a new research direction for the lab in the field of skeletal muscle phosphoproteomics, an area of science I knew nothing about at the time, was all I needed to be successful here at the University of Minnesota. For this, I am grateful.

Next, I would like to thank my co-mentors/BICB advisors: Dr. Laurie Parker, Dr. Yue Chen, and Dr. Yuk Sham, for their instrumental guidance on my research projects herein. I could not have completed these projects without our continual meetings and discussions about phosphoproteomics, experimental design, and especially, data analysis of these large, complex proteomic datasets. I am eternally grateful to you for imparting your expertise to me. In addition, I would like to thank our Center for Mass Spectrometry and Proteomics Core; your help was integral to these projects.

To my thesis committee: Dr. Brendan Dougherty, Dr. LeAnn Snow, Dr. Laurie Parker, and Dr. Yuk Sham, thank you for your time advising me during my PhD training. I am grateful for the unique insight each of you brings to my research projects. Your guidance has helped me shape my science, storytelling, and, importantly, the clinical significance of my research.

I want to acknowledge the University of Minnesota Graduate School for awarding me the Graduate School Fellowship and the Diversity of Views and Experiences Fellowship, as well as the Department of Biochemistry, Molecular Biology, and Biophysics

for awarding me the T32 fellowship. These awards allowed me to maximize my PhD training through career development activities and workshops to enhance my research projects and skills. I want to acknowledge and thank Dr. Noro Andriamanalina, Dr. Cori Bazemore-James, and Dr. Yuk Sham for their guidance and wisdom in navigating graduate school and lab life. Your words of wisdom and encouragement helped me tremendously throughout these years. I will forever remember them.

I want to also acknowledge the Postbaccalaureate Research Education Program (PREP) at the Mayo Clinic. Through PREP, I had the opportunity to cultivate my research skills in the lab of Dr. Carlos Mantilla and Dr. Gary Sieck. The research skills I acquired as a PREP fellow in their lab were pivotal and laid the foundation for me as a research scientist. In addition, I want to thank all my Mayo Clinic mentors: Dr. Dennis Mays, Dr. Luis Lujan, Dr. Carlos Mantilla, and Dr. Gary Sieck, for their continued support throughout my graduate training. Even though I was at the University of Minnesota, you continued to give me your time and expertise. Thank you for listening to me practice my presentations, supporting me by coming to my oral presentation at EB, writing me letters of recommendation, and helping me craft my research stories. I am forever thankful for the continued support, discussions, and mentorship.

I would also like to thank Dr. Christopher Pritchett, my undergraduate research experience with you sparked my passion for research and to become a scientist. You not only shared your love of science and research but also mentored beyond the lab. I thank you for your guidance and insights.

To my kindred spirits — Joshua, Mako, and Paul. I am so lucky our roads crossed. You stuck with me — lifting me up

when I was down and celebrating my successes with me. They say, “Good friends are like stars. You don’t always see them, but you know they’re always there.” You are my stars, and I look up to all of you. Your compassion, dedication, and hard work exemplify who I want to become. I know I can always rely on you if I have a body to bury, but most importantly, a home to return to. Thank you for being my framily.

Last but not least, to my husband and best friend, Lee — words cannot express how much you mean to me. You are my pillar of support. I honestly can say I would not be here defending if not for you pushing me along and believing in me. Coming from a traditional collectivistic patriarchal family where the pursuit of higher education was frowned upon for females, I was shunned from the family. I felt alone until I met you. Being post-bacs together at the Mayo Clinic was fun, and competing for our first author manuscript was motivating. Now, being your partner, your wife, has been an honor. You are always a few steps ahead of me but patiently waiting and paving a path for me to reach you. Watching you become the scientist you are now and the amazing PI you will one day become inspires me to become a better scientist and be the best me. Thank you for listening to me vent my frustrations, supporting me throughout the woes and joys of research and life, and being the best rationale soundboard. I know that we will be able to accomplish anything together. I cannot wait to see what the future holds for us! I love you to infinity and beyond.

DEDICATION

I dedicate this dissertation to Collin and Pheng Seng. You two are my number one fans. Love you to the moon and back.

Abstract

Dynapenia, the age-related loss of muscle strength without the loss of muscle mass, significantly impacts the physical function and overall quality of life in older adults, thereby decreasing their health span. Skeletal muscle strength loss has been shown to occur earlier and is greater in aging females than males. Furthermore, clinical and preclinical studies have measured associations between skeletal muscle strength loss and the age at which circulating estrogen begins to decline in females. Despite copious years of skeletal muscle research, the molecular mechanisms underlying muscle strength loss in aging females remain poorly understood. Age-related protein phosphorylation changes have been reported in skeletal muscle of males, and protein phosphorylation alterations have been shown in cardiac muscle across age and sex. However, the extent and magnitude of these changes in the skeletal muscle phosphoproteome of females in response to estrogen deficiency have yet to be determined. This dissertation aims to further our molecular understanding of how estrogen deficiency impacts skeletal muscle function (i.e., the force-generating capacity of muscle) in females by investigating the skeletal muscle phosphoproteome using high-throughput mass spectrometry coupled with bioinformatic analyses and computational modeling. First, using an ovariectomy model, we determined the physiological remodeling of the skeletal muscle phosphoproteome associated with estrogen deficiency. Next, due to the controversies related to using an ovariectomy model to implicate estrogen-related changes in aging females and because the primary function of skeletal muscle is contraction (i.e., molecular force generation), we sought to discern estrogen deficiency-associated protein phosphorylation alterations in contracted skeletal muscle via

evoked electrical stimulations in ovariectomized and natural aging ovarian-senescent female mice compared to their respective controls. Examining the phosphoproteomic alterations in resting, non-contracted, and contracted skeletal muscle of estrogen-deficient females, we identified novel phosphosites, candidate kinases and phosphatases, as well as illuminated key pathways that are sensitive to estrogen levels that may contribute to the loss of skeletal muscle strength. This dissertation provides new avenues for further research and novel targets for the development of therapeutics and interventions to mitigate the loss of skeletal muscle strength in females.

TABLE OF CONTENTS

LIST OF TABLES

LIST OF FIGURES

LIST OF ABBREVIATIONS

AMPK	5’ AMP-activated protein kinase
CAST	Calpastatin
CDK6	Cyclin dependent kinase 6
DES	Desmin
DRX	Disordered-relaxed state
MAPK1	Mitogen-activated protein kinase 1
MYH2	Myosin heavy chain 2
MYOZ2	Myozenin 2
OBSCN	Obscurin
Ovx	Ovariectomized
PRKACA	Protein kinase A catalytic subunit alpha
PRKCE	Protein kinase C epsilon
pRLC	Regulatory light chain phosphorylation
SRX	Super-relaxed state
TPM3	Tropomyosin alpha chain 3
YAP1	Yes-associated protein 1

Chapter 1

Introduction

Globally, the proportion of older adults in the population is expected to increase dramatically. Older adults aged 60 and older are predicted to increase 2-fold, and those aged 80 and older are predicted to increase 3-fold by 2050 [1]. This shift in the distribution of older adults in the world population will bring about global challenges in healthcare, economic disparities, and disease burden. Skeletal muscle is the most abundant tissue in the human body, making up approximately 40% of total body mass in a healthy adult. They are crucial for controlling our movements and posture, protecting internal organs and tissues, storing energy, and regulating body temperature and metabolism. With age, skeletal muscle strength begins to decline and can start as early as the fourth decade of life [2–6]. This age-related loss of muscle strength without the loss of muscle mass is coined dynapenia [7,8]. Dynapenia significantly impacts the activities and quality of life of the aging population [9–12]. Therefore, understanding the underlying molecular mechanisms of skeletal muscle strength loss is paramount in combating the onslaught of challenges associated with aging, as well as preserving the health span into old age.

Historically, skeletal muscle function has been primarily studied in males, humans and rodents [13,14]. However, skeletal muscle strength loss affects both men and women at

differing rates [9,15]. Studies have shown that skeletal muscle strength loss occurs earlier in females than males in both human and rodent studies [16,17]. Preclinical and clinical studies have measured associations between when skeletal muscle strength loss occurs, around middle age in females (~40 years old in humans and ~16 months old in female mice), and the decline of circulating estrogen [16–18]. Estrogen deficiency has been shown to contribute to reduced muscle force and blunted recovery of strength after injury [18–21]. Conversely, estrogen-base hormone therapy in humans or ovariectomized (Ovx) mice supplemented with estradiol (E2) has been shown to mitigate or rescue strength loss [20–27].

Skeletal muscle contraction (i.e., molecular force generation) depends not only on the interaction of myosin and actin but also in conjunction with many muscle proteins to properly propagate the force throughout the muscle fiber. It has been well established that myosin regulatory light chain phosphorylation (pRLC) contributes to muscle activation in smooth muscle and potentiates muscle force in striated muscles [28,29]. More, the discovery of the super-relaxed (SRX) state of myosin and differing myosin conformational states that may also be regulated by myosin pRLC has advanced our understanding of the contractile regulation in molecular force generation [30]. The reduction of muscle force in Ovx

female mice has been correlated with reduction in both myosin pRLC and the SRX state compared to Sham mice [31–33]. Presently, there is limited information on the molecular mechanisms underpinning skeletal muscle strength loss in females. Accumulating evidence indicates protein phosphorylation alterations and adaptations in activities of kinases and phosphatases sensitive to estrogen levels may mediate molecular and cellular responses involved in muscle strength loss of females [32,34].

Therefore, the first aim of this dissertation examines the impact of estrogen deficiency on the skeletal muscle phosphoproteome in resting, non-contracted muscles of ovariectomized (Ovx) via surgical ovariectomy (to disrupt the production of ovarian hormones, particularly estrogen) compared to Sham mice. The second aim examines the skeletal muscle phosphoproteome of Ovx and natural aging, ovarian-senescent female mice compared to their respective controls in contracted muscles, as skeletal muscle contraction is an external stimulus that induces protein phosphorylation. Taken together, this dissertation comprehensively examines the skeletal muscle phosphoproteome in two conditions, resting, non-contracted, and contracted muscles of estrogen-deficient female mice, using high-throughput mass spectrometry discovery-based phosphoproteomics. Our phosphoproteomic

analyses combined with bioinformatic tools and computational modeling identified novel candidate phosphosites, kinases, and phosphatase targets sensitive to estrogen levels for further evaluation of their physiological significance to skeletal muscle strength loss in female mice.

Chapter 2

Literature Review

2.1 Skeletal muscle

2.1.1. Skeletal muscle anatomy

Skeletal muscle, the largest organ in the body, is a voluntary muscle comprised of muscle fascicles that are made up of muscle fibers (i.e., muscle cells) [35]. The bundles of muscle fibers are composed of packages of myofibrils. Each set of bundles is sheathed with connective tissue. The epimysium wraps the entire skeletal muscle, whereas the perimysium wraps the group of fasciculi, and the endomysium surrounds the muscle fibers. The endomysium layer also contains capillaries and nerves and covers the sarcolemma, the muscle fiber's cell membrane. The sarcolemma is a barrier between extracellular and intracellular compartments like the plasma membrane of other cells; however, a unique feature of the sarcolemma is that it invaginates into the muscle cell forming transverse tubules. Myofibrils are made up of myofilaments - the thick filaments are composed of primarily myosin along with myosin binding protein-C, titin, myomesin, and obscurin, and the thin filaments are composed of primarily actin along with tropomyosin and troponin. The thick and thin filaments are anchored to the Z-discs and arranged in a sequential repeating unit called sarcomere, which is ~2μm from end to end and is considered the foundational unit in the myofibril, giving skeletal muscle its striated

appearance. Skeletal muscle fibers are multi-nucleated with both the nuclei and satellite cells (i.e., myogenic stem cells) located on the periphery of the muscle fiber. The sarcoplasmic reticulum, a mesh-like sheath, wraps around myofilaments and is a storage for calcium. A unique feature of skeletal muscle is that it encompasses four different myosin heavy chain (MHC) isoforms that make up the different types of skeletal muscle fibers: one slow type fiber, type I comprised of MHC-beta and three fast type fibers: type IIa with MHC-IIa, type IIb with MHC-IIb, and type IIx with MHC-IIx [36].

2.1.2 Skeletal muscle contraction

Excitation of skeletal muscle is triggered by the binding of acetylcholine from the motor neuron to acetylcholine receptors at the motor endplate, causing the muscle cell to depolarize and generate an action potential. The action potential is then propagated down the sarcolemma, stimulating the sarcoplasmic reticulum to release calcium. Calcium binds to troponin C, evoking a conformational change in tropomyosin to reveal the myosin-binding site on actin. Through the cross-bridge cycle, a power stroke ensues in which actin is pulled and slides past myosin creating force at the molecular level that leads to a muscle contraction.

Briefly, the cross-bridge ATPase cycle of skeletal muscle myosin is intricate. First, the binding of ATP to the myosin head causes the dissociation of the actin-myosin complex [37]. Next, the myosin head hydrolyzes ATP into ADP and inorganic phosphate (P_i) and becomes energized, weakly binding to actin and creating a cross-bridge [37]. When the myosin head releases P_i, it becomes strongly bound to actin and subsequently initiates a power stroke [37]. With this power stroke, actin is pulled, and slides passed myosin toward the M line of the sarcomere. After the power stroke, the myosin head releases ADP and returns the actomyosin cross-bridge to the rigor complex, where the myosin head is still strongly bound to actin until another ATP binds to release the myosin head from actin [38].

2.1.3 Myosin conformational states

Myosin belongs to the family of mechanoenzymes known as molecular motors [39]. The myosin isoform found in skeletal muscle is myosin II, which forms the thick filament and is crucial in generating molecular force for muscle contraction. Myosin II exists in three different states – the active state that binds actin only during contraction, and then two relaxed states, the super-relaxed state (SRX) and disordered relaxed state (DRX), that predominate in non-contracting muscle (i.e., during relaxation). The myosin states in relaxation

are in dynamic equilibrium, where the “off” state is the SRX state (myosin heads folded back towards the tail), and the “on” state is the DRX state (myosin heads interacting and perpendicular to the tail). The ATP turnover rate drastically differs among the active, DRX, and SRX states, being less than 1s, less than 30 s, and greater than 100 s, respectively [39]. The regulation of contraction was originally thought to be dependent on the number of available myosin binding sites on actin; however, the discovery of the super-relaxed state and ensuing studies on myosin’s role as a mechanosensor have advanced our understanding of the intricate regulation of muscle contractility. Mechano-sensing of force, piperine (i.e., black pepper), or the phosphorylation of myosin regulatory light chain will transition myosin from the SRX state to the DRX state; whereas, interaction with myosin bind protein-C will transition myosin from the DRX state to the SRX state [30,40–42]. Studies have shown that only myosin heads in the DRX are able to move to the active state, bind to actin, and generate molecular force [43].

Cryo-electron microscopy has contributed structural detail to the SRX and DRX states, revealing the structure of myosin heads in the SRX state. In the SRX state, the myosin heads are folded back towards the tail, and this structure is termed the interacting-heads motif (IHM). It has been shown

that when calcium binds the essential light chain (ELC) of myosin, it shifts the myosin heads to an “on” state from the IHM (the off state) and may act as a molecular linker switch regulating the DRX/SRX states in cardiac muscle [39,44]. However, there is limited work on the ELC in striated muscle, particularly skeletal muscle, and what factors, such as estrogen, have on modulating the ELC is yet to be determined.

2.1.4 Myosin conformational states and aging

Several pieces of evidence to suggest that female sex hormones influence myosin and muscle contraction. Using an ovariectomy mouse model (i.e., surgical bilateral removal of the ovaries to mimic the loss of estrogen in menopause), estrogen deficiency disrupted the SRX of myosin by decreasing the ATP turnover rate in Ovx mice compared to Ovx + E2 (Ovx mice treated with estradiol)[45]. In addition, Phung et al. showed that age and sex affect the relaxation states of myosin in skeletal muscle fibers of female mice compared to male mice, shifting the DRX/SRX equilibrium [33]. Further, reduction in myosin regulatory light chain phosphorylation (pRLC), which regulates the transition of myosin into the DRX state from the SRX state in skeletal muscle, after potentiation of isometric twitch force was found to be correlated with the loss of muscle force potentiation in OVX mice compared to sham mice [32]. In the same study, using the C2C12 muscle cell

line, dose-dependent phosphorylation of RLC by estradiol was demonstrated [32]. However, a study by Fillion et al., using the same ovariectomy mouse model, found no impact of estrogen deficiency on pRLC or potentiation of concentric twitch force [46]. The disruption of myosin dynamics (DRX to SRX and vice versa) during the relaxed state and decreased myosin pRLC may lead to increased weakness with age resulting from slower cross-bridge kinetics [39]. Thus, more work is needed to examine age- and estrogen deficiency-related molecular mechanisms regulating myosin pRLC and phosphorylation of other sarcomeric proteins and their contribution to force generation in females.

2.2 Skeletal muscle aging

2.2.1 Age-related loss of skeletal muscle mass

Skeletal muscle mass begins to decline in the fourth decade of life at a rate of ~3 – 8% per decade [47]. This rate increases to ~8% per decade between 50 – 70 years of age and then an accelerated loss of ~15% per decade after 70 [48–51]. Studies in men and women have reported a loss of 30 – 50% skeletal muscle mass between the ages of 40 and 80 [9,12,52].

Loss of muscle fibers may result from the loss of motor units with age leading to denervation of the muscle fibers and fiber death [35,55]. The loss of skeletal muscle mass can be attributed to losing muscle fibers, thereby altering muscle

fiber-type composition. Preclinical and clinical studies have shown an increase in Type IIa fibers and a decrease in Type II fibers [49,50,53,54]. In addition to the loss of muscle fibers, muscle fiber-type atrophy (i.e., decrease in muscle fiber cross-sectional area) contributes to the loss of skeletal muscle mass with age. Specifically, atrophy of type I and type II fibers [55–57]. The loss of muscle mass is further accelerated with the beginning of menopause, which will be discussed in a later section [58].

2.2.2 Age-related loss of skeletal muscle strength

The loss of muscle strength, which leads to the loss of skeletal muscle function with age, is a component of sarcopenia, the age-related loss of skeletal muscle mass and function. There is supporting evidence that the loss of muscle strength does not necessarily correlate with the loss of muscle mass. This age-related loss of muscle strength without the loss of muscle mass is termed dynapenia. It is well known that muscle strength declines with age and that muscle strength decline faster than muscle mass [7,8,49,59]. Compared to 20-year-old individuals, muscle strength is 20-40% less in those 70 or older and 50% less in those 90 and older [12]. A study examining hand grip and knee extensor strength in men and women between the ages of 20 to 80 showed a dramatic decline in strength in women after age 55, which is during

the time around menopause [60]. Menopause and muscle strength loss will be discussed further in the next chapter. A recent meta-analysis examining isometric and isokinetic torque in knee extensors of human males and females across ages from 57 different studies showed that the loss of isokinetic torque declined 25 years earlier in females than in males [61]. Likewise, the loss of muscle force in the hindlimb muscle, soleus, of male and female mice across ages showed the same pattern [17].

Muscle strength loss with age may result from changes in the contractile apparatus and between contractile protein interactions. Moran et al. showed a significant reduction in the number of strong-binding myosin heads during muscle activation, thus reducing muscle force [18]. Additionally, there is evidence that aging decreases myosin expression and myosin-actin cross-bridge kinetics that may result from the reduction in pRLC of myosin [62–64]. Reduction in pRLC has been shown to correlate with decrements in muscle force [32]. However, it is unlikely that RLC is the only contractile protein whose phosphorylation state is modified by aging. Further studies examining phosphorylation of skeletal muscle proteins and muscle contraction is needed as much of the literature on phosphorylation of contractile proteins stem from smooth and cardiac literature.

2.3 Estrogens and estrous cycle

2.3.1 Estrogens

In females, the primary sex steroid hormones are estrogens. There are four types of estrogens: estrone (E1), estradiol (E2), estriol (E3), and estetrol (E4). E2 is the predominant product in the biosynthesis of estrogens and is the most potent biological estrogen [65–68]. In premenopausal women, E2 is the primary estrogen, whereas, in postmenopausal women, E1 is the predominant estrogen [68,69]. Although E1 is the predominant estrogen in postmenopausal women, it is a weak estrogen (i.e., it is less potent to stimulate estrogenic activities), and its estrogenic potency stems from its conversion to E2; thus, it acts as a prohormone of E2 [70]. E3 and E4 levels are only detectable during pregnancy, where E3 becomes the most synthesized estrogen during pregnancy by the placenta, and E4 is produced solely by the fetal liver.

Estrogens are steroid hormones derived from a common precursor, cholesterol. The synthesis of estrogens occurs primarily in the ovaries, placenta, corpus luteum, and small amounts from nongonadal organs, such as the heart, liver, skin, adipose tissue, and brain [65,66,68,71–73]. It is important to note that in young non-reproductive females or postmenopausal females, the major site of estrogen synthesis is in extragonadal sites, where synthesized estrogen acts locally;

whereas, in reproductive females, the major sites are the ovaries where synthesized estrogen is primarily released into the bloodstream [69].

In the ovary, the thecal and granulose cells are involved in the synthesis of E2 (Figure 7). Both thecal and granulose cells can perform the first two steps of E2 biosynthesis: 1) cholesterol is converted into pregnenolone, catalyzed by the cytochrome p450 side-chain cleavage enzyme (P45scc), and 2) pregnenolone is converted into progesterone, catalyzed by 3beta-hydroxysteroid dehydrogenase (3beta-HSD). Where they diverge is that thecal cells are only able to synthesize androgens from progesterone catalyzed by cytochrome P450 17alpha-hydroxylase (P45017alpha) and 17beta-hydroxysteroid dehydrogenase (17beta-HSD) but unable to complete the biosynthesis of E2. In contrast, granulosa cells can complete the biosynthesis of E2 but not the synthesis of androgens. Thus, androgens synthesized in the thecal cells are released from growing follicles to be transported to the granulosa cells in order to complete the biosynthesis of E2. On the other hand, granulose cells are unable to synthesize androgen. Therefore, progesterone has to be transported into the thecal cells for androgen synthesis. However, once androgens are transported to the granulosa cells, the

synthesis of E2 via aromatase (P450Arom) from androgens can be completed.

2.3.2 Mouse estrous cycle

Female mice reach sexual maturity ~ 4 weeks (26 days) after birth, and the estrous cycle begins with the opening of the vagina [74,75]. The estrous cycle length is 4 to 5 days and is divided into 4 phases: proestrus, estrus, metestrus, and diestrus [74–76]. The proestrus phase lasts less than 24 hours, the estrus phase lasts from 12 – 24 hours, the metestrus phase lasts from 8 – 24 hours, and finally, the diestrus phase from 48 – 72 hours [74]. Unless the cycle is interrupted by anestrus, pseudopregnancy, or pregnancy, it will repeat every 4 – 5 days. The proestrus phase parallels the human follicular stage, which is associated with increased circulating E2 levels up to about 40 pg/ml [74]. The rise in E2 level leads to an increase in luteinizing hormone and the release of follicle-stimulating hormone (FSH) [74]. The peak of FSH concentrations marks the estrus phase, with estradiol levels rapidly declining to around 15 pg/ml and correlating to ovulation. Without interruptions, the cycle will proceed into metestrus and diestrus, which are analogous to the human early and late luteal stage with increased progesterone levels [74].

In the rodent estrous cycle, the uterine lining is reabsorbed, and the reduction in the number of follicles in

the ovaries leads to ovarian senescence, similar to menopause in humans [73]. However, some female rodents may also enter into different reproductive-aging states. They may experience irregular estrous cycles around 9 – 12 months of age and transition into a polyfollicular anovulatory state of persistent estrus resulting in sustained levels of E2 [77–79]. From this persistent estrus state, they can transition into an anestrous state, where ovulatory cycles stop, and gonadal steroid levels are low or pass through a repetitive pseudopregnancy before the anestrous state [76,79]. At times, they may even stay in the pseudopregnancy state until the end of their lifespan, thus, generating high progesterone levels [76]. Due to the complexity of estrogen status in female rodents, a sensitive and reliable method of confirming their cycling status, such as vaginal cytology or measuring serum estradiol, such as ELISA or LC-MS/MS should be applied.

2.4 Estrogen receptors

Estrogen receptors (ERs) are proteins found in the cytosol or on the extracellular membrane, with expression of ERs heavily dependent on tissue type. ERs can further be sub-categorized based on their cellular localization, with intracellular ERs falling into the nuclear receptor family of receptors. In contrast, the receptors found on the extracellular membrane belong to the membrane-bound receptor

family. There are two nuclear ERs (ERa and ERb) which are historically thought to contribute to all estrogen-mediated signaling; however, over the last two decades, the membrane-bound estrogen receptors (approximately 10-15%), which are splice variants of the nuclear receptors, have also been shown to contribute to overall estrogenic effects 80. The membrane-bound estrogen receptors, including another ER, the G-protein-coupled estrogen receptor (GPER), are exposed to different stimuli and display different signaling kinetics compared to the nuclear receptors.

The genomic effects of estrogen are mediated by successful binding to the nuclear receptors ERα and ERβ with the concept of ligand-mediated changes in ER conformation central to the mechanism of action. Once estrogen enters the cell via passive diffusion through the cell membrane, it binds to the nuclear ER and translocate into the nucleus. After this initial binding event, the ER undergoes several conformational changes that result in receptor dimerization. This dimerization increases the affinity and rate of receptor binding to DNA. Various ER dimers can be produced (ERα homodimers, ERβ homodimers, ERα / ERβ heterodimers) depending on numerous factors within the cell [81].

Nevertheless, the ER dimer is responsible for binding the estrogen response elements (ERE) located in the promoter

region of target genes. This ER-DNA complex then recruits a cascade of coactivators and other proteins to the promoter regions forming the transcription machinery. It should be noted that transcriptional regulation occurs on the time scale of hours to days.

GPER is a membrane-bound estrogen receptor falling into the superfamily of G-protein coupled receptors (GPCRs) as their signaling cascade is dependent on G protein activity. Upon ligand binding, GPER can mediate several rapid changes in cellular function primarily mediated via secondary messenger pathways (Ca2+, NO, cAMP) [71]. Importantly, it is possible through activation of GPER to induce tyrosine kinases such as EGRF, IGF1R, and other essential protein/lipid kinases (PI 3-kinase, Akt, MAPK), bringing to light the large swatches of biologic activity estrogen signaling may contribute [71]. It should be noted that the effects mediated by membrane-bound estrogen receptors occur on the time scale of seconds to minutes.

2.5 Estrogen-mediated signaling pathways

Four major estrogen-mediated signaling pathways are currently identified: two ER-dependent pathways and two ER-independent pathways [69]. Estrogen-mediated signaling is primarily through the ERs mentioned above, with the classical genomic signaling through ERα and ERβ. ER-dependent pathways

can be initiated in the cytoplasm or the plasma membrane [69]. The estrogen-independent pathway triggered by IGFR, DAR, or EGFR can also lead to ER transcriptional activities. Non-transcriptional activities can occur by the membrane ERs, GPER, or passive diffusion of E2 into the cell in ER-dependent or ER-independent pathways.

Although we and others have shown that E2 and E2-ER signaling is important for muscle contraction and the generation of force in skeletal muscle, dissecting the molecular mechanism of estrogen-mediated signaling in skeletal muscle has been minimally investigated. We have shown that estrogen impacts protein phosphorylation of myosin RLC; however, estrogen may also impact the phosphorylation-base signaling of other sarcomeric proteins. Thus, it is crucial to investigate how estrogen may affect the phosphoproteome and phosphorylation-base signaling in females.

2.6 Estrogen and skeletal muscle

Estrogen has been shown to have a beneficial, protective effect on skeletal muscle, affecting muscle structure and function, muscle damage, post-damage muscle inflammation, and post-damage muscle repair [82–84]. There are at least three prevailing thoughts for how estrogen exerts its protective effects on skeletal muscle: 1. estrogen acts as an

antioxidant, stimulating expression and activities of other antioxidant enzymes to limit oxidative damage, 2) estrogen contributes to membrane-stabilizing effect by inserting itself within membrane phospholipids, and 3) estrogenic regulation of downstream genes and molecular targets such as contractile proteins [85]. Preclinical and clinical studies have shown a significant effect of E2 treatment or hormone therapy on muscle strength, which will be described in further detail below.

2.6.1 Menopause

Women live through three distinct phases in their life-span — the reproductive phase, the menopausal transition phase, and the postmenopausal phase. More than one-third of a woman's life is now spent in the postmenopausal phase in the majority of western countries [27] Menopause is a natural biological process defined as the stage in a woman's life where she is no longer fertile and is indicated by the end of menstrual cycles. Typically, this occurs between the ages of 40 — 50, with an average age of 51 in the United States. It is an age-dependent physiological condition resulting from the decline of reproductive hormones (E2 and progesterone); however, it can also be triggered by other causes such as chemotherapy, radiation therapy, hysterectomy, and primary ovarian insufficiency (i.e., when the ovaries produce

insufficient levels of reproductive hormones due to autoimmune diseases or genetic factors)[86–88].

Menopause is characterized by a natural decline in estrogen, increasing visceral fat mass, and decreases in bone mass density, muscle mass, and strength [89]. Estrogen has been shown to contribute to the overall health of organ systems and tissues. The decline in E2 level may contribute to adverse health effects and functional decline of postmenopausal women. The effects of menopause have been examined on the health and well-being of women, ranging from their appetite and the gastrointestinal system, the heart and cardiovascular system, bone health to the neuromuscular system. Within one year before and after the last menstrual cycle in the menopausal transition phase, there is a substantial decline in estrogen secretion [27]. Following this, in the early postmenopausal years, there is a further gradual decline of E2, with levels declining to 0.04 nM or less [27,68]. As mentioned above, E1 becomes the primary estrogen in postmenopausal females. It is synthesized in adipose tissue, where testosterone and androstenedione are converted to E1, thus replacing the production of E2 in the ovaries [27]. The decrease of estrogen in menopause has been associated with many adverse outcomes in skeletal muscle, such as an increase in muscle

weakness and injury, reduced power, and delayed recovery from injuries [85].

2.6.2 Estrogen and skeletal muscle mass

The loss of estrogen during menopause is associated with body composition changes, particularly the decline of skeletal muscle mass and an increase of intramuscular fat that may be related to a loss of muscle strength [58,89]. A cross-sectional study in menopausal women showed a decline of 0.6 % per year of muscle mass. In the first three years of menopause, the total body potassium, a marker of lean body mass, was also shown to decrease significantly [89]. A study examining non-contractile muscle tissue per unit of muscle cross-sectional area reported that postmenopausal women (65 to 80 years old) had two times the amount of non-contractile muscle tissue compared to premenopausal women (23 to 57 years old) [90]. Additionally, the loss of estrogen may also influence muscle contractile properties and intensify muscle damage, inflammation, and recovery [91]. Other important factors contributing to reducing muscle mass in postmenopausal women are protein uptake, oxidative stress, and physical inactivity [89].

2.6.3 Estrogen and skeletal muscle strength

Poor muscle strength in postmenopausal women is a strong risk factor for total mortality [91]. The loss of muscle strength

in females has been shown to decline dramatically around menopause [60,92,93]. In human studies, to investigate estrogen-related strength loss, many studies have been conducted examining premenopausal women versus postmenopausal women and postmenopausal women versus postmenopausal women on estrogen-based hormone therapy. These studies show that strength loss was prevented and/or reduced in perimenopausal women and postmenopausal women on estrogen-based hormone therapy [22,93,94]. In addition, a meta-analysis by Greising et al. found that postmenopausal women receiving estrogen-based hormone therapy had ~5% greater strength than postmenopausal women who did not receive treatment [95]. Compared to their male counterparts, postmenopausal women experience decreased functional capacity, more significant strength declines, impairments in muscle repair, and increased rates of sarcopenia and osteoporosis with age [58,89].

Using the OVX mouse model, estrogen deficiency has been shown to decrease muscle strength. In animal studies, female rodents supplemented with estradiol exhibited less muscle fiber injury and inflammation after exercise-induced muscle injury, and influenced the activation and proliferation of satellite cells in the post-damage repair process [85]. Force normalized to contractile proteins (i.e., actin and myosin) was significantly reduced in the soleus and extensor

digitorum muscle of OVX mice compared to sham mice across [18,23]. Further, when OVX mice were treated with E2, force was restored to control levels [23]. Using electron magnetic spectroscopy, Moran et al. showed that force generation in OVX mice was significantly decreased and resulted from reduced strong-binding myosin during contraction and that force generation and myosin function was rescued with E2 treatment [23]. In addition, examining the recovery of strength after injury in wild-type mice, Kosir et al. found that OVX mice had a significant blunted recovery of strength compared to sham mice [19]. The molecular mechanisms underlying the loss of muscle strength in females are not entirely known; however, studies indicate that pRLC and changes in myosin conformational states impact force generation/muscle strength. It is unlikely that myosin is the only protein in skeletal muscle affected by estrogen-mediated signaling, as protein phosphorylation plays a key role in signal transduction.

2.7 Phosphoproteomics

2.7.1 Protein phosphorylation

Post-translational modifications (PTMs) are modifications on proteins during or after their assembly by addition, removal, or folding of functional groups, which can regulate protein structure, activity, interactions, and

location [96–98]. Today, there are over 400 types of PTMs [96,98]. Protein phosphorylation, a reversible modification, is one of the most well-studied PTM due to its importance in signal transduction and disease [99–101]. About 30% of the proteome is estimated to be modified by phosphorylation with more than 500,000 potential phosphorylation sites [101,102]. In eukaryotes, O-phosphorylation occurs on the amino acids: serine, threonine, and tyrosine, with the frequency of phosphorylation occurring at a ratio of ~1,800:200:1, respectively [98]. The addition of the γ-phosphate group by the universal donor, adenosine triphosphate (ATP), to the hydroxyl oxygen of the amino acid residue is mediated by protein kinases [99]; whereas the removal of phosphorylation is catalyzed by protein phosphatases.

Protein phosphorylation with the addition of one or more phosphate groups has a profound effect on the biological function of the modified protein. It can activate or inactivate a protein and modulate molecular interactions and signaling [100]. The advent of high throughput phosphoproteomic studies with mass spectrometry (MS), identification of peptides, and localization of phosphorylation sites, has prompted the creation of many software tools and bioinformatics pipelines. More, utilizing kinase-specific phosphorylation motifs in order to predict kinase-substrate

interactions has resulted in the creation of prediction tools such as Inference of kinase activities from phosphoproteomics (IKAP), NetworKIN, NetPhorest, Ingenuinity Pathway Analysis, and others.

2.7.2 Mass spectrometry

MS has become a powerful tool for the analysis of phosphoproteins. Using high-resolution mass spectrometry, the detection of mass to charge (m/z) ratio can measure the mass difference between a phosphorylated peptide compared to an unphosphorylated peptide, as phosphorylation adds a mass shift of 79.99 Da to the modified peptide. However, due to the positive ion mode of the MS, phosphopeptide signals and ionization efficiency are low [103]. Therefore, phosphopeptide enrichment is advantageous prior to liquid chromatography coupled tandem mass spectrometry (LC-MS/MS). Higher-energy collisional dissociation (HCD) is used for further MS/MS fragmentation instead of collision-induced dissociation (CID), as it preserves the labile phosphate groups on the peptide backbone, thus, allowing for confident phosphosite assignment [104]. Although CID with a linear ion trap is traditionally used because of its sensitivity and speed, MS/MS spectra from HCD fragmentation with an orbitrap mass analyzer are of higher quality as utilizing both allows for high-resolution ion detection, increased ion fragments, and

no low-mass cutoff [105,106]. Other fragmentation techniques that can be utilized are electron capture dissociation and electron transfer dissociation.

2.7.3 Phosphoproteomic profiling of skeletal muscle

Technological advancements in phosphoprotein enrichment strategies and profound improvements to mass spectroscopy, resulting in faster and more sensitive data acquisition, have dramatically increased the power of global phosphoproteomic analyses [102]. Although there have been phosphoproteomic studies of skeletal muscle using cell culture, this section will primarily focus on seminal studies from which skeletal muscle tissue from human and rodent studies were utilized and in the context of aging and/or sarcopenia/dynapenia.

The first phosphoproteomic analysis on aged skeletal muscle (gastrocnemius) was performed in young and old male rats (3 months old vs. 30 months old, respectively) by Gannon et al. in 2008 to investigate muscle degeneration in a sarcopenic rodent model [107]. Two-dimensional gel electrophoresis was performed – first dimension separation by the protein's isoelectric point value, then second dimension separation by the protein's molecular weight, followed by a silver stain, fluorescent phosphoprotein Pro-Q Diamond stain, and total protein-dye with Ruthenium II Bathophenathroline disulfonate chelate (RuBPs). No difference in protein

abundance between the groups was found with the silver and RuBPs stain; however, 22 protein spots were differentially expressed between young and old rats with the Pro-Q Diamond phosphostain. The 22 protein spots were analyzed by matrix-assisted laser desorption/ionization time-of-flight (MALDI-ToF) mass spectrometry for mass spectrometric fingerprinting analysis, and 14 of the 22 protein spots were identified. Out of the 14 identified differentially expressed phosphorylated proteins in old compared to young rats, ten proteins had increased phosphorylation expression of myosin light chain (MLC) 2, Golgi reassembly stacking protein I, tropomyosin-alpha, lactate dehydrogenase, desmin, alpha-1-actin, albumin, down syndrome critical region homolog 6, alpha-actin, and aconitase 2, and 4 had decreased phosphorylation expression of 2 cytochrome c oxidase proteins, creatine kinase, and enolase 3-beta. The results from this study indicated that there was an age-dependent modification of protein phosphorylation in skeletal muscle. Of the 22 differentially expressed phosphoproteins, 63% had increased phosphorylation, and 36% had decreased phosphorylation with age. This paper was restricted by technology, as 2D gel phosphoproteomics is limited in sensitivity; thus, the results may not fully represent phosphoproteomic alterations in muscle aging. In addition, females were not included in the study.

The first large-scale phosphoproteomic study examining the human skeletal muscle phosphoproteome was done by Højlund et al. in 2009. Skeletal muscle tissue (vastus lateralis muscle) from 3 healthy young lean males (32 – 48 years old) under basal condition were analyzed [108]. Strong cation exchange was performed, followed by titanium oxide (TiO_2) phosphopeptide enrichment, and then HPLC-ESI-MS/MS was performed on a hybrid linear ion trap (LTQ)-Fourier Transform Ion Cyclotron Resonance (FTICR) mass spectrometer. They were able to identify 127 phosphoproteins and 306 unique phosphosites. Of these, 26% of the phosphoproteins were sarcomeric proteins, and 53% of the unique phosphosites were related to skeletal muscle contractile function.

Miller et al. in 2013 performed a phosphoproteomic study in humans, examining specifically myofibrillar proteins from the vastus lateralis muscle in young and older males and females [109]. Investigators performed phosphoprotein-specific gel staining coupled with LC-MS. They identified alpha-tropomyosin, troponin T, fast and slow skeletal myosin binding protein -C isoforms, myosin regulatory light chain-2, MLC 2s, and MLC-2f (fast isoform). LC-MS determined absolute phosphorylation of only MLC-2s and MLC-2f. From this, it was determined that only MLC-2f protein showed a significant age-related decrease in phosphorylation level in

older women (1.8 ± 0.1-fold decrease) compared to the other groups (Miller, 2013). These results highlight the potential contribution of differentially expressed isoforms of myosin regulatory light chain to muscle force contraction.

Lastly, Gregorich et al. performed a targeted top-down proteomics study examining the phosphorylation of myosin regulatory light chain (RLC) [110]. Using young (6 months old) and old (36 months old) male rats, they found a decline in RLC phosphorylation with age. These four studies demonstrate that the skeletal muscle phosphoproteome changes with age. Specifically, phosphorylation of contractile proteins, particularly myosin regulatory light chain phosphorylation in humans and rodents, has been shown to impact muscle force generation.

It is important to note that there have been many other phosphoproteomic studies in skeletal muscle tissue related to exercise, insulin-signaling, calorie restriction, high-fat diets, etc.; however, the majority of the studies are in males, whether in human or rodent studies. Thus, global phosphoproteomic profiling of skeletal muscle in females is unknown, and whether the effects of aging, specifically, the loss of estrogen with age in females, impact the phosphoproteome and phosphorylation signaling networks in skeletal muscle remains to be determined.

To overcome the limitations of these previous studies due to technology and address the lack of research in females investigating altered protein phosphorylation in skeletal muscle, we employed high-throughput mass spectrometry discovery-based phosphoproteomic analysis of skeletal muscle in female mice. Our first important question was to establish whether estrogen deficiency remodeled the skeletal muscle phosphoproteome in female mice. To examine the impact of estrogen deficiency on the skeletal muscle phosphoproteome, we used an ovariectomy model coupled with label-free mass spectrometry to globally profile the changes in resting, non-contracting muscles of Ovx compared to Sham female mice. This led to my first major project presented in Chapter 3 of this dissertation.

Chapter 3

Global phosphoproteomic profiling of skeletal muscle in ovarian-hormone deficient mice

Global phosphoproteomic profiling of skeletal muscle in ovarian-hormone deficient mice

Mina P. Peyton[1,2], Tzu-Yi Yang[3], LeeAnn Higgins[3], Todd W. Markowski[3], Cha Vue[1], Laurie L. Parker[2,3], and *Dawn A. Lowe[1,4]

[1]Department of Rehabilitation Medicine, Division of Rehabilitation Science, University of Minnesota – Twin Cities, Minneapolis, Minnesota 55455, United States

[2]Department of Computer Science, Bioinformatics and Computational Biology Program, University of Minnesota, Minneapolis, Minnesota 55455, United States

[3]Department of Biochemistry, Molecular Biology, and Biophysics, University of Minnesota – Twin Cities, Minneapolis, Minnesota 55455, United States

[4]Department of Rehabilitation Medicine, Division of Physical Therapy, University of Minnesota – Twin Cities, Minneapolis, Minnesota 55455, United States

***Corresponding author**

*Email: lowex017@umn.edu

Orcid: 0000-0002-5784-9289

Supplemental material available at:

DOI: https://doi.org/10.6084/m9.figshare.20043392

The contents of this chapter are published in *APS Physiological Genomics*.

OVERVIEW

Protein phosphorylation is important in skeletal muscle development, growth, regeneration, and contractile function. Alterations in the skeletal muscle phosphoproteome due to aging have been reported in males; however, studies in females are lacking. We have demonstrated that estrogen deficiency decreases muscle force which correlates with decreased myosin regulatory light chain phosphorylation. Thus, we questioned whether the decline of estrogen in females that occurs with aging might alter the skeletal muscle phosphoproteome. C57BL/6J female mice (6 mo) were randomly assigned to a sham-operated (Sham) or ovariectomy (Ovx) group to investigate the effects of estrogen deficiency on skeletal muscle protein phosphorylation in a resting, non-contracting condition. After 16 weeks of estrogen deficiency, the tibialis anterior muscle was dissected and prepped for label-free nano-liquid chromatography tandem mass spectrometry phosphoproteomic analysis. We identified 4,780 phosphopeptides in tibialis anterior muscles of ovariectomized (Ovx) and Sham-operated (Sham) control mice. Further analysis revealed 647 differentially regulated phosphopeptides (Benjamini – Hochberg adjusted p-value < 0.05 and 1.5-fold change ratio) that corresponded to 130 proteins with 22 proteins differentially phosphorylated (3 unique to Ovx, two unique to

Sham, six upregulated, and 11 downregulated). Differentially phosphorylated proteins associated with the sarcomere, cytoplasm, and metabolic and calcium signaling pathways were identified. Our work provides the first global phosphoproteomic analysis in females and how estrogen deficiency impacts the skeletal muscle phosphoproteome.

KEYWORDS: females, estrogen, ovariectomy, sarcomere, AMPK, YAP, and calcium signaling

INTRODUCTION

Protein phosphorylation is one of the most well studied reversible, post-translational modifications due to its importance in signal transduction and disease [99–101]. It is estimated that about 30% of the proteome in mammals is modified by phosphorylation, with more than 500,000 known phosphorylation sites identified to date [101,102]. The addition of one or more phosphate groups can have profound effects on the biological function of the modified protein. Phosphorylation can either activate or inactivate a protein as well as modulate molecular interactions and signaling [100]. Thus, examining phosphorylation status of proteins in a given condition at a given time provides further understanding of their role in physiological or pathophysiological states.

Skeletal muscle mass and strength begin to decline with age, increasing the risk of poor balance, impaired mobility, falls, and overall mortality [111–113]. Preclinical and clinical studies have shown that loss of muscle strength occurs earlier in females than males, and this decline in muscle strength in females is associated with the reduction of circulating estrogen, specifically 17beta-estradiol (E2), as a result of menopause [17,18,114]. To understand the impact of estrogen deficiency on molecular aspects of skeletal muscle function,

rodent ovariectomy models were used to show that loss of estrogen significantly attenuates force generation by reducing the number of strong-binding myosin heads during contraction (10–11), which could be restored by supplementation of E2 (12). Similar effects of estrogen deficiency on myosin function have been indicated in muscles of postmenopausal women [94,116]. Protein phosphorylation, including myosin, has been shown to play a significant role in regulating signal transduction pathways that contribute to fiber-type differentiation, muscle hypertrophy, plasticity, regeneration, excitation-contraction coupling, and contractile function [32,117–126]. Estrogen modulates myosin regulatory light chain (RLC) phosphorylation in striated muscle; however, in skeletal muscle, whether phosphorylation of other proteins is sensitive to estrogen is yet to be determined [32,127,128]. Broader phosphoproteomic analysis could aid in identifying candidate phosphoproteins to elucidate further how estrogen deficiency affects the molecular characteristics of muscle proteins and function in females.

Previous studies examining the skeletal muscle phosphoproteome have been predominantly performed with samples from males, with only limited global phosphoproteomic studies in females [107,108,129,130]. Phosphoproteomic analysis of aged male compared to young male rat muscle via 2D gel

electrophoresis and phosphostaining demonstrated altered phosphorylation in 22 muscle proteins [107]; however, females were not included in that study, and 2D gel phosphoproteomics is limited in sensitivity, so the results may not fully represent the role of phosphorylation in muscle aging. Changes specifically in myosin phosphorylation and kinetics have been examined across young and aged humans (both male and female), and decreased myosin RLC phosphorylation and kinetics were only observed in aged females [130], suggesting potential estrogen-related differences; however, broader phosphoproteomics data on those differences have been lacking. We sought to investigate the functional landscape of the skeletal muscle phosphoproteome in estrogen-deficient females to identify whether broader scale changes beyond just those observed in RLC phosphorylation were occurring. We hypothesized that loss of estrogen in females would remodel the skeletal muscle phosphoproteome, affecting phosphoproteins of the sarcomere, the basic contractile unit of the muscle fiber critical for muscle function.

In this study, we used bilateral ovariectomy to model the loss of estrogen in menopause because it induces the deficiency of ovarian hormones, including the primary estrogen, E2. We performed label-free phosphoproteomic analysis on the tibialis anterior (TA) muscle of

ovariectomized (Ovx) and control mice that had undergone a sham ovariectomy surgery (Sham) to determine how estrogen deficiency impacts the skeletal muscle phosphoproteome in females during a basal, non-contracting condition. Differentially phosphorylated proteins associated with the sarcomere, cytoplasm, and muscle-relevant canonical pathways, such as metabolic and calcium signaling pathways, were identified. These observations suggest that estrogen loss contributes to remodeling the skeletal muscle phosphoproteome, which could have downstream implications for the molecular function of proteins critical to muscle strength in aging females.

MATERIALS AND METHODS

Animals

Female C57BL/6J (6 mo) mice were purchased from Jackson Laboratories (Bar Harbor, ME, USA). Female C57BL/6J (6 mo) mice were purchased from Jackson Laboratories (Bar Harbor, ME, USA). All mice were housed in groups of four to five in a room maintained on a 14:10 h light/dark cycle. All experiments and procedures were approved by the University of Minnesota Institutional Animal Care and Use Committee.

Experimental Design

The study design to evaluate the skeletal muscle phosphoproteome in Ovx and Sham control mice is summarized in Fig 1A. Female C57BL/6J mice were randomly assigned to a Sham or ovariectomy surgery. Vaginal cytology was performed 4 wk post-surgery, and uterine mass was measured at the time of sacrifice to confirm estrous cycling and successful ovariectomy. Mice had access to phytoestrogen-free food (2019 Teklad Global 19% Protein Rodent Diet, Harland Teklad, Madison, WI, USA) and water *ad libitum* until sacrifice. TA muscles from anesthetized mice (1.75% isoflurane and 200 ml O_2 per min) were dissected 16 wk post-surgery. Tissues were harvested between 0900 — 1300 hours corresponding to the dark cycle of the mice. The TA muscle was chosen because it is a well-characterized hindlimb mouse muscle studied across aging and disease and because it is amenable to physiological contractile measurements [131], potentially important for subsequent phosphoproteomic studies. Muscles were TA muscles from anesthetized mice (1.75% isoflurane and 200 ml O_2 per min) were dissected 16 wk post-surgery, immediately flash-frozen in liquid nitrogen, and stored at -80ºC until sample preparation and phosphopeptide enrichment for nanoflow LC-MS/MS acquisition.

Sham and Ovariectomy surgeries

Anesthetized (1.75% isoflurane and 200 ml O_2 per min),

mice received a subcutaneous injection of slow-release buprenorphine (1mg/kg) immediately prior to surgeries. Two dorsal lateral incisions were made to locate the ovaries, which were excised in mice assigned to the Ovx group, and located but not removed in mice assigned to the Sham group. The incisions were closed with 6—0 silk sutures, and 7 mm wound clips closed the skin incision.

Protein extraction, digestion, and phosphopeptide enrichment

Frozen TA muscles were pulverized into powder with a cryo-grinder (liquid nitrogen-cooled mortar and pestle), lysed (10 μl lysis buffer per mg of tissue) in protein lysis buffer (7M urea, 2M thiourea, 0.4M Tris pH7.5, 20% acetonitrile, four mM TCEP) with 1X HALT Protease & Phosphatase Inhibitor Cocktail (78440, Thermo Fisher Scientific, Rockford, IL, USA), and sonicated for 5 s using a probe sonicator (Branson Digital Sonifer, Emerson, St. Louis, MO, USA) set at 30% amplitude. After sonication, a 160 μl aliquot of each lysate was placed in the Barocycler® NEP2320 (Pressure Biosciences, South Easton, MA) at 37ºC, with pressure cycles set at 35,000 psi for 20 s, then 0 psi for 10 s for 60 cycles for further protein homogenization. Once pressure cycling was complete, samples were transferred to a new 1.5 ml Eppendorf protein LoBind tube, and a 200 mM

chloroacetamide stock solution was added for a final concentration of 8 mM to alkylate proteins (1:24 dilution) and incubated for 15 min. Samples were spun down at 15,000 x *g* for 10 min at 18ºC. Two 1 μl aliquots of supernatant were used to determine protein concentration using the Bradford assay. For trypsin digestion, 500 μg total protein was digested with 20 μl Promega sequencing grade modified trypsin (0.625 μg/μl trypsin) and incubated at 37ºC in a warm air incubator overnight (~ 16 h). Samples were acidified and extracted using Waters Oasis 1 CC HLB Solid Phase Extraction cartridge for clean-up, following the manufacturer's instructions. Peptides were eluted with 1.2 mL 80% acetonitrile and vacuum dried to remove acetonitrile. Lysates were stored at -80ºC until phosphopeptide enrichment. Phosphopeptide enrichment was performed with a TiO_2 phosphopeptide enrichment kit (ThermoFisher Scientific). Eluted peptides were dehydrated using a speed-vac and desalted using homemade C18 Stage-tips [132].

Nanoflow LC-MS/MS

Approximately 600 ng of peptide mixture per sample was analyzed in a data dependent acquisition mode by liquid chromatography (LC)-nanoESI mass spectrometry (MS) with a Proxeon Easy nLC 1000 Nano-UPLC system online with an Orbitrap Fusion Tribrid mass spectrometer (Thermo Fisher Scientific,

Rockford, IL, USA). Peptides were separated at a flow rate of 300 nL/min over a 146 min gradient, consisting of 5-22% solvent B over 75 min, 22-35% solvent B over 45 min, 90% solvent B held for 20 min, and 5% solvent B held for 6 min. Solvent A was water with 0.1% formic acid, and solvent B was 80% acetonitrile with 0.1% formic acid. The column was packed using 3 μm C18 beads in a 100 μm x 50 cm PicoTip (r119.aq.0001, ReproSil-Pur 120 C18-AQ 1.9 μm, Dr. Maisch, Ammerbuch-Entringen, Germany). Precursor ions were detected by the orbitrap at a resolution of 120,000 at 200 m/z and a mass range of 380 – 1580 m/z. MS/MS spectra were acquired in the Orbitrap analyzer with an isolation window of 1.6 m/z after fragmentation at 30% higher energy collision dissociation energy at a resolution of 30,000.

Phosphoproteomic database search, phosphoprotein, and phosphopeptide quantification

The raw MS files were processed by Proteome Discoverer v2.4. MS/MS spectra were searched against the UniProtKB *Mus musculus* database (55,474 entries, UniProt UP000000589, downloaded November 2019) with the Sequest HT search engine embedded in Proteome Discoverer v2.4. Parameters were set as follows: MS1 tolerance of 15 ppm, MS/MS mass tolerance of 0.05 Da, trypsin (full) digestion with a maximum of two missed cleavages, minimum peptide length of 6, and maximum of 144

amino acids. Cysteine carbamidomethylation (57.02 Da) was set as a fixed modification, and methionine oxidation (15.99 Da), asparagine and glutamine deamidation (0.98 Da), acetylation of the N-terminus (42.01 Da), and phosphorylation of tyrosine, serine, and threonine (79.97 Da) were set as dynamic modifications. A false discovery rate (FDR) of 1% was set for peptide-to-spectrum matches using the Percolator algorithm (v3.02.1) and protein assignment. Phospho-localization scoring was performed with the IMP-ptmRS v2.0 node, and only phosphopeptides with a localization score > 0.8 were used for quantification. Precursor abundance quantification was based on area and normalized by total peptide amount. All peptides were used for normalization for protein quantification; however, only phosphorylated peptides were used for pairwise ratios and protein roll-up. Unique and razor peptides were used for protein quantification.

Label-free quantification (LFQ) of proteins and peptides was performed with normalized abundances using the Proteome Discoverer LFQ algorithms. The protein ratio was calculated as the geometric median of the peptide ratios, and the peptide ratios were calculated as the geometric median of all combinations of ratios from all the biological replicates in the study. Phosphopeptides and phosphoproteins with a 1% FDR confidence and normalized abundance (intensity) observed in

at least three biological replicates in at least one of the groups were used for further analysis. Phosphoproteins, phosphopeptides, and phosphosites were considered significant and differentially phosphorylated (proteins) or regulated (peptides and sites) if they had a Benjamini – Hochberg adjusted p-value < 0.05 and was defined as downregulated if they had a fold change ratio (Ovx/Sham) ≤ -1.5 or upregulated if they had a fold change ratio ≥ 1.5.

Kyoto Encyclopedia of Genes and Genomes (KEGG), Reactome, and Gene Ontology (GO) enrichment analysis

Significant and differentially regulated phosphopeptides were mapped back to their precursor protein, and the list of phosphoproteins was used for overrepresentation analysis. Using the clusterprofiler and ReactomePA packages in R v4.1.1, KEGG and Reactome pathways and GO annotation terms for molecular functions, cellular components, and biological processes enriched in the dataset were identified [133–135]. For GO molecular process enrichment analysis, hierarchical clustering was applied with average linkage to identify the top 5 clusters. Overrepresented pathways and GO annotation terms were considered significant if they had a Benjamini – Hochberg adjusted p-value < 0.05.

Ingenuity Pathway Analysis (IPA)

IPA (Qiagen, Redwood City CA, USA) was used to perform a core analysis on the phosphopeptides, analyzing associations of observed phosphoproteins with canonical pathways, molecular and cellular functions, physiological system development and functions, and upstream regulators using IPA's functional analysis algorithm and the curated Ingenuity Knowledge Base library. IPA's Downstream Effects analytics and prediction algorithm were used to compute an activation Z-score to predict the activation states of pathways, functions, and upstream regulators. Molecules from the dataset that met the cutoffs of a Benjamini-Hochberg adjusted p-value < 0.05 and 1.5-fold change ratio were considered for analysis.

Statistical analyses

Body and uterine masses were analyzed with Student's two-tailed t-tests (Sham vs. Ovx) using Graphpad Prism 9.1 (San Diego, CA, USA). All data are reported as the mean ± standard deviation (SD). Relative phosphoprotein and phosphopeptide quantification were analyzed in Proteome Discoverer v2.4 (ThermoFisher) using Student's t-tests. Fisher's exact test was used in IPA to calculate p-values for the association or overlap between the identified molecules in the dataset and a given pathway/process/function. Benjamin-Hochberg's posthoc analysis was used to correct for

multiple comparisons. The predicted activation states in IPA's pathways/functions/upstream regulators were measured as Z-scores. The Z-score measures how closely the observed expression pattern of the molecules in the dataset compared to the expected expression pattern based on the literature for a particular annotation. Significantly activated or inhibited state was accepted at a $-2 \geq$ Z-score ≥ 2. Significance was accepted at $\alpha < 0.05$ level.

RESULTS

Comparative skeletal muscle phosphoproteomic analysis

To investigate the impact of estrogen deficiency on the skeletal muscle phosphoproteome in females, we employed an nLC-MS/MS label-free global phosphoproteomics profiling approach for relative quantification of phosphoproteins and phosphopeptides between Ovx and Sham female mice (n = 4/group; Fig. 1A). Successful removal of ovarian tissue was confirmed by examining body mass, uterine mass, and estrous cycling. 16 wk post-surgery, body mass and uterine mass between Sham and Ovx mice were significantly different ($p < 0.001$; Fig. 1 B & C), with mean body masses of 26.2 ± 1.4 and 33.9 ± 1.0 g, respectively, and mean uterine masses of 200.1 ± 26.6 mg and 15.6 ± 6.2 mg, respectively. Vaginal cytology 4 wk post-surgeries further confirmed estrous cycling in Sham mice and

persistent diestrus in Ovx mice.After 16 weeks, tibialis anterior (TA) muscles were dissected, prepared via protein extraction, trypsin digestion, phosphopeptide enrichment, and analyzed by LC-MS/MS. Using label-free quantification as

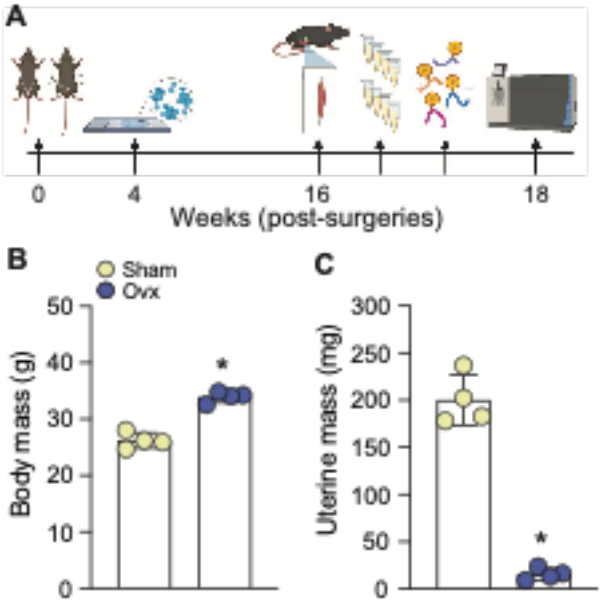

Figure 3.1 Experimental design and mouse characteristics. Female mice were assigned to a surgical group and underwent their respective surgeries, Sham or ovariectomy, with body and uterine mass measured 16 wk later at the time of sacrifice. (A) Schematic of experimental design — created with Biorender.com. Vaginal cytology was performed 4 wk post-surgeries. At 16 wk, tibialis anterior muscles were dissected and digested with trypsin for peptide extraction. The lysate underwent TiO_2 phosphopeptide enrichment for label-free phosphoproteomic analysis, and nLC-MS/MS was performed on the Orbitrap Fusion Tribrid mass spectrometer. (B) Body mass ($p < 0.001$) and (C) uterine mass ($p < 0.001$) of Sham and Ovx mice. Data were analyzed by a Student's t-test (Sham vs. Ovx); n = 4/group. Values represent means ± SD. *significantly different from Sham.

described in the Methods, phosphopeptides were identified and mapped to proteins, and abundance levels were compared between the Sham and Ovx groups. In total, 4,780 phosphopeptides comprising 5,493 phosphorylation sites were

identified, 109 were unique to Ovx, 234 were unique to Sham, and 4437 were detected in both Ovx and Sham (Fig. 2A). Among these 4,780 phosphopeptides, phosphorylation was most prevalent on serine (S) residues, representing 80% of the sites identified, followed by threonine (T, 17%) and tyrosine (Y, 4%), which is consistent with known distributions for S, T and Y phosphorylation (Fig. 2B)[136]. Further analysis identified 647 significant and differentially regulated phosphopeptides, with 444 downregulated and 203 upregulated in Ovx compared to Sham (Fig. 2C). After filtering for robustness (abundance detected in at least three biological replicates in at least one of the Sham or Ovx groups), 189 phosphopeptides were identified that corresponded to 130 proteins (Fig. 2D) of which 22 were differentially phosphorylated: 3 unique to Ovx, two unique to Sham, and 11 downregulated and 6 upregulated in Ovx relative to Sham (Table 1). Four out of the 22 differentially phosphorylated proteins were sarcomeric proteins: tropomyosin alpha 3 (TPM3), obscurin (OBSCN), myosin heavy chain 2 (MYH2), and myozenin-2 (MYOZ2). Interestingly, TPM3 was unique only to Sham and absent in Ovx, and the other three were downregulated in Ovx compared to Sham mice. More, out of the 130 phosphosites identified on the 22 differentially phosphorylated proteins, only 26 phosphosites were identified as differentially

regulated (Table 1). Taken as a whole, these data show that the skeletal muscle phosphoproteome is altered under a resting, non-contracting condition in Ovx female mice.

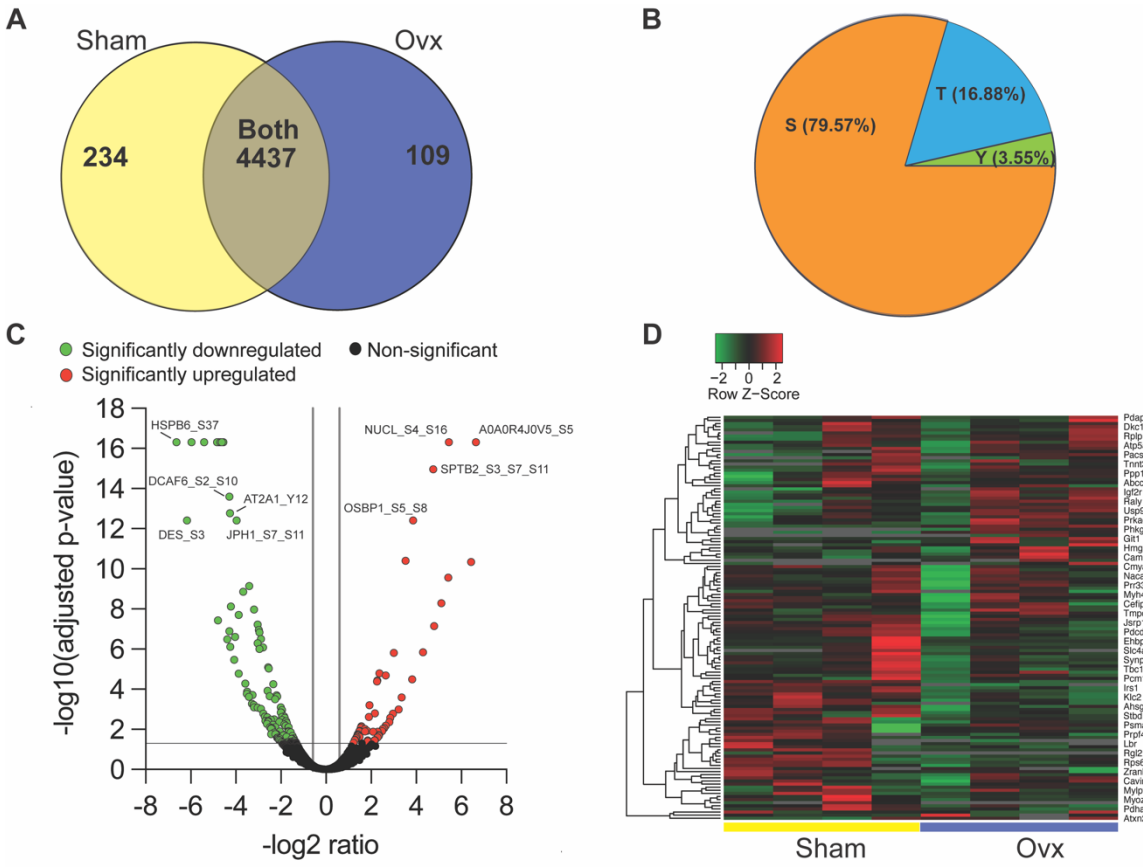

Figure 3.2 Characteristics of the phosphoproteome. Proteome Discoverer (v2.4) was used for database search and identification of phosphopeptides and phosphoprotein analysis. (A) Venn diagram of all identified phosphopeptides identified in muscle from Sham and Ovx mice. (B) Pie chart of modification sites there were phosphorylated on residues serine (S), threonine (T), and tyrosine (Y) in the dataset. (C) Volcano plot of differentially regulated phosphopeptides. Green and red dots represent downregulated and upregulated significantly regulated phosphopeptides (Benjamini – Hochberg adjusted p-value < 0.05 and 1.5-fold change ratio), respectively, whereas black dots represent non-significant phosphopeptide. (D) Significantly regulated phosphopeptides were mapped back to their precursor proteins. The list of phosphoproteins was submitted to Heatmapper. Heatmap of 130 phosphoproteins clustered according to average linkage using Pearson Correlation. Color scheme represents $\log_2$ ratio of each phosphoprotein for each biological sample. Gray = missing data.

Table 3.1 Significantly differentially phosphorylated proteins and phosphosites in Ovx relative to Sham mice.

Uniprot AcessionID	Gene Symbol	Description	Phosphosite (Score)	Log2 ratio	Differential regulation
Q99LI7	*Cstf3*	Cleavage stimulation factor subunit 3	S691(100)	6.64	Only Ovx
D3Z472	*Phkg1*	Phosphorylase b kinase gamma catalytic chain	S61(98.8)	6.64	Only Ovx
O54818	*Tpd52l1*	Tumor protein D53	S149(99.2)	6.64	Only Ovx
Q9WU42	*Ncor2*	Nuclear receptor corepressor 2	S149(100); S152(100)	4.79	Upregulated
A0A0R4J0Z3	*Aqp4*	Aquaporin 4, isoform CRA_a	S276(95.1); S285(99.9)	2.19	Upregulated
B1ARU1	*Macf1*	Microtubule-actin cross-linking factor 1	S1517(100); S1520(100)	2.17	Upregulated
G3X9Q6	*Larp4*	La-related protein 4	S642(97.7)	1.39	Upregulated
Q8BJS4	*Sun2*	SUN domain-containing protein 2	S12(100); S120(99.9); S122(97.8); S135(99.6); S281(100)	0.75	Upregulated
Q4FE56	*Usp9x*	Probable ubiquitin carboxyl-terminal hydrolase FAF-X	S1600(100); S2443(100)	0.59	Upregulated
A0A0R4J1P2	*Tpm3*	Tropomyosin alpha-3 chain OS=Mus musculus	Y60(100); T108(100); Y162(100); S206(100); Y221(100); T237(100); S245(100); T282(98.6)	-6.64	Only Sham
Q61193	*Rgl2*	Ral guanine nucleotide dissociation stimulator-like 2	S619(98.8)	-6.64	Only Sham
Q8C142	*Ldlrap1*	Low-density lipoprotein receptor adapter protein 1	S198(99)	-3.03	Downregulated
Q8BHL3	*Tbc1d10b*	TBC1 domain family member 10B	T138(99.1)	-2.21	Downregulated
A7E1Z5	*Slc4a4*	Anion exchange protein	S68(98.6)	-2.14	Downregulated

Q3U9G9	*Lbr*	Delta (14)-sterol reductase LBR	S101(100)	-2.07	Downregulated
Q8CAP3	*Rad23a*	Rad23a protein	S123(97.9); S216(95)	-1.93	Downregulated
P62754	*Rps6*	40S ribosomal protein S6	S235(100); S236(98.7); S240(100); S244(100)	-1.90	Downregulated
Q78JW9	*Ubfd1*	Ubiquitin domain-containing protein UBFD1	S131(99.9)	-1.50	Downregulated
Q9JJW5	*Myoz2*	Myozenin-2	T107(98.5); T111(100); S116(100); S158(100)	-1.35	Downregulated
G3UW82	*Myh2*	Myosin, heavy polypeptide 2, isoform CRA_d	T202(100); T218(100); T257(100); T381(100); Y413(100); T444(100); S650(100); T667(100); S745(100); T761(100); T918(100); T944(100); S955(100); T967(100); T986(100); T1000(100); T1026(100); S1044(100); S1095(100); S1135(100); S1147(100); S1165(99.2); T1195(100); S1206(100); S1240(100); S1246(100); S1268(100); T1289(100); S1306(100); S1309(100); T1316(100); S1360(100); S1373(100); Y1382(100); T1424(100); Y1467(98.8); S1483(100); Y1495(99.1);	-1.06	Downregulated

			T1504(100); S1517(100); T1520(100); S1577(100); S1603(100); S1614(100); Y1650(100); S1717(100); T1728(100); S1729(97.4); T1733(100); T1739(100); S1742(100); T1767(100); T1782(99.4); S1835(100); T1861(100); S1901(100); S1922(100)		
E9QQ96	*Obscn*	Obscurin	S135(100); S236(100); S3254(100); S4708(100); S4893(100); T5568(100); S5632(100); T5636(100); S5639(100); S5665(97.8); T5670(99); S5683(97); S5686(100); S5687(100); S5711(100); S5916(98); T6134(100); S6236(100); S6445(100); T6451(100); S6455(100); S6551(100); T6680(100); S6837(100); S7083(100); S7134(100); S7147(100); S7149(100); S7167(98.6); S7223(100)	-1.03	Downregulated
Q920Q6	*Msi2*	RNA-binding protein Musashi homolog 2	S6(100); S12(97.7)	-1.00	Downregulated

Note. The red font denotes significantly differentially regulated phosphosites.

KEGG, Reactome, and GO overrepresentation analysis

To gain more insight into the differential impact of estrogen deficiency in the skeletal muscle phosphoproteome, differentially regulated phosphopeptides were mapped back to their precursor protein. The list of phosphoproteins was used in R for pathway and GO term overrepresentation analysis. The top 15 most overrepresented KEGG and Reactome pathways were related to calcium signaling, hypoxia-inducible factor (HIF) 1-alpha signaling, insulin signaling, muscle contraction, ion homeostasis, and mTOR signaling (Fig. 3A and B). GO molecular function (MF) was enriched for actin and actinin binding, mRNA binding, translation initiation factor binding, phosphatidylinositol phosphate binding, and structural constituent of muscle and post-synapse. These, in turn, resulted in strong enrichment in GO cellular components (CC) associated with the contractile apparatus and components of the muscle fiber, including the Z-disc, I-band, sarcoplasmic reticulum, T-tubules, sarcolemma, as well, as the cytoskeleton (Fig. 3C and D). The five main clusters from the GO biological process analysis emulated previous pathways and GO term enrichments. Clusters relating to calcium signaling and ion activities were highlighted in both KEGG (calcium signaling) and Reactome (muscle contraction) and are

associated with calcineurin-NFAT signaling, which has been shown to be involved in gene regulation pertaining to skeletal muscle differentiation, fiber-type switching, and muscle hypertrophy. The metabolic signaling and activities cluster is associated with glucagon/insulin signaling in KEGG and pyruvate metabolism and TCA cycle in Reactome. The striated cell assembly development cluster is associated with GO MF and CC enrichment pertaining to maintenance of and structural components of the muscle cell, such as cytoskeleton – actin binding, sarcomere, structural constituent of muscle and post-synapse, and translation regulation – mRNA binding and translation initiation factor binding (Fig. 3E). Overall, all pathway and GO enrichment analyses show overrepresented proteins associated with calcium and metabolic signaling pathways and functions related to muscle cell maintenance and structural integrity.

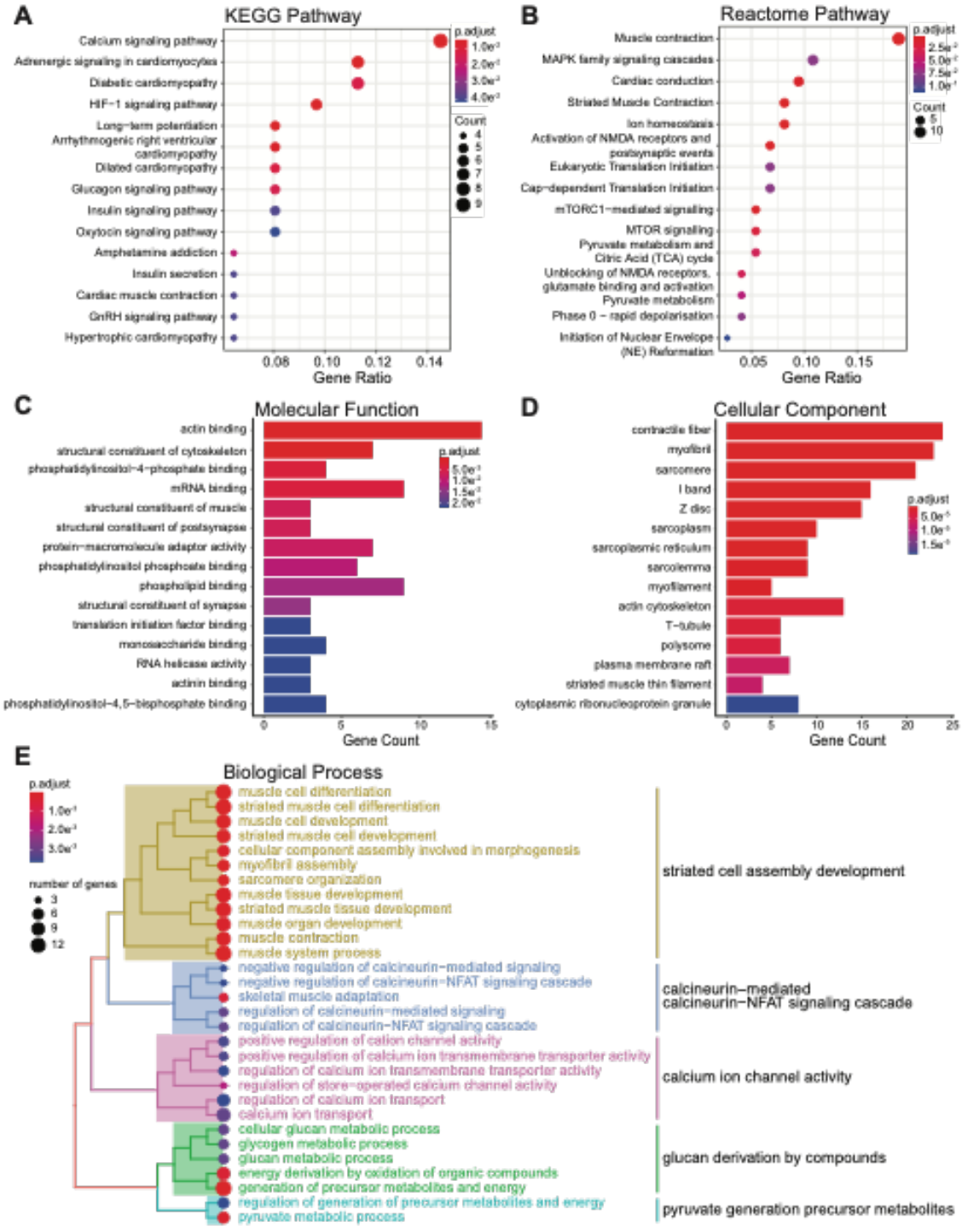

Figure 3.3 KEGG, Reactome, and GO term enrichment analyses. Differentially regulated phosphopeptides that were quantified in at least three biological replicates or absent in all biological replicates (unique phosphopeptides) in at least one group were mapped back to their precursor protein, and the list of

phosphoproteins was submitted for enrichment analysis using the R package clusterprofiler. The top 15 pathways overrepresented in the dataset are shown in (A) KEGG and (B) Reactome pathways. (C-D) Overrepresented GO terms in molecular function and cellular component in the dataset and (E) overrepresented GO terms in biological process with hierarchical clustering according to average linkage to identify the top 5 clusters are presented.

Differentially overrepresented IPA canonical pathways

Next, to evaluate potential differential downstream effects from the changes in the phosphoproteome in Ovx mice, all 4,780 phosphopeptides were uploaded to IPA, 377 of which mapped to molecules characterized in the IPA database. The top 10 canonical pathways enriched in the dataset are shown in Fig. 4A. Consistent with the KEGG, Reactome, and GO analyses, the calcium signaling pathway was the most significantly enriched IPA annotated canonical pathway ($p < 0.05$, 12% overlapping molecules) with 50 observed molecules mapping to the pathway, 31 molecules downregulated, and 19 molecules upregulated in Ovx relative to Sham muscles out of IPA's 226 total annotated pathway molecules (Supplementary Fig.1). IPA's activation Z-score algorithm was unable to predict the activation state of calcium signaling (i.e., pathway directionality – activation or inhibition). However, visualizing the mapping of observed phosphoproteins to the IPA "resting muscle cell" model indicated that phosphorylation of the SERCA, calsequestrin and ryanodine receptor proteins were altered in Ovx compared to Sham muscles

(log_2FC = -0.32, -0.27, 0.04 and BH p-values = 0.889, 0.948, 0.808, respectively) (Fig. 4B). Two metabolic pathways had significant predicted inhibition with IPA Z-scores of -2.12: glycolysis I ($p < 0.05$, 32% overlap, nine molecules downregulated and two molecules upregulated out of 25 annotated pathway molecules) and gluconeogenesis I ($p < 0.05$, 32% overlap, nine molecules downregulated and three molecules upregulated out of 25 annotated pathway molecules). These observations all indicate that essential metabolic and calcium signaling functions in skeletal muscle are affected in estrogen-deficient mice, which could, in turn, contribute to changes in muscle function overall.

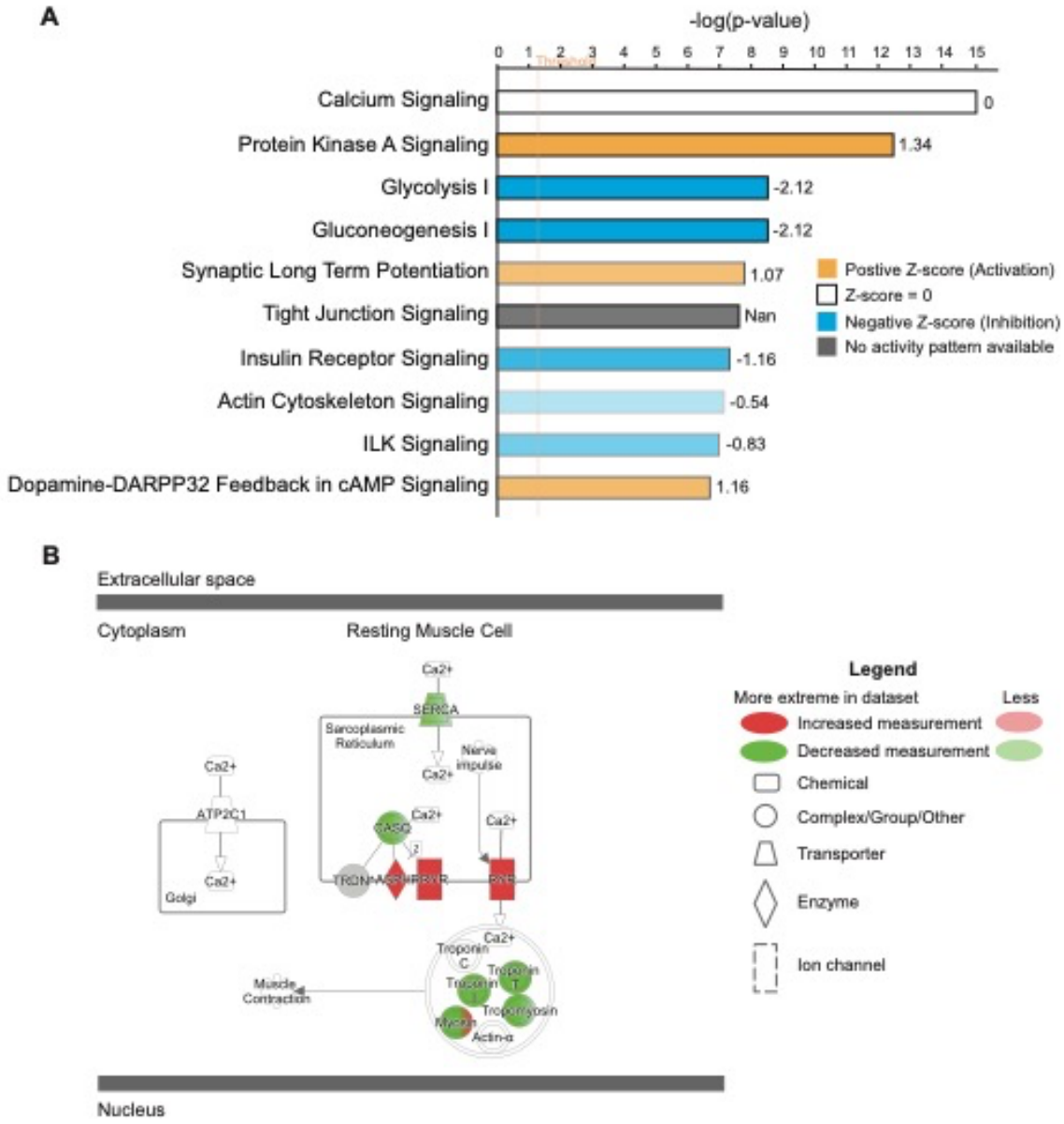

Figure 3.4 Changes in canonical metabolic pathways and calcium signaling pathways induced by ovariectomy. Phosphopeptides identified in the dataset were submitted to IPA's Downstream Effects analytics and prediction algorithm to analyze molecules associated with IPA's annotated canonical pathways. (A) The top 10 significantly associated canonical pathways from the dataset and predicted inhibition or activation state, with a $-2.0 \geq$ Z-score ≥ 2.0, respectively. (B) Calcium signaling pathway in a resting, i.e., non-contracting muscle cell and the phosphorylation state of proteins from the dataset is illustrated. Decreases or increases in protein phosphorylation measurements from Ovx muscle relative to Sham muscles are shown in green and red, respectively.

IPA's functional analysis

To further explore the biological significance of the molecular alterations induced by estrogen deficiency within the skeletal muscle phosphoproteome, we employed IPA functional analysis to predict the impact of phosphoproteome alterations on molecular and cellular functions and physiological system development and functions. The top 10 functional parent groups that mapped to molecules observed in the Ovx/Sham dataset are shown in Fig. 5A, with IPA's skeletal and muscular system development and function (SMSDF) group exhibiting the strongest association ($p < 0.05$) with 113 observed molecules mapping to this function. Deeper analysis into the physiological subfunctions assigned by IPA to the SMSDF group predicted a significant inhibition of contractility of muscle in estrogen-deficient mice (Fig. 5B). Two other functional parent groups, cellular assembly and organization with 165 observed molecules mapping to this function ($p < 0.05$) and cellular function and maintenance with 179 observed molecules mapping to this function ($p < 0.05$), had three overlapping subfunctions with significant activation Z-scores. There was significant predicted inhibition in the formation of phagosomes (Fig. 5C) and vesicles (Fig. 5D) and significant predicted activation in disruption of cytoskeleton (Fig. 5E). In summary, estrogen

deficiency perturbs skeletal muscle and cellular functions that may lead to impaired contractile function and compromised cellular and cytoskeleton integrity.

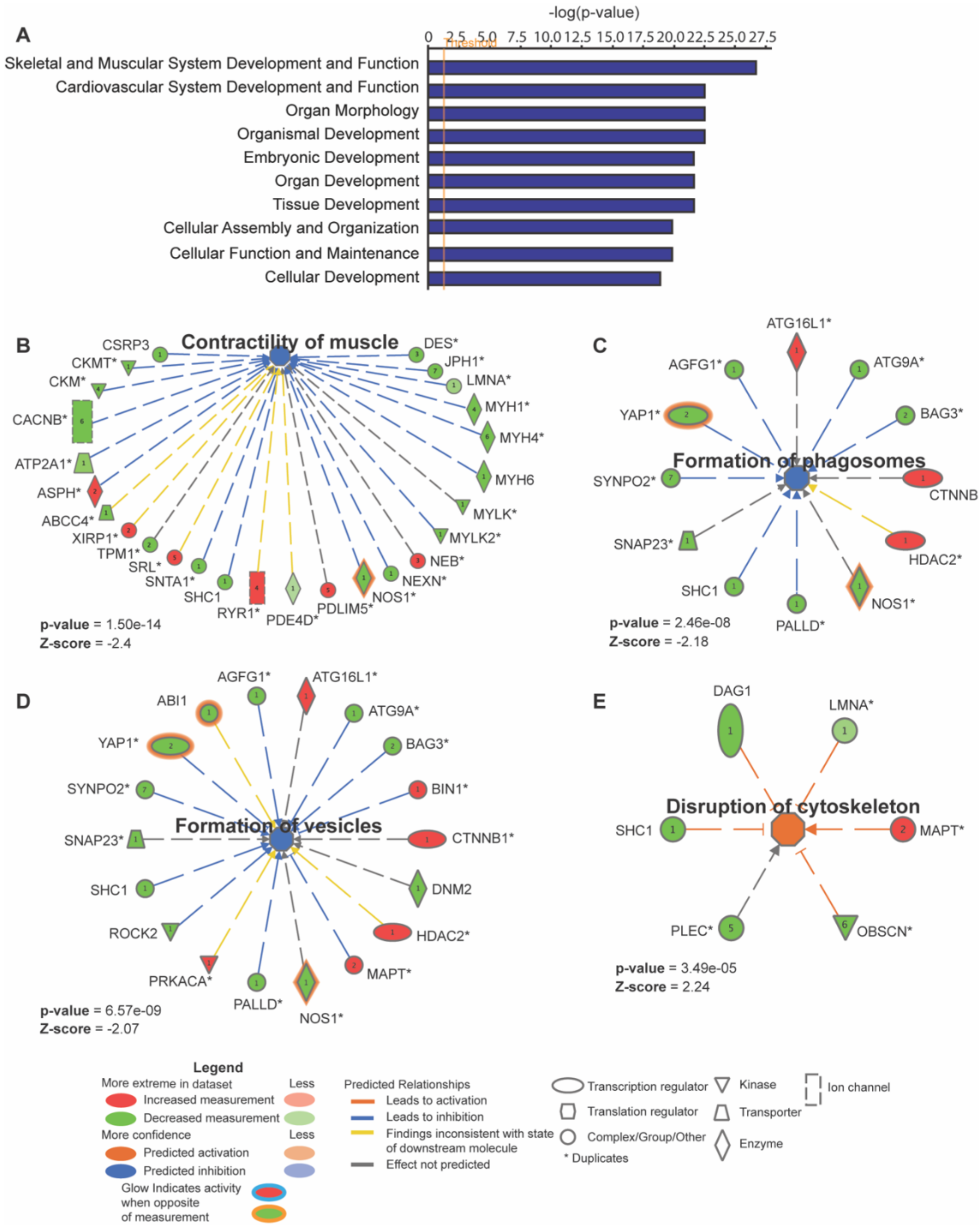

Figure 3.5 Changes in molecular, cellular, and physiological system development functional analyses in estrogen-deficient mice. Phosphopeptides identified in the dataset were submitted to IPA's Downstream Effects analytics and activation Z-score prediction algorithm to analyze and predict molecular and cellular functions and physiological system development and

functions. (A) The top 10 significantly enriched IPA functional parent groups from the dataset are summarized. Significant inhibition (-2.0 ≥ Z-score) or significant activation (Z-score ≥ 2.0) of subfunctions predicted from the dataset are shown in B) contractility of muscle, C) formation of phagosomes, D) formation of vesicles, and E) disruption in cytoskeleton. The number in the upper right box next to the molecule denotes the number of phosphopeptides observed in the dataset for the molecule. Green and red color of the molecule represents decreased or increased phosphorylation measurement of the protein in Ovx relative to Sham mice, and the glow around the molecules indicates their activity status when opposite to the phosphoprotein measurement. The blue and orange color of a subfunction or molecule represents the activation status — inhibition or activation, respectively. The color, orange, blue, yellow, or gray, of the edge (line) predicts the relationship between the two nodes (molecules), indicating activation, inhibition, inconsistent, or no prediction, respectively. The arrowhead or inhibition line at the end of the edge reflects the relationship proportionality (i.e., the inhibition line reflects the inverse proportionality, and the arrowhead reflects direct proportionality between two nodes).

Upstream regulator analysis and mechanistic network of E2

Using IPA's activation Z-score prediction algorithm and Ingenuity Knowledge Base library, we examined kinase activity inferred by the changes in the phosphoproteome dataset; we identified the top four potentially inhibited or activated kinases, revealing potential inhibition of CDK6 (Table 2). We next sought to determine whether previously known E2-related alterations in protein phosphorylation could be observed through phosphoproteins directly detected in our dataset (Supplementary Fig.2A). Overall, we identified nine proteins linked to E2 in IPA that were observed in our data—with increased phosphorylation on beta-catenin (CTNNB1), eukaryotic translation initiation factor 4E-binding protein 1 (EIF4EBP1), histone deacetylase 2 (HDAC2), and microtubule-

associated protein tau (MAPT), and decreased phosphorylation on insulin receptor substrate 1 (IRS1), nitric oxide synthase 1 (NOS1), 40S ribosomal protein S6 (RPS6), SHC-transforming protein 1 (SHC1), and stromal interaction molecule 1 (STIM1). In addition, other functional effects of estrogen loss were represented indirectly in our phosphoprotein observations, including changes annotated in IPA as being directly (AMPK, IGF1, RPS6KB1, and D-glucose) or indirectly (TP53, PPARGC1a, and NR0B2) affected by estrogen deficiency (Supplementary Fig. 2B).

Table 3.2 Upstream kinases affecting the phosphoproteome in Ovx mice.

Kinase	Predicted Activation State	Activation Z-score	Target Molecules in Dataset
CDK6	Inhibited	-2.0	ABI1, LPIN1, SRSF1, SYNPO2
PRKCE		-1.96	IRS1, RPS6, SHC1, VDAC1
PRKAA1		-1.347	EIF4EBP1, IRS1, PDHA1, RPS6, STIM1, YAP1
ROCK1		-1.091	INSR, IRS1, MYL2, MYLPF, RPS6
CAMK2A		1	ABI1, CAMK2A, CTNNB1, MAPT
ROCK2		1.029	MYL2, MYLPF, PPP1R12A, ROCK2
MAPK1		1.097	EIF4EBP1, IRS1, MAPKAPK2, MAPT, NCOR2, NEFH, NEFM, PKM, PLCG1, POLR2A, PXN, RPS6KA3, SEC16A, SHC1, YBX3
PTK2		1.262	ARHGEF11, GIT1, IRS1, MYL2, PLCG1, PXN, SHC1

Note. Decreased or increased phosphorylation measurements of the target molecule are represented by the green and red font color, respectively.

To illustrate how the observations of differential

phosphoproteins in TA muscle from Ovx/Sham muscle may connect to canonical effects of estrogen on cell signaling, we used IPA to build a mechanistic network (Fig. 6). This shows the direct relationships between E2 and the nine phosphoproteins observed, as well as two kinases, predicted to be altered by estrogen deficiency (AMPK and RPS6KB1) but not directly observed in the dataset. Inhibition of E2 is associated with a predicted inhibition of AMPK that results in a predicted activation of Yes-associated protein1 (YAP1) and predicted inhibition of autophagy-related 9A (ATG9A). Both YAP1 and ATG9A had decreased phosphorylation observed in our dataset and were associated with maintaining muscle homeostasis. In addition, inhibition of E2 is directly related to the increase in phosphorylation that we observed of CTNNB1, EIF4EBP1, and HDAC2, which are all involved in transcription regulation. This upstream prediction analysis reveals how estrogen deficiency may modulate other regulators and co-activators of transcription factors important for maintaining muscle fiber integrity and function.

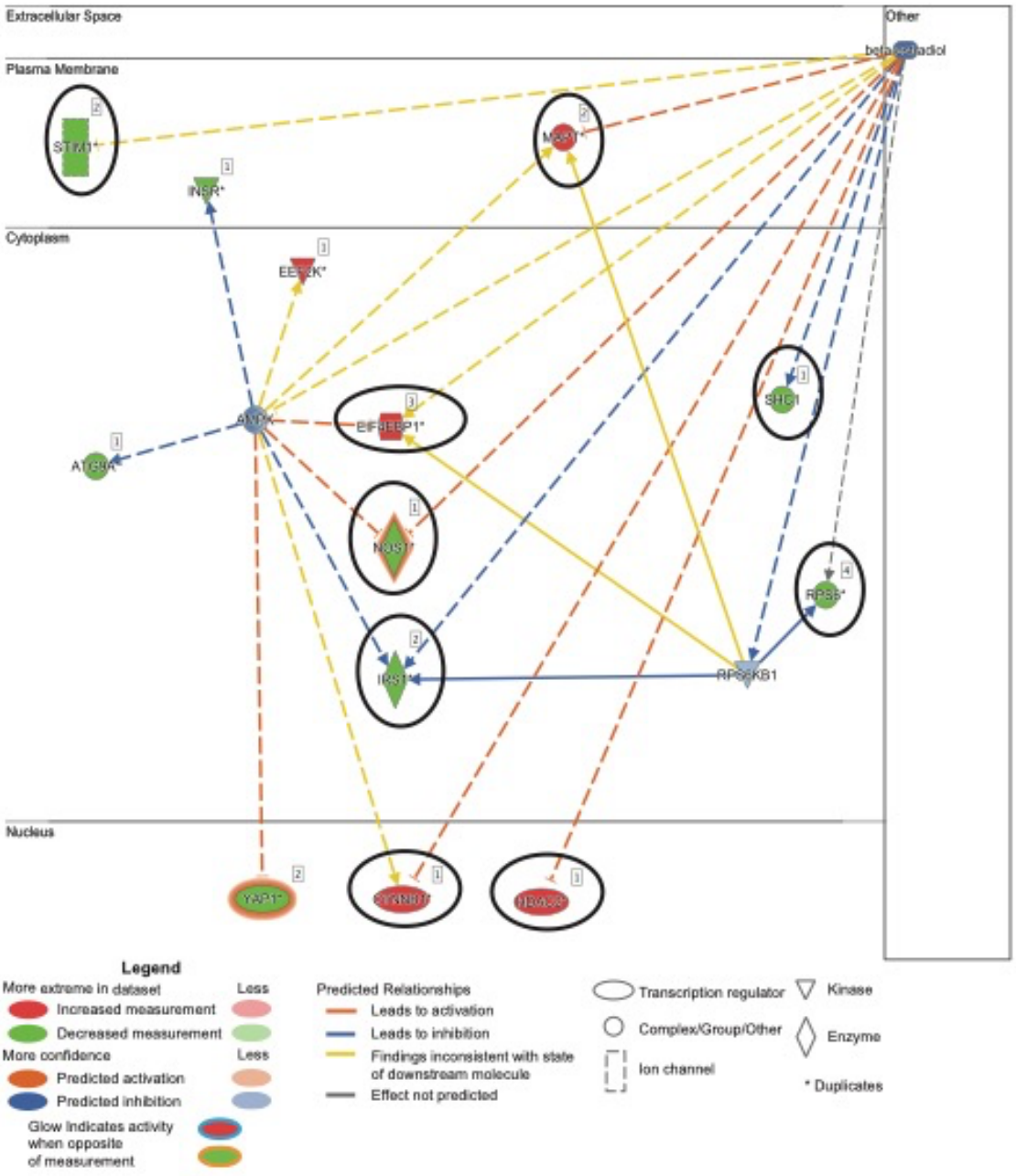

Figure 3.6 Beta-estradiol (E2) mechanistic network. Phosphopeptides identified in the dataset were submitted to IPA's activation Z-score prediction algorithm to predict kinase activity inferred from the Ovx/Sham dataset. A mechanistic network of E2 and its relationship to other regulators and the dataset was created. The number in the upper right box next to the molecule denotes the number of phosphopeptides observed in the dataset for the molecule. E2 inhibition was predicted from the expression profile of nine molecules observed in our

phosphoproteomics dataset (circled in black). See Figure 5 for explanation of color scheme, edges, and nodes.

DISCUSSION

Recent phosphoproteomic analyses of skeletal muscle have provided a greater understanding of the complex pathophysiology associated with skeletal muscle aging and strength loss. The majority of previous phosphoproteomic studies were conducted on muscle from males, and in this analysis of female skeletal muscle, we identified a number of proteins in agreement with those studies, showing that the majority of the phosphopeptides were from sarcomeric proteins and they were overrepresented amongst the peptides observed [108,137,138]. For example, clinical phosphoproteomic analysis of the vastus lateralis muscle in a resting condition from three healthy males identified phosphoproteins related to the Z-disc, contractile apparatus, and calcium signaling proteins, among others—which is consistent with our results [108]. The present study identified phosphorylation alterations of sarcomeric proteins and perturbed calcium handling and skeletal muscle function in estrogen deficient muscle.

We identified four sarcomeric proteins in our dataset, TPM3 Thr-282, OBSCN Ser-7167, MYH2 Ser-1835, and MYOZ2 Thr-107 and Thr111 (Table 1), revealing decreased phosphorylation

at the identified phosphosites and overall decreased phosphorylation at the protein level in muscle from Ovx compared to Sham mice. In contrast, a sarcopenic male rat model showed increased phosphorylation of the sarcomeric proteins (no specific phosphosite listed): myosin light chain 2 (MYL2), desmin (DES), and tropomyosin alpha in male muscles [107]. The effect of phosphorylation on the four altered sarcomeric proteins identified in our dataset is poorly understood in skeletal muscle. However, studies examining the phosphorylation of TPM3 indicate that hyperphosphorylation contributes to the pathophysiology of myopathies and cardiomyopathies [139,140]. Conversely, decreased phosphorylation of these proteins may suggest loss of function leading to less active proteins and muscle dysfunction.

Relating observed phosphoproteomic alterations to functional outcomes is challenging, particularly given the known complexity of muscle structure, Z-disc, and contractile proteins. However, using enrichment analysis in conjunction with IPA's predictive modeling, we identified overrepresentation in calcium and metabolic signaling consistent with IPA's enriched canonical pathways (Fig. 3 & 4). As cardiomyocytes and skeletal muscle fibers are both striated and their cellular structural components and contractile function are similar, it is not surprising to see

many pathways relating to cardiomyocytes/cardiomyopathy. Thus, it is reasonable that our data, would be enriched in parallel pathways and functions related to cardiac muscles, and our perturbation of estrogen-mediated phosphorylation would suggest a compromise in muscle function as shown with the enrichment of cardiomyopathy pathways. Our study affirms that the phosphorylation alterations detected in Ovx mice may be relevant to decrements in muscle function due to estrogen loss. Not surprisingly, as calcium is critical for skeletal muscle function, our dataset showed significant enrichment in calcium signaling and calcium ion channel activity-related functions and pathways. Altered calcium handling has been shown in aging and diseased striated muscles [141–146]. More, in Ovx mouse hearts, estrogen deficiency has been shown to perturb intracellular Ca^{2+} homeostasis by increasing spontaneous Ca^{2+} release from the sarcoplasmic reticulum and reducing myofilament Ca^{2+} sensitivity [147]. Therefore, it is likely that estrogen deficiency may alter calcium handling in skeletal as well as cardiac muscle, in line with our enrichment analyses. Altered calcium handling could be attributed to increased RYR protein phosphorylation found in Ovx compared to Sham rats [148]. We detected increased RYR phosphorylation and decreased phosphorylation of SERCA and CASQ in Ovx relative to Sham muscles, but differences were

not statistically significant. Overrepresentation results associated with metabolic functions and predicted inhibition of IPA-derived canonical metabolic pathways are also not surprising, as it is well established that estrogen deficiency perturbs skeletal muscle metabolism including reports that Ovx mice have increased fat mass, impaired mitochondrial function, and inhibited MTOR complex 1 signaling [149]. In addition, metabolic changes associated with Ovx have been attributed at least in part to altered skeletal muscle metabolism, the regulation of glycogen synthase and citrate synthase [150], as well as reduced mitochondrial biogenesis and increased oxidative stress [151–154].

IPA's functional analysis revealed inhibition of skeletal muscle function and cellular and maintenance functions with estrogen deficiency (Fig. 5B). These predicted dysregulated functions suggest a potential impairment in contractile activity and mechanisms involved in skeletal muscle maintenance and repair. Muscle undergoes constant plasticity requiring gene regulation and cellular adaptations to stimuli, including contractile activity (e.g., in response to endurance exercise), loading and unloading conditions (e.g., resistance training and atrophy from disuse, respectively), changes in environmental factors such as nutrition or hypoxia, and injuries (e.g., exercise-induced or

traumatic injuries). The predicted disruption in cellular maintenance and function were further related to vesicle and phagosome formation and cytoskeleton disruption, which may be attributed in part to our observation of decreased ATG9A phosphorylation, as ATG9A is critical for autophagosome formation and maintaining muscle homeostasis through autophagy-mediated proteolysis [155]. The autophagy-mediated proteolysis in skeletal muscle is critical for maintaining muscle homeostasis under basal, non-contracting conditions as well as during physical activity. Appropriate autophagic flux is required to remove and degrade damaged proteins and cell organelles in muscle, and inhibition of autophagy induces atrophy and myopathies [156,157]. Estrogen deficiency, via ovariectomy, aging, or in a diseased state, decreases the ability of skeletal muscle to generate force and reduces recovery of muscle strength from injury [18,19,158–162]. Accordingly, the IPA predicted inhibition in contractility of muscle in estrogen-deficient mice supports what we and others have observed *in vitro* and *in vivo* in skeletal muscle and sheds light on underlying molecular mechanisms.

Furthermore, AMPK was identified as an upstream regulator sensitive to estrogen deficiency and was predicted to be inhibited (Fig.6), which is consistent with literature reporting that Ovx mice had significantly reduced levels of

AMPK phosphorylation in skeletal muscle at rest [163]. Inhibition of AMPK was associated with a predicted activation in YAP1 activity, which is consistent with the observed decreased in YAP1 phosphorylation. Increase in YAP1 activity is intriguing, as there are conflicting reports on its role in skeletal muscle. Overexpression of a constitutively active YAP1 S127A in skeletal muscle *in vivo* for 5 – 7 wks has been shown to induce muscle atrophy and myopathy [164]. In contrast, YAP2 overexpression for a shorter duration resulted in skeletal muscle hypertrophy [165,166]. However, further studies determined YAP2 overexpression at supraphysiological levels did indeed induce muscle hypertrophy, but it also induced a muscle fiber degeneration phenotype [165]. Our ovariectomy model displayed a chronic loss of estrogen, which could potentially suggest a high level of YAP1 activity in resting, non-contracting muscles, as we observed decreased YAP1 phosphorylation in Ovx compared to Sham mice. Thus, downregulation in YAP1 phosphorylation may contribute to skeletal muscle dysfunction in Ovx mice. Furthermore, YAP has emerged as a key player in mechanotransduction [167,168], also suggesting that altered YAP-mediated signaling may contribute to skeletal muscle dysfunction in Ovx female mice.

The present study used an ovariectomy model to investigate how the loss of estrogen affects the skeletal

muscle phosphoproteome. Our work along with others have shown that estradiol is the main contributing hormone associated with skeletal muscle strength loss in female rodents (preclinical studies) and postmenopausal women (clinical studies). Nonetheless, it is important to note that hormones in addition to estrogen are impacted in this surgical model including progesterone, testosterone, follicle stimulating hormone, and luteinizing hormone [169–174], and may potentially contribute to skeletal muscle dysfunction in females as well. Further studies on how the overall perturbation of the hypothalamic-pituitary-gonadal axis in females impact skeletal muscle will be needed.

CONCLUSION

Our study is the first global phosphoproteomic profiling of the skeletal muscle phosphoproteome in female mice under two estrogenic conditions. The dataset combined with bioinformatic tools and computational predictive modeling demonstrates that estrogen deficiency is associated with distinct changes in the skeletal muscle phosphoproteome that may significantly affect muscle function and strength. Results support the concept that phosphorylation of sarcomeric proteins is responsive to estrogen levels. In particular, phosphorylation alterations relating to calcium

sensitive proteins suggests disruption in calcium handling may be involved in the pathogenesis of skeletal muscle strength loss in aging females. Additionally, identification of AMPK as an upstream regulator sensitive to estrogen levels may be a potential driver of the phosphorylation alterations observed in this study. Importantly, the results provide testable hypotheses for future studies to elucidate the molecular mechanisms underlying how estrogen deficiency affects skeletal muscle contractile function.

In summary, this study established remodeling of the skeletal muscle phosphoproteome in resting, non-contracting muscles of Ovx female mice compared to Sham mice. The main findings from this study identified novel phosphosites related to sarcomeric proteins (TPM3 Thr-282, OBSCN Ser-7167, MYH2 Ser-1835, and MYOZ2 Thr-107 and Thr111) that had significantly decreased phosphorylation, and pathways that are sensitive to estrogen deficiency, such as the calcium signaling pathway and metabolic pathways. We also identified two upstream regulators, CDK6 and PRKCE, predicted to be significantly inhibited due to estrogen deficiency. In addition, we propose that the observed downregulation of YAP1 phosphorylation by its predicted upstream regulator, AMPK, as possibly contributing to skeletal muscle dysfunction in estrogen deficient female mice. The results from this project

led us to question whether estrogen deficiency altered protein phosphorylation during force generation (i.e., during muscle contraction) in skeletal muscle, which could possibly underlie the muscle strength loss observed in Ovx and aging female mice. This led to my next major project presented in Chapter 4 of this dissertation.

Chapter 4

Natural aging and ovariectomy induces parallel phosphoproteomic alterations in skeletal muscle of female mice

Natural aging and ovariectomy induces parallel phosphoproteomic alterations in skeletal muscle of female mice

Mina P. Peyton[1,2], Tzu-Yi Yang[3], LeeAnn Higgins[3], Todd W. Markowski[3], Laurie L. Parker[2,3], and *Dawn A. Lowe[1, 4]

[1]Department of Rehabilitation Medicine, Division of Rehabilitation Science, University of Minnesota – Twin Cities, Minneapolis, Minnesota 55455, United States

[2]Department of Computer Science, Bioinformatics and Computational Biology Program, University of Minnesota, Minneapolis, Minnesota 55455, United States

[3]Department of Biochemistry, Molecular Biology, and Biophysics, University of Minnesota – Twin Cities, Minneapolis, Minnesota 55455, United States

[4]Department of Rehabilitation Medicine, Division of Physical Therapy, University of Minnesota – Twin Cities, Minneapolis, Minnesota 55455, United States

***Corresponding author**

*Email: lowex017@umn.edu

Orcid: 0000-0002-5784-9289

The contents of this chapter are under final preparation to be submitted to *Innovation in Aging*.

OVERVIEW

Background and Objectives: Skeletal muscle strength loss mid-life in females is associated with the decline of estrogen. With the average life expectancy of women being 81.1—84.3 years and menopause occurring between the ages of 40—50 years in the United States, more than one-third of a woman's life is now spent in the postmenopausal phase, i.e., in an estrogen-deficient state. Preclinical and clinical studies show that reduction in estrogen decreases muscle force and blunts recovery of strength after injury. More, in ovariectomized (Ovx) mice and aged women, decreased force was associated with reduced myosin regulatory light chain phosphorylation compared to ovary-intact and young women. Therefore, we questioned how estrogen deficiency impacts the overall skeletal muscle phosphoproteome after contraction and force generation.

Research Design and Methods: We performed label-free phosphoproteomic analyses of the tibialis anterior muscle after contraction in two mouse models of estrogen deficiency, ovariectomy (Ovx vs. Sham) and age-induced ovarian senescence (Old vs. Young).

Results: We examined fold-changes between Ovx or Old contracted muscles compared to their control Sham or Young contracted muscles and identified a total of 2,593 and 3,507

phosphopeptides in the Ovx/Sham and Old/Young datasets, respectively. Comparative analysis of both datasets using Ingenuity Pathway Analysis's (IPA) activation Z-score found parallel patterns of inhibition and activation across IPA-defined canonical signaling pathways, such as AMPK signaling, 14-3-3-mediated signaling, and calcium signaling. Likewise, similar activation patterns for IPA's functional analysis were related to muscle contractile function, muscle integrity, and RNA expression and translation. IPA's upstream regulator analysis identified MAPK1 and PRKACA as candidate kinases sensitive to estrogen levels.

Discussion and Implications: Our findings highlight key molecular signatures and pathways suggesting that the similarities identified across both datasets could elucidate molecular mechanism(s) that may contribute to skeletal muscle strength loss due to estrogen deficiency.

Translational Significance

This study examines the complex changes in regulation of protein phosphorylation in skeletal muscle of two estrogen-deficient mouse models using high-throughput mass spectrometry based phosphoproteomic analysis. We identified upregulation in phosphorylation of calpastatin at Ser-82 as a unique phosphosite and potential upstream regulators that may be involved in the dysregulation of skeletal muscle

function. Identification of altered protein phosphorylation substrates, phosphosites, and upstream regulators will advance our understanding of how estrogen deficiency impacts the force-generating capacity of skeletal muscle and may aid in identifying novel targets to mitigate strength loss in aging females.

Keywords: estrogen deficiency, ovarian senescence, calpastatin, MAPK, PKA, and calcineurin

BACKGROUND AND OBJECTIVES

Skeletal muscle is the most abundant tissue in the human body, making up approximately 40% of total body mass in a healthy adult. Muscle is crucial in controlling our movements and posture, protecting internal organs and tissues, storing energy, and regulating body temperature and metabolism. As muscle contracts, the sarcomere, the basic contractile unit in skeletal muscle, shortens and generates molecular force (i.e., muscle strength). The loss of muscle strength significantly impacts the activities and quality of life of the aging population. Age-related muscle strength loss occurs earlier in females than males [94,175]. Compared to male counterparts, postmenopausal women experience decreased functional capacity, greater strength declines, impairments in muscle repair, and increased sarcopenia and osteoporosis rates with age [58,89]. Poor muscle strength in postmenopausal women is identified as a strong risk factor for total mortality [176].

Decline in muscle strength mid-life in females associates with the reduction of estrogen, specifically estradiol (E2), the primary circulating estrogen. Reduction in ovarian hormones (E2 and progesterone) is a natural biological process that concludes with menopause, which occurs between the ages of 40 – 50 in the United States [177].

With the average life expectancy of women being 81.1 – 84.3 years (non-Hispanic white females and Hispanic females, respectively) in the United States, more than one-third of a woman's life is now spent in the postmenopausal phase, i.e., in an estrogen-deficient state [178]. In addition, females may also undergo estrogen deficiency due to other events [86–88,179,180], thereby, extending this estrogen-deficient state in the life of many women.

Traditionally, studies of age-related loss of skeletal muscle function and strength have been lacking in females. However, clinical and preclinical studies have shown that estrogen deficiency contributes to muscle strength loss in females [18,181–184]. For example, some studies highlight that strength loss was prevented and/or reduced in perimenopausal women and postmenopausal women on estrogen-based hormone therapy compared to postmenopausal women and those not on therapy [95,116,185]. Similarly, in rodent studies, skeletal muscle force generation is lower in ovariectomized (Ovx) females and those treated with E2 had muscle force restored to ovarian-intact females [23]. Furthermore, E2 has been shown to confer an overall beneficial effect on skeletal muscle, such as increased muscle mass after disuse atrophy [186], less muscle fiber injury and inflammation [187], and increased activation and proliferation of satellite cells [188] directly implicating

E2 as the critical ovarian hormone in skeletal muscle function.

Protein phosphorylation, a reversible post-translational modification that fine tunes cellular function and signaling, contributes and regulates a host of skeletal muscle activity, such as fiber-type differentiation, muscle hypertrophy, plasticity, regeneration, excitation-contraction coupling, calcium (Ca^{2+}) sensitivity, and contractile function [32,117,120–126,189,190]. Skeletal muscle contraction also acts as an external stimulus that induces phosphoproteomic alterations [189,190]. In particular, phosphorylation of myosin regulatory light chain (pRLC) has been shown to regulate conformational states of myosin, impacting myosin kinetics and binding to actin during contraction. Preclinical studies have reported that pRLC is 1.8-fold lower in muscle of older compared to younger women, while there was no difference between young and older men [34]. Furthermore, Ovx female mice had ~20% decrease in muscle force *in vitro*, which correlated with 50% decreased pRLC compared to Sham mice [32]. As myosin is one of many proteins of the sarcomere, we hypothesized that estrogen deficiency, via Ovx or natural aging, will modulate phosphorylation of other muscle proteins in response to contraction and force generation. We used two mouse models of estrogen deficiency:

an ovariectomy model (to represent physiological loss of estrogen) and a natural aging ovarian senescence model (to represent aging more comprehensively, including estrogen loss and other factors), and compared their phosphoproteomic profiles to their respective controls. Performing a comparative analysis across both datasets, the present work identified parallel alterations in protein phosphorylation and molecular and cellular signatures. Importantly, identification of novel altered phosphosites and candidate kinases and phosphatases sensitive to the presence of estrogen will help advance our understanding of the contributions of estrogen deficiency to muscle strength loss in aging females.

RESEARCH DESIGN AND METHODS

Animals

Female C57BL/6J (6, 4, and 24 mo) mice were purchased from Jackson Laboratories (Bar Harbor, ME, USA). All mice were housed in groups of four to five with access to phytoestrogen-free food and water ad libitum. The room was maintained on a 14:10 h light/dark cycle. All experiments and procedures were approved by the University of Minnesota Institutional Animal Care and Use Committee.

Experimental Design

The study design to investigate the skeletal muscle phosphoproteome after contraction in two models of estrogen deficiency, ovariectomy (Ovx vs. Sham) and natural aging (Old vs. Young) (n = 3-4/group), is summarized in Figure 1A. C57BL/6J female mice (6 mo) were randomly assigned to a sham or ovariectomy surgery. Sham and Ovx mice were 14 mo at the terminal experiment and Ovx mice were estrogen deficient for 32 wk. Vaginal cytology was performed 4 weeks post-surgery and uterine mass was measured at the terminal experiment. Old (24 mo) and Young (4 mo) mice were purchased from Jackson Lab and were acclimatized for two weeks before the terminal experiment. We chose aged mice of 24 mo of age as C57BL/6J mice are ovarian-senescent between 16-20 mo [191]. An *in vivo* muscle contraction protocol of the anterior crural muscles was performed on each mouse in all four groups. The protocol (detailed below) primarily consisted of one maximal isometric tetanic contraction. A single tetanic contraction was chosen to mitigate potential complications of muscle fatigue that might occur with multiple maximal contractions. Immediately following the muscle contraction protocol, the contracted tibialis anterior (TA) muscles from anesthetized mice were dissected within 5 min, flash frozen in liquid nitrogen, and stored at -80ºC until sample preparation and phosphopeptide enrichment for nanoflow LC-MS/MS acquisition.

Sham and Ovariectomy surgeries

Anesthetized (1.75% isoflurane and 200 ml O_2 per min) mice received a subcutaneous injection of slow-release buprenorphine (1mg/kg) immediately prior to surgeries. Bilateral ovariectomy via abdominal incisions were made to locate the ovaries which were excised in Ovx mice, and located but not removed in Sham mice. The abdominal muscle wall incisions were closed with 6—0 silk sutures and 7 mm wound clips closed the skin incision.

***In vivo* muscle contraction protocol**

Mice were anesthetized (1.25% isoflurane and 125 O_2 per min) and positioned on a temperature-controlled platform as previously described [159]. Briefly, the left knee was immobilized and the left foot secured to an aluminum “shoe” that was attached to the shaft of an Aurora Scientific 300B servomotor. Utilizing sterilized platinum needle electrodes (FE212, Grass Technologies Warwick, RI, USA), inserted to stimulate the left common peroneal nerve, voltage and electrode placement were optimized with 3-5 twitch contractions (0.1 ms pulse). Following optimization, an isometric tetanic contraction of the anterior crural muscles (the TA being the primary muscle in that group) was elicited (1000 Hz for 1000 ms with 0.1 ms pulses), with a twitch

contraction performed 10 s prior and two post-tetanic twitch contractions at 2 s and 30 s after the tetanic contraction.

Protein extraction, digestion, and phosphopeptide enrichment

Frozen dissected TA muscles as described above in the Methods were pulverized into powder with a cryo-grinder (liquid nitrogen cooled mortar and pestle), lysed (10 μl lysis buffer per mg of tissue) in protein lysis buffer (7M urea, 2M thiourea, 0.4M Tris pH7.5, 20% acetonitrile, 4 mM TCEP) with 1X HALT Protease & Phosphatase Inhibitor Cocktail (Thermo Fisher Scientific, Rockford, IL, USA), and sonicated for 5 s using a probe sonicator (Branson Digital Sonifer, Emerson, St. Louis, MO, USA) set at 30% amplitude, all done on ice. After sonication, a 160 μl aliquot of each lysate was placed in the Barocycler® NEP2320 (Pressure Biosciences, South Easton, MA, USA) at 37ºC, with pressure cycles set at 35,000 psi for 20 s, then 0 psi for 10 s for 60 cycles for further protein homogenization. Once pressure cycling was complete, samples were transferred to a new 1.5 ml Eppendorf protein LoBind tube and 200 mM chloroacetamide stock solution was added for a final concentration of 8 mM to alkylate proteins (1:24 dilution) and incubated for 15 min at room temperature. Samples were spun down at 15,000 x *g* for 10 min at 18ºC. Aliquots of supernatant were used to determine protein concentration using the Bradford assay. For trypsin

digestion, 500 μg total protein was digested with 12.5 ug sequencing grade modified trypsin (Promega, Madison, WI, USA) and incubated at 37ºC in a warm air incubator overnight (~ 16 h). Samples were acidified to 0.2% trifluoroacetic acid (TFA) to a final volume of 1 ml and extracted using 1 cc Oasis HLB Solid Phase Extraction cartridges (Waters Corporation, Milford, MA, USA) for clean-up. Briefly, 1cc HLB cartridges were equilibrated by passing 1 mL of 80% acetonitrile, 0.1% TFA over the cartridge followed by passing 1 mL of 0.1% TFA. The sample was passed over the cartridge followed by washing the sample with 1 mL 1% acetonitrile, 0.1% TFA over the cartridge. Peptides were eluted with 0.5 mL 50% acetonitrile, 0.1% trifluoroacetic acid and vacuum dried to remove acetonitrile. Lysates were stored at -80ºC until phosphopeptide enrichment. Phosphopeptide enrichment was performed with the High-Select™TiO_2 Phosphopeptide Enrichment Kit (Thermo Fisher Scientific, Rockford, IL, USA). Eluted peptides were dehydrated using a speed-vac.

Nanoflow LC-MS/MS

Approximately 600 ng of peptide mixture, contained in a 1 μl aliquot of 98:2, water:acetonitrile, 0.1% formic acid, were analyzed in data dependent acquisition mode by liquid chromatography (LC)-nano ESI-mass spectrometry (MS) with an Ultimate 3000 Dionex RSLC nano LC system online with an

Orbitrap Fusion Tribrid mass spectrometer (Thermo Fisher Scientific, Rockford, IL, USA). Peptides were separated during a linear gradient with the following profile: 5-22 % solvent B in 70 min, 22-35 % solvent B over 35 min, and 90% solvent B held for 10 min. Solvent A was water with 0.1% formic acid and solvent B was 80% acetonitrile with 0.1% formic acid. The 50 cm column was packed in house using ReproSil-Pur 120 C18-AQ 1.9 μm (Dr. Maisch, Ammerbuch-Entringen, Germany) in a PicoTip 75 μm inner diameter (New Objective, Littleton, MA, USA). Data acquisition was acquired with the following MS parameters: ESI voltage 2.1 kV, ion transfer tube 275 °C; Easy-IC internal calibration; Orbitrap MS1 scan 120k resolution in profile mode from 380 — 1580 *m/z* with 100 msec injection time; 100% (4 x 10E5) automatic gain control (AGC); MS2 was triggered on precursors with 2 — 6 charges above 5 x 10E4 counts; MIPS (monoisotopic peak determination) was set to Peptide; MS2 settings were: 1.6 Da quadrupole isolation window, higher energy collisional dissociation activation at 35% collision energy, Orbitrap detection with 60K resolution at 200 *m/z*, first mass fixed at 110 *m/z*, 150 msec max injection time, 100% (5 x 10E4) AGC and 40 sec dynamic exclusion duration with +/- 10 ppm mass tolerance.

Phosphoproteomics database search, phosphoprotein and phosphopeptide quantification

The raw MS files were processed by Proteome Discoverer v2.4 (Thermo Fisher Scientific, Rockford, IL, USA). MS/MS spectra were searched against the UniProtKB/Swiss-Prot *mus musculus* database (55,474 entries, UniProt UP000000589, downloaded November 2019) with the Sequest HT search engine embedded in Proteome Discoverer v2.4. Parameters were set as follows: MS1 tolerance of 15 ppm, MS/MS mass tolerance of 0.05 Da, trypsin (full) digestion with a maximum of two missed cleavages, minimum peptide length of 6 and maximum of 144 amino acids. Cysteine carbamidomethylation (57.02 Da) was set as a fixed modification, and methionine oxidation (15.99 Da), asparagine and glutamine deamidation (0.98 Da), acetylation of the N-terminus (42.01 Da), and phosphorylation of tyrosine, serine, and threonine (79.97 Da) were set as dynamic modifications. A false discovery rate (FDR) of 1% was set for peptide-to-spectrum matches using the Percolator algorithm (v3.02.1) and for protein assignment. Phospho-localization scoring was performed with the IMP-ptmRS v2.0 node and only phosphopeptides with a localization score > 0.8 were used for quantification. Unique and and razor peptides were used for quantification. Precursor abundance quantification was based on area and normalized by total peptide amount. All peptides

were used for normalization for protein quantification; however, only phosphorylated peptides were used for pairwise ratios and protein roll-up.

Label-free quantitation (LFQ) of phosphopeptides were performed with normalized abundances using the Proteome Discoverer LFQ algorithms. The protein ratio was calculated as the geometric median of the phosphopeptide group ratios, and the phosphopeptide group ratios were calculated as the geometric median of all combinations of phosphopeptide ratios from all the biological replicates in the study. Phosphopeptides that had a high 1% FDR confidence were used for further analysis. We applied a maximum p-value filter of 0.05 and a minimum relative fold change of phosphoprotein and phosphopeptide expression at 1.4 to the PD quantification results. Phosphoproteins and phosphopeptides were considered significantly and differentially regulated if they had an adjusted p-value < 0.05 and were defined as downregulated if they had a fold change ≤ -1.4 or upregulated if they had a fold change ≥ 1.4.

Kyoto Encyclopedia of Genes and Genomes (KEGG), Reatome, and Gene Ontology (GO) enrichment analysis

Significantly and differentially regulated phosphopeptides were mapped back to their precursor protein and the list of phosphoproteins was used for

overrepresentation analysis using the clusterprofiler package in R v4.1.1 [133,134]. Comparative enrichment analysis of the Ovx/Sham and Old/Young datasets were performed for GO terms in all three domains: cellular component, molecular function, and biological process. Additionally, KEGG and Reactome pathway enrichment analyses was performed with clusterprofiler and the ReactomePA packages in R [135]. Cluster analysis using the Kmeans algorithm was performed on the top 10 KEGG and Reactome pathways. Overrepresented pathways and GO annotation terms were considered significant if they had a Benjamini – Hochberg adjusted p-value < 0.05.

Ingenuity Pathway Analysis (IPA)

IPA (Qiagen, Redwood City CA, USA) was used to perform core analyses on the on the phosphopeptides from Ovx/Sham and Old/Young datasets. A comparative analysis across both core analyses was performed in IPA using the activation Z-score algorithm to predict the activation states of pathways, functions, and upstream regulators from both datasets. The Z-score measures how closely the observed expression pattern of the molecules from the datasets compare to the expected expression pattern based on the literature for a particular annotation. Molecules from the dataset that met the cutoffs, ≤ 1.4-fold change ratio and adjusted p-value < 0.05 were considered for analysis.

Statistical analyses

Relative phosphoprotein quantification was analyzed in Proteome Discoverer v2.4 (Thermo Fisher Scientific, Rockford, IL, USA) using a background t-test. Fisher's exact test was used in IPA to calculate p-values for the association or overlap between the identified molecules in the dataset and a given pathway/process/function. Benjamini-Hochberg post-hoc analysis was used to correct for multiple comparisons. The predicted activation state in the pathways/functions/upstream regulators in IPA were measured as a Z-score. Significant activation or inhibition was accepted at $|Z| \geq 2$. Significance was accepted at $\alpha < 0.05$ level.

RESULTS

Mouse Characteristics

Significant differences in body mass across the groups were measured ($p < 0.001$) (Fig. 1B). Mean body mass for Sham, Ovx, Young, and Old mice are 35.8 ± 3.9, 38.4 ± 6.2, 22.3 ± 1.0, and 30.1 ± 5.4, respectively. Uterine mass was significantly different between Ovx and Sham mice ($p < 0.016$), with the mean uterine masses being 19.3 ± 5.1 and 135.7 ± 70.2, respectively (Fig. 1C). In addition, cytology confirmed persistent diestrus in Ovx mice and estrous cycling in Sham mice, as expected.

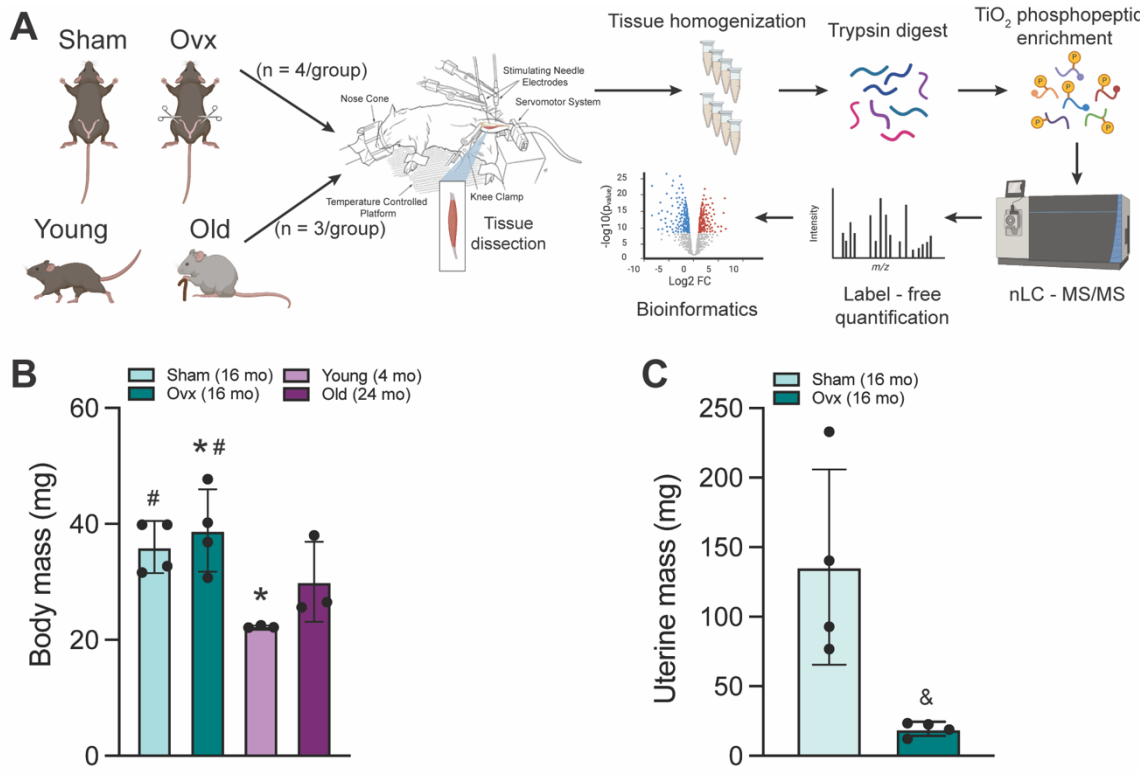

Figure 4.1. Schematic of experimental design created with Biorender.com and mouse demographics. A) 6 mo C57BL/6J female mice were assigned to a Sham or Ovx group and underwent their respective surgeries. Young and Old mice were 4 mo and 24 mo, respectively. The left leg of anesthetized mice was subjected to *in vivo* contractions and then tibialis anterior muscles were immediately dissected. Frozen TA muscles underwent peptide extraction with trypsin digestion and TiO_2 phosphopeptide enrichment. nLC-MS/MS was performed on the Orbitrap Fusion Tribid mass spectrometer for label-free phosphoproteomic analysis. B) Body mass of all four groups of female mice measured before the terminal contraction experiment. Data were analyzed by a one-way ANOVA and a main effect of group was found ($p < 0.001$); n = 3-4/group. C) Uterine mass of Sham and Ovx mice after the terminal contraction experiment. Data were analyzed by a pooled t-test (Ovx vs. Sham, $p = 0.016$); n = 4/group. Values represents mean ± SD. # Significantly different from Young, *Significantly different from Old, and & Significantly different from Sham.

Comparative skeletal muscle phosphoproteomes in Ovx/Sham and Old/Young mice

In the two models of estrogen-deficient mice, a total of 2,593 phosphopeptides and 3,507 phosphopeptides were identified in Ovx/Sham and Old/Young TA muscles, respectively (Figs. 2A & B). Phosphorylation was most prevalent on serine (Ser, ~ 78%), followed by threonine (Thr, ~ 17%), and tyrosine (Tyr, ~ 4%), which is consistent with literature and was similar across both datasets (Figs. 2C & D)[192], demonstrating reproducible sample preparation and peptide detection. Further analysis identified 222 and 408 significantly and differentially regulated phosphopeptides in Ovx/Sham and Old/Young datasets, respectively (Figs. 2E & F).

The datasets were processed to identify intersecting proteins and phosphosites, which were then deemed to be associated with estrogen deficiency. After filtering for robustness (i.e., relative abundance detected in at least 3 out of the 4 biological replicates in Ovx or Sham and 2 out of 3 biological replicates in Old or Young groups), 66 estrogen-deficiency associated phosphoproteins were identified (Supplemental Table 1). From these 66 phosphoproteins, four were significantly and differentially expressed (eukaryotic translation initiation factor 4E-binding protein 1, ankyrin repeat domain-containing 2, heat shock protein beta-6, and heterogeneous nuclear ribonucleoprotein U-like protein 2) in the Old/Young dataset.

Two (phosphoacetylglucosamine mutase and myc box-dependent interacting protein1) were significantly and differentially expressed in the Ovx/Sham dataset.

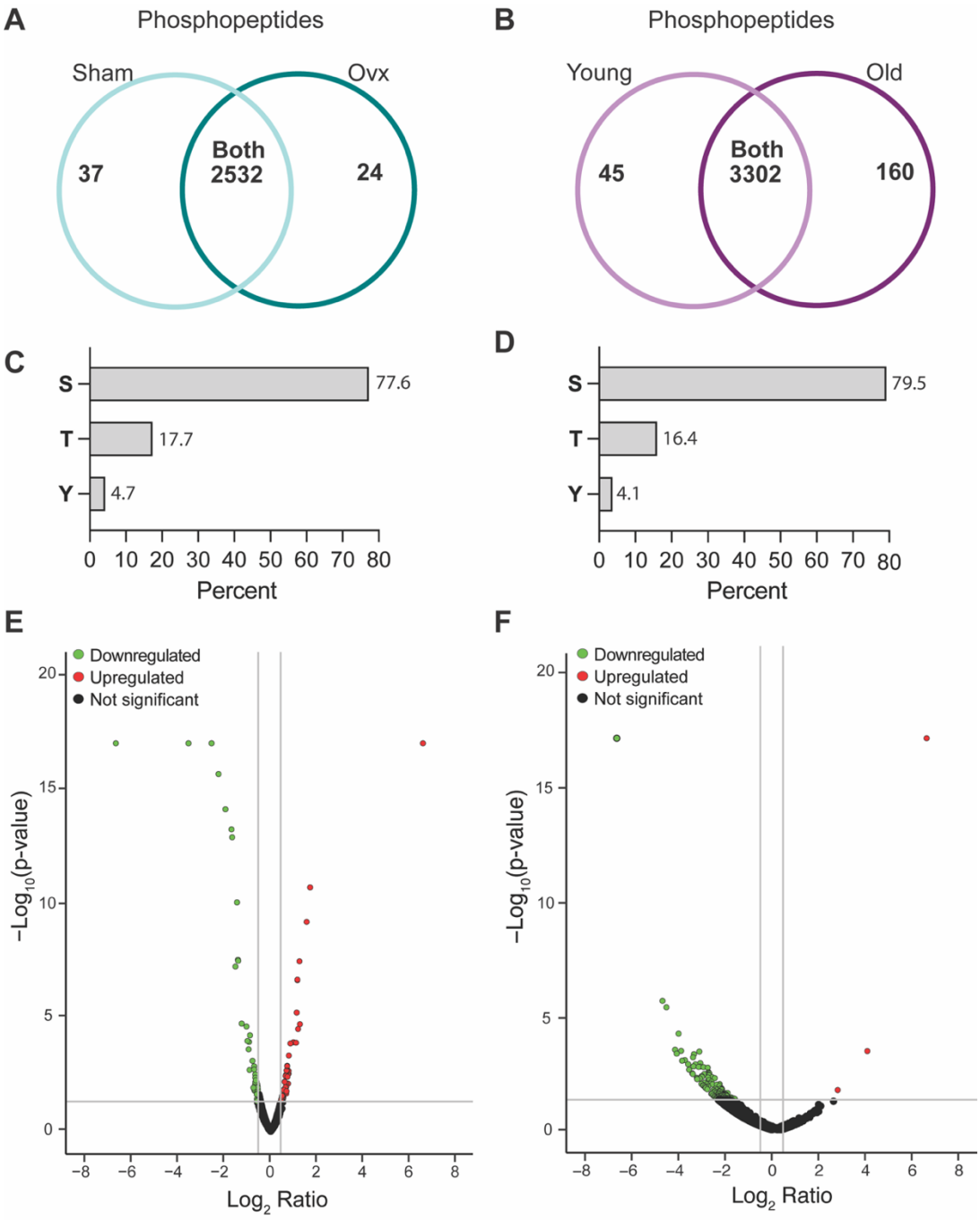

Figure 4.2. Characteristics of the Ovx/Sham and Old/Young phosphoproteomes. Proteome Discoverer (v2.4) was used for database search and identification of phosphopeptides analysis. Venn diagram of identified phosphopeptides unique to each group and common to both groups in A) Ovx/Sham and B) Old/Young datasets. Prevalence of phosphorylation on amino acid residues serine (S), threonine (T), and tyrosine (Y) in C) Ovx/Sham and D) Old/Young datasets. Volcano plots of differentially regulated phosphopeptides ($p < 0.05$ and 1.4-fold change) in E) Ovx/Sham and F) Old/Young mice.

A total of 21 estrogen-deficiency-associated phosphosites were found across the two datasets, of which 4 phosphosites were significantly and differentially regulated in both, tumor protein D54 Ser-166, ATP synthase subunit alpha Ser-521, calpastatin Ser-82, and H/ACA ribonucleoprotein complex subunit DKC1 Ser-481 (Table 1). Calpastatin (CAST) Ser-82 and H/ACA ribonucleoprotein complex subunit DKC1 Ser-481 were the only two phosphosites that had the same directionally across both datasets (downregulated in the estrogen-deficient groups). Although we did identify estrogen-deficiency associated phosphosites on six sarcomeric proteins (myozenin-1 Ser-134, desmin Ser-28, nexilin Ser-559, junctophilin-1 Ser-501, troponin T Ser-2, and myosin regulatory light chain 2 Ser-16), only myozenin-1 Ser-134 was significantly and differentially regulated in the Old/Young; whereas, myozenin-1 Ser-164 and troponin T Ser-2 were significantly and differentially regulated in the Ovx/Sham datasets. These data show that Ovx and Old mice compared to their respective control, Sham or Young, had some similar phosphoproteomic alterations in contracted muscles induced by estrogen deficiency.

Table 4.1. Estrogen-deficiency associated phosphosites in Ovx/Sham and Old/Young datasets.

Uniprot Accession ID	Gene Symbol	Protein Description	Phosphosite (Score)	Log2 ratio: Ovx / Sham	Log2 ratio: Old / Young
A2AUD5	*Tpd52l2*	Tumor protein D54	S166(100)	6.64	-6.64
Q03265	*Atp5f1a*	ATP synthase subunit alpha, mitochondrial	S521(100)	1.61	-6.64
Q8CE04	*Cast*	Calpastatin	S82(100)	6.64	6.64
Q9CQH3	*Ndufb5*	NADH dehydrogenase [ubiquinone] 1 beta subcomplex subunit 5, mitochondrial	S182(100)	1.04	-6.64
Q9ESX5	*Dkc1*	H/ACA ribonucleoprotein complex subunit DKC1	S481(100)	-6.64	-6.64
Q9JK37	*Myoz1*	Myozenin-1	S134(100)	3.23	6.64
Q5EBG6	*Hspb6*	Heat shock protein beta-6	S16(100)	-0.80	-3.38
A0A1D5RLD8	*Gm10358*	Glyceraldehyde-3-phosphate dehydrogenase	T182(100)	-0.58	-2.88
P31001	*Des*	Desmin	S28(100)	-0.87	-2.53
P48678	*Lmna*	Prelamin-A/C	S390(100)	-0.93	-2.18
A0A494B9J0	*Ankrd2*	Ankyrin repeat domain-containing protein 2	S321(100); T325(100)	-1.09	-2.28
G5E8J6	*Hrc*	Histidine rich calcium binding protein	S104(100)	-3.25	-1.33
Q9CYR6	*Pgm3*	Phosphoacetylglucosamine mutase	S64(100)	1.30	-1.51
A0A0G2JEX1	*Nexn*	Nexilin	S559(100)	3.54	-1.40
A0A0A0MQC7	*Mapt*	Microtubule-associated protein	S188(100)	-6.64	-0.61
G5E8J6	*Hrc*	Histidine rich calcium binding protein	S354(100)	0.36	-1.17
P48678	*Lmna*	Prelamin-A/C	S390(100); S392(100)	-0.10	-1.19
Q9ET80	*Jph1*	Junctophilin-1	S501(100)	3.43	1.14
Q9JK37	*Myoz1*	Myozenin-1	S164(100)	-6.64	-1.40
A0A0R4J1B1	*Tnnt3*	Troponin T	S2(100)	-6.64	-0.42
P97457	*Mylpf*	Myosin regulatory light chain 2	S16(99)	0.45	-0.01

Note. The red font denotes significantly and differentially regulated phosphosites (BH p-value <0.05 & |FC| > 1.4).

GO term overrepresentation analysis

To gain insight on the biological significance of estrogen deficiency in the skeletal muscle phosphoproteome

after contraction in Ovx and Old mice, a comparative GO term overrepresentation analysis was performed. The top 10 most overrepresented GO terms for cellular compartment, molecular function, and biological process are shown in Fig. 3A, B, and C, respectively. There was significant overrepresentation of GO terms (FDR < 0.05) across all GO domains with numerous similarities between both datasets. GO molecular function analysis had similar terms enriched in both datasets relating to actin/actin filament binding, structural constituent of the cytoskeleton and muscle, calmodulin binding, tropomyosin binding, and translation regulator activity. However, there was a preferential enrichment in phosphatase activity in the Ovx/Sham dataset; whereas, a preferential enrichment in translation activity in the Old/Young dataset (Fig. 3A). All top 10 GO cellular component terms pertaining to the muscle fiber were enriched across both datasets, with reduced enrichment in the myosin complex in the Old/Young dataset. Likewise, all GO biological process terms except one, glycogen metabolic process, was enriched across both datasets. Overall, the top 10 GO term enrichments across many molecular functions, and essentially all cellular components and biological processes were consistent in the Ovx/Sham and Old/Young datasets suggesting that estrogen deficiency confer

parallel changes in the skeletal muscle phosphoproteome after force generation.

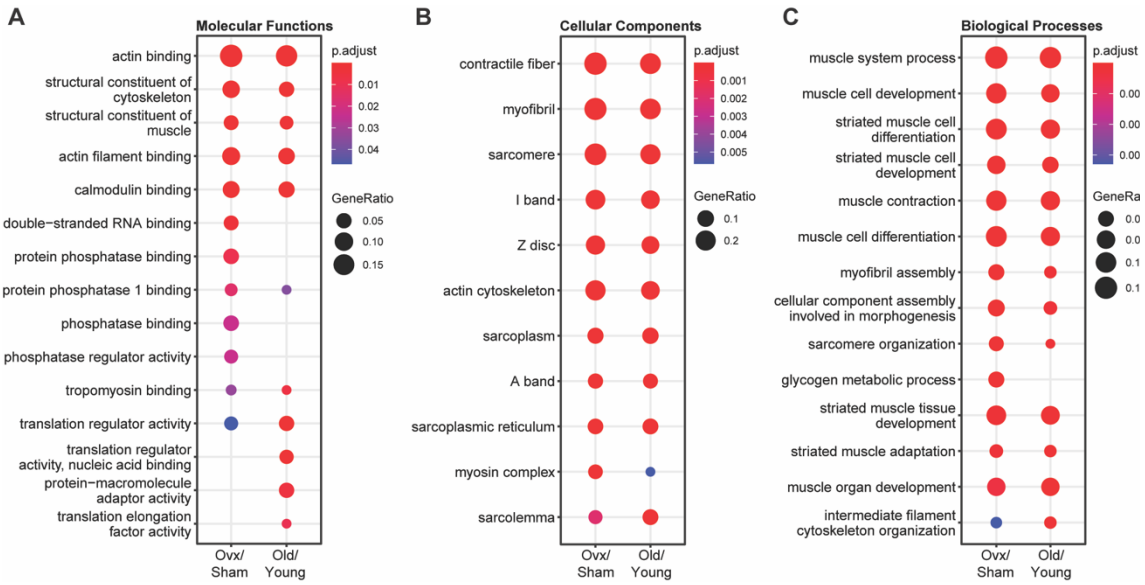

Figure 4.3. Comparative GO term enrichment analysis between Ovx/Sham and Old/Young. Phosphopeptides were mapped back to their precursor protein and submitted for Gene Ontology (GO) overrepresentation analysis using the clusterProfilier package in R. The top 10 overrepresented GO terms in the dataset for A) molecular functions, B) cellular components, and C) biological processes are listed. P-value was adjusted using Bejamini – Hochberg post-hoc analysis for multiple comparison. Significant GO terms were accepted at p.adjusted < 0.05.

KEGG and Reactome Pathway overrepresentation analysis

To further explore biological pathways associated with estrogen deficiency in the datasets, overrepresentation analysis of KEGG and Reactome pathways was performed. Using the K-means clustering algorithm, mutual overlapping pathways were clustered together via the similarity between nodes, and the stronger the similarity, the shorter and thicker the connecting lines (Fig. 4). Similar to the GO term analyses,

among the top 10 pathways, all but one KEGG and three Reactome pathways were associated across both datasets. Only the “pathways of neurodegeneration – multiple diseases” from the KEGG analysis was unique to the Old/Young dataset. Out of the four apoptosis related pathways from the Reactome analysis, three were unique to the Ovx/Sham dataset suggesting that apoptosis was more of a factor for Ovx than it was for Old “natural” aging mice. In summary, many enriched KEGG and Reactome pathways were similar across both datasets suggesting that these pathways may be sensitive to estrogen levels and may contribute to muscle contractile dysfunction.

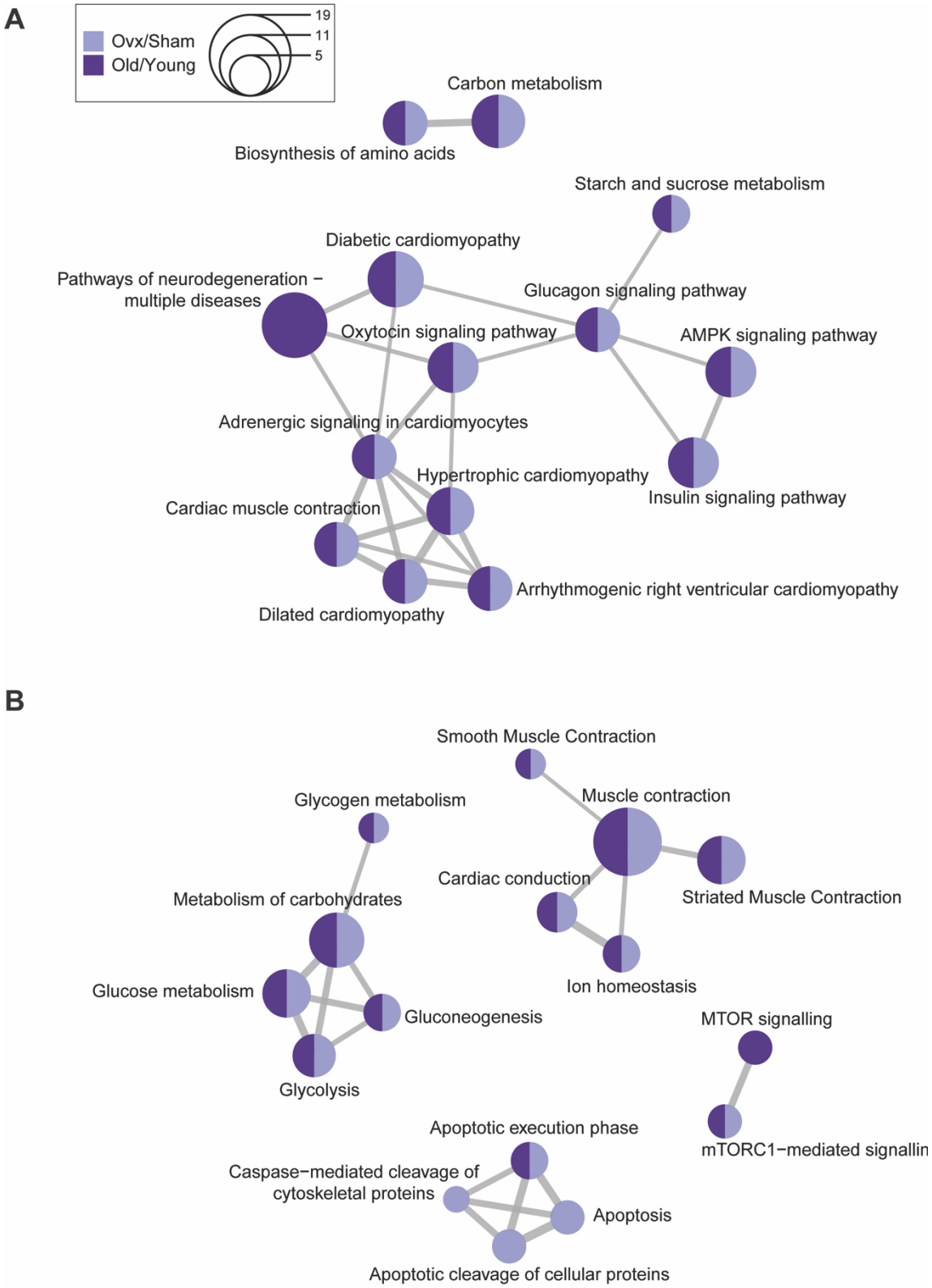

Figure 4.4. Comparative KEGG and Reactome pathway enrichment analysis between Ovx/Sham and Old/Young. Phosphopeptides that had a significant differentially regulated phosphorylation site (p value < 0.05 and -0.38 ≥ log2 ratio ≥ 0.38) were mapped back to

their precursor protein and the list was submitted to R for analysis of KEGG and Reactome pathways. The top 10 overrepresented A) KEGG and B) Reactome pathways were clustered using Kmeans clustering. The size of the circle represents the number of proteins associated to the pathway.

IPA's Predicted Downstream Effects and Upstream Regulator Analytics

Next, the identified phosphopeptides from the Ovx/Sham and Old/Young datasets were submitted to IPA to perform core analyses. A comparative analysis between the two core analyses was then performed to identify parallel activation states via IPA's Z-score algorithm across IPA-derived molecular and cellular functions, canonical pathways, and upstream regulators. For reference, IPA's Z-score indicates a predicted overall activation or inhibition of functions/pathways and activated or inhibited upstream regulators, where a negative Z-score signifies an inhibition and a positive Z-score signifies activation [193].

IPA Molecular and Cellular Functions Analysis

Seventeen biological processes were identified across both datasets with similar directionality of activation and were broadly related to muscle quantity and function, filament formation and stabilization, transport of molecules, autophagy, and RNA expression and translation (Fig. 5A). Four molecular and cellular functions (quantity of muscle, necrosis, force generation, and expression of RNA) were in

activated states with necrosis being significantly activated (Z-score = 2.52) in the Old/Young dataset. The remaining molecular and cellular functions were in inhibited states with polymerization of filaments being the most inhibited (Z-score = 1.94) in the Ovx/Sham dataset. These parallel molecular and cellular functions identified across both datasets suggest a compromise not only in the force generating capacity of skeletal muscle but also mechanisms involved in skeletal muscle maintenance and integrity when estrogen is deficient.

IPA Canonical Pathway Analysis

Seven canonical pathways were identified having the same directionality of activation across both datasets, with all showing inhibition except for 14-3-3 protein mediated signaling which was activated in an estrogen deficient condition (Fig. 5B). All pathways were significantly enriched ($p < 0.05$) across both datasets except for phagosome formation in the Old/Young dataset ($p = 0.299$). The top three canonical pathways, AMPK signaling, 14-3-3 protein mediated signaling, and calcium signaling, had significant activation Z-scores in the Ovx/Sham dataset (-2.23, 2.0, and -2.0, respectively). The similarities in inhibition or activation of canonical pathway profiles indicate important calcium, kinase, and cellular signaling in skeletal muscle that may be compromised

in estrogen-deficient mice, which could in turn contribute to changes in muscle force generation.

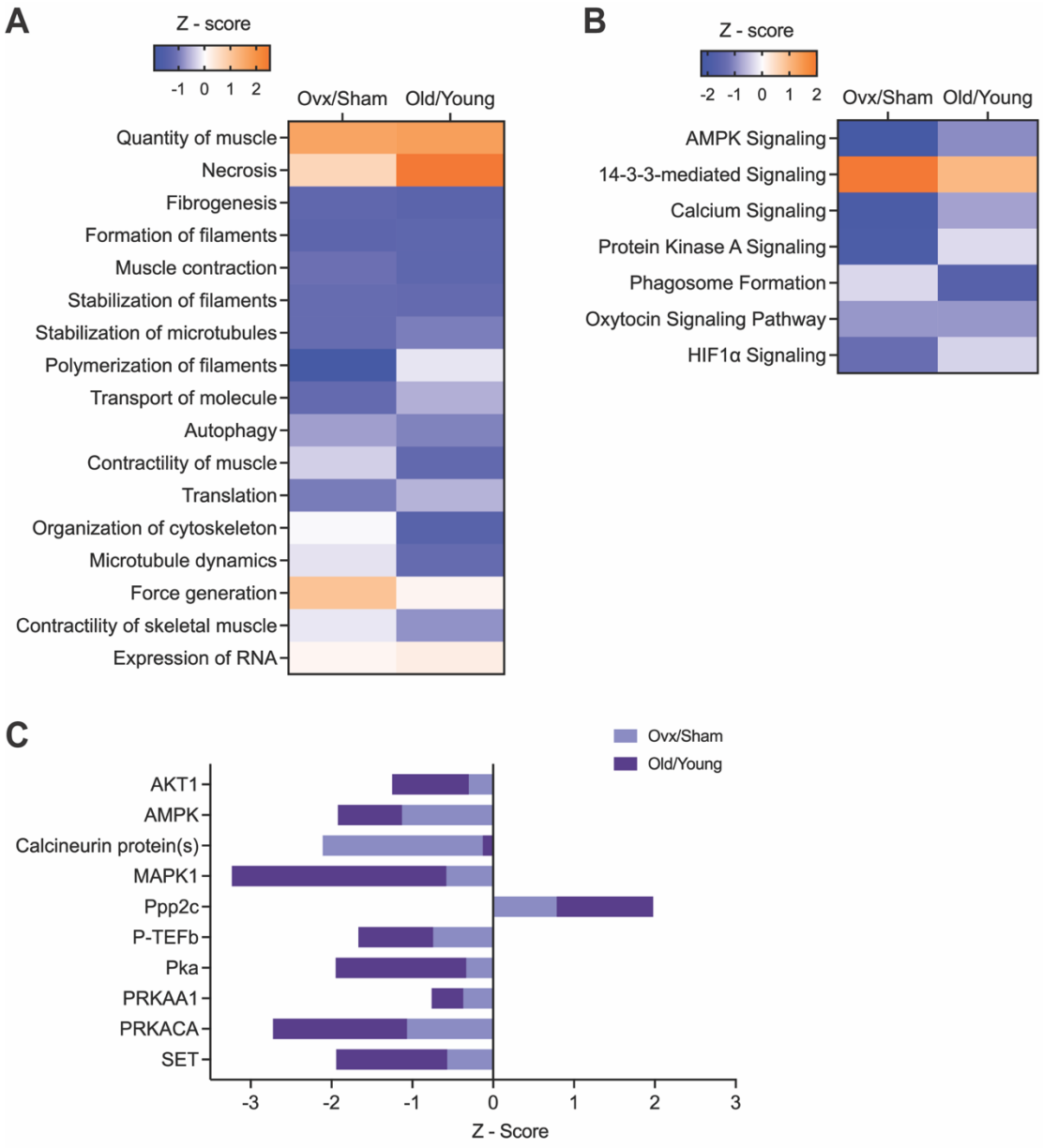

Figure 4.5. IPA's predictive downstream effect and upstream regulator analytics between Ovx/Sham and Old/Young. Phosphopeptides identified in both the Ovx/Sham and Old/Young datasets were submitted to IPA for comparative analysis of A) canonical pathways, B) functions, and C) kinases and phosphatases using IPA's predictive activation Z-score to determine downstream and upstream effects of estrogen deficiency. Pathways, functions, and kinases identified in both datasets are represented. Significant Z-scores were accepted at $|Z| \geq 2$.

IPA Upstream Regulatory Analysis

Ten upstream regulators (i.e., candidate kinases and phosphatases) were identified across both datasets (Fig. 5C). All candidate kinases and phosphatases were inhibited (negative Z-scores) with the exception of serine/threonine-protein phosphatase 2A catalytic subunit (PPP2C) being activated in both the Ovx/Sham (Z-score = 0.79) and Old/Young (Z-score = 1.98) datasets. Mitogen activated protein kinase 1 (MAPK1 also known as ERK2, Z-score = -3.23) and cAMP-dependent protein kinase (PKA) catalytic subunit alpha (PRKACA, Z-score = -2.74) were significantly inhibited and SET (Z-score = -1.94) and AMPK (Z-score = -1.92) was highly inhibited in the Old/Young compared to the Ovx/Sham dataset (Z-scores = -0.58, -1.07, -0.57, and -1.13 for MAPK1, PRKACA, SET, and AMPK, respectively). Calcineurin proteins(s) (Z-score = -2.11) was the only phosphatase regulator that was significantly inhibited in the Ovx/Sham dataset compared to the Old/Young (Z-score = -0.13). Overall, the parallel activation status of these candidate kinases and phosphatases across both datasets suggests sensitivity to the loss of estrogen in skeletal muscle of female mice, with more robust inhibited or activated status in the Old/Young group potentially due to compounded effects of aging.

DISCUSSION AND IMPLICATIONS

The purpose of this study was to utilize two models of female estrogen deficiency, ovariectomy and natural aging-induced ovarian senescence, to identify estrogen sensitive alterations in the phosphoproteomic landscape of skeletal muscle after contraction. We identified parallel alterations in molecular and cellular signatures and pathways in both models related to skeletal muscle contractile function and structural integrity coupled with enriched pathways for AMPK, 14-3-3, and calcium signaling. This work provides insight into phosphorylation alterations and potential candidate kinases and phosphatases impacting the force-generating capacity of skeletal muscle due to estrogen deficiency that may underlie muscle strength loss in females.

Significant upregulation of calpastatin (a calpain inhibitor) phosphorylation combined with altered phosphorylation of calpain substrates - downregulation of desmin and troponin T in both datasets and downregulation of myosin regulatory light chain phosphorylation in Old/Young dataset with upregulation in the Ovx/Sham dataset highlighted in our study may imply abrogation of calpain activities. Hyperphosphorylation of calpastatin positively regulates calpain inhibition [194], and modifications on calpain substrates, such as phosphorylation or dephosphorylation, has been shown to regulate the susceptibility of the substrate to

calpain degradation [195]. Calpain-mediated proteolytic activities in skeletal muscle are crucial for myofibrillar protein turnover and aid in muscle plasticity through disassembly of the myofibril [196]. For example, reduced desmin degradation coupled with increased calpain inhibition may not only be indicative of aberrant proteolytic activities required for muscle remodeling, but may also lead to the retention of damage proteins. Particularly, desmin fragments/misfolding can form desmin-derived amyloids; thereby, disrupting myofibrillar organization and functions [197]. Impaired proteostasis, by decreased proteolytic activity and/or increased protein aggregation – a hallmark in skeletal muscle aging [198], may contribute to the loss of strength in females due to estrogen deficiency.

The present study suggests that loss of estrogen modulates kinase and phosphatase activities that may affect the force-generating capacity of muscle in female mice, as predicted by the significant changes in activation status from IPA's upstream regulator analysis. All identified kinases and phosphatases had analogous directionality of activation in both models of estrogen deficiency with MAPK1/ERK2 and PRKACA predicted to be significantly inhibited in the Old/Young dataset. Identification of the involvement of the MAPK pathway via MAPK1/ERK2 as a potential candidate

kinase sensitive to estrogen level is consistent with previous work [32]. Total MAPK1/ERK2 levels have also been reported to be significantly decreased in skeletal muscle from Ovx compared to Sham mice after a fatiguing contraction protocol [199], and reduced activation was observed after a bout of resistance exercise in older men compared to younger men [200]. Furthermore, C2C12 cells exposed to hydrogen peroxide exhibited cytoskeleton disorganization, mitochondrial redistribution, and fragmented nuclei – features associated with apoptosis, and were rescued upon E2 pretreatment, which was found to exert anti-apoptotic effects via ERK and p38 MAPK activation [201]. Therefore, downregulation of MAPK1/ERK2 activity may indicate increased activation in apoptotic pathways and increased perturbations of the cytoskeleton, consistent with our enrichment analyses.

Another candidate kinase identified from IPA's upstream regulator analysis was PRKACA. PRKACA is the catalytic subunit alpha of PKA that is released upon binding of cAMP to the regulatory subunit dimer of PKA. Unlike MAPK1/ERK2, there is limited information on the specific role of PRKACA in skeletal muscle. However, PKA was also identified as a potential candidate kinase sensitive to E2 [32]. Overexpression of the PKA catalytic domain in skeletal muscle was revealed to inhibit Forkhead box O activity and contribute to muscle

remodeling [202]. In addition, incubation of skeletal muscle single fibers with PKA enhanced contractile function by modifying protein-binding protein C in old compared to young men [203]. Importantly, it is well established that PKA regulates calcineurin [204], which was also predicted to be downregulated in both estrogen deficient models. Calcineurin inhibition has been shown to induce muscle defects, such as fiber atrophy, immature myotube formation, calcification, and inflammation [205].The impact of PKA and/or calcineurin have been extensively studied and details on their impact on hypertrophy, regeneration, metabolism, and muscle disorders in skeletal muscle can be found in a number of exceptional reviews [206–211]. The implication of both PKA and calcineurin being inhibited in our two models suggest comprised contractile function, fiber maturation, and muscle remodeling that may in turn contribute to decreased force-generating capacity of skeletal muscle in estrogen-deficient females, whether via Ovx or aging ovarian-senescent.

In summary, the current study examining the impact of estrogen deficiency in the skeletal muscle phosphoproteome after contraction and force generation, identified corresponding alterations in protein phosphorylation, pathways, and upstream regulators in both Ovx and natural aging ovarian-senescent female mice. The results provide two

rich datasets for further study of estrogen deficiency-induced phosphoproteomic alterations in female skeletal. Our study highlights, calpastatin phosphorylation at Ser-82 as a candidate phosphosite, and MAPK1/ERK2, PRKACA, and calcineurin as potential upstream regulators sensitive to estrogen deficiency that may contribute to changes in the force-generating capacity of skeletal muscle. Future studies based on these bioinformatic and computational analyses, and potentially incorporating estrogenic treatments, will be key confirmatory experiments to test the extent to which the predicted candidate phosphosites, kinases and phosphatases, and pathways affect muscle strength in aging females.

Acknowledgements

We thank the University of Minnesota Center for Mass Spectrometry and Proteomics for their service, Dr. Yue Chen for his discussions on phosphoproteomic analysis, and Dr. Shawna McMillan for her critical reading.

Funding

This work was supported by the National Institute of Aging [R01 AG031743-13 to D.A.L.]; and National Institute of Arthritis and Musculoskeletal and Skin Diseases [T32 AR007612 to M.P.P].

Competing interests

The authors declare that they have no competing financial interests.

Authors' contributions

MPP, TY, LH, TWM, LLP, and DAL contributed to experimental design and conceptual framework. MPP, TY, TWM, and LH contributed to data collection and analysis. MPP, TY, and LH contributed to data curation and formal analysis. MPP prepared all figures and drafted the original manuscript. All authors contributed to the edits and revisions of the manuscript and have given approval to the final version of the manuscript.

Supporting Information

Supplemental materials and methods and figures can be found online.

The mass spectrometry proteomics data have been deposited to the ProteomeXchange Consortium via the PRIDE partner repository with the dataset identifier PXD035171. Username: reviewer_pxd035171@ebi.ac.uk, Password: SuCF3XI6

In summary, results from this project revealed protein phosphorylation changes and predicted altered kinases and phosphatase activity that may underlie the decreased in force generation observed in Ovx and ovarian, senescent aged female mice. Similar phosphoproteomic alterations identified across molecular and cellular signatures and pathways in both

datasets were related to decreased DES Ser-12 phosphorylation, increased CAST Ser-1 phosphorylation, and inhibition in AMPK signaling, 14-3-3 protein mediated signaling, and calcium signaling. Additionally, identified upstream regulators sensitive to estrogen deficiency that had predicted inhibition in activity were MAPK1/ERK2, PRKACA, and calcineurin. Taken together, the similarities identified in both datasets could elucidate the molecular characteristics of proteins that might contribute to decrements in muscle strength observed in Ovx and Old female mice due to estrogen loss.

Chapter 5

Overall discussion and conclusions

Dynapenia severely impacts the physical function and health span of the aging population. While the best intervention to offset the loss of skeletal muscle strength remains to be exercise via resistance training and continued physical activity, potential therapeutics, such as estrogen replacement therapy in women and E2 treatment in female mice, have been shown to help prevent skeletal muscle strength loss. However, the controversies and risks of using estrogen replacement therapy remain and push the field of female skeletal muscle biology to identify not only the underlying mechanisms of strength loss but also potential novel targets to aid in the development of therapeutics to help mitigate strength loss in aging females. The projects undertaken in this dissertation aimed to reveal potential mechanisms and novel targets of muscle strength loss using mass spectrometry discovery-based phosphoproteomics coupled with bioinformatic tools and computational predictive modeling.

In Chapter 3, we investigated protein phosphorylation alterations in skeletal muscle induced by estrogen deficiency. We hypothesized that estrogen deficiency would remodel the skeletal muscle phosphoproteome in Ovx compared to Sham female mice. Agreeing with our hypothesis, estrogen deficiency altered protein phosphorylation in Ovx compared to Sham mice. Among these phosphoproteomic alterations included

sarcomeric proteins (TPM, MYH2, MYO2, and OBSCN) and proteins related to calcium and metabolic signaling. Furthermore, our predictive modeling found inhibition of contractility, consistent with what we and others have observed *in vitro* and *in vivo*, along with other predicted deficits in skeletal muscle function, such as inhibition of phagosome formation and activation in dysregulation of the cytoskeleton. Importantly, we identified two novel upstream regulators, CDK6 and PRKCE, as candidate kinases potentially sensitive to estrogen levels that may regulate the phosphoproteomic alterations observed and contribute to skeletal muscle strength loss in females. We also proposed dysregulation in AMPK-YAP1 mediated signaling to also contribute to skeletal muscle dysfunction. Findings from this study of resting, non-contracted muscle revealed an already modified skeletal muscle phosphoproteome in estrogen deficient mice that could alter force generation. Therefore, we next sought to investigate the skeletal muscle phosphoproteome in contracted muscles.

Chapter 4 examined estrogen-deficiency associated protein phosphorylation alterations in contracted muscles of Ovx and ovarian senescent, aged female mice compared to their respective controls (Sham and young mice, respectively). As ovariectomy is a well-used model of female aging to probe the

primary estrogen biology loss with age, it is nonetheless a model and one that is imperfect. Therefore, to address whether the estrogen deficiency-related phosphoproteomic alterations and predictions are truly associated with female aging, we performed a comparative analysis across both the surgical (Ovx/Sham) and aging (Old/Young) groups. The similarities found across both groups in protein phosphorylation alterations, GO terms, signaling pathway patterns (KEGG and Reactome pathways), and predicted upstream regulators suggests that these parallel findings are likely estrogen deficiency-induced. Specifically, we identified increased CAST Ser-82 phosphorylation in both Ovx and Old female mice. In addition, we identified three upstream regulators across both analyses, MAPK1/ERK2, PRKACA, and calcineurin, to potentially be sensitive to estrogen deficiency. Thus, both experiments provide bi-directional support for each other (i.e., ovariectomy is a reasonable model of aging in our experiment, and the changes observed in aging are due to the loss of estrogen since that is the key downstream outcome of ovariectomy).

Overall, this dissertation provides robust datasets for future investigations on how estrogen deficiency impacts the female skeletal muscle phosphoproteome. Notably, the results from these projects reveal that skeletal muscle protein

phosphorylation is altered in estrogen-deficient females, which may, in turn, contribute to dynapenia. Future studies investigating the physiological significance of these two comprehensive phosphoproteomic analyses through loss of function or gain of function studies may generate valuable insight into the molecular regulators and signaling cascades contributing to the debilitating clinical phenotype of skeletal muscle strength loss. Specifically, mechanistic studies from this work include but are not limited to the following:

1. Functional testing of identified candidate phosphosites, kinases, and phosphatase to validate their physiological relevance and significance
2. Development of targeted phosphoproteomic parallel reaction monitoring mass spectrometry method to assay protein phosphorylation sites associated with muscle strength loss
3. Creation of a biomarker panel for skeletal muscle strength loss
4. Development of treatments and therapeutic interventions to help mitigate muscle strength loss.

BIBLIOGRAPHY

1. Ageing and health. Accessed July 22, 2022. https://www.who.int/news-room/fact-sheets/detail/ageing-and-health
2. Keller K, Engelhardt M. *Strength and Muscle Mass Loss with Aging Process. Age and Strength Loss*. Vol 3.; 2013.
3. Metter EJ, Conwit R, Tobin J, Fozard JL. Age-associated loss of power and strength in the upper extremities in women and men. *Journals of Gerontology - Series A Biological Sciences and Medical Sciences*. 1997;52(5):B267-B276. doi:10.1093/gerona/52A.5.B267
4. Tieland M, Trouwborst I, Clark BC. Skeletal muscle performance and ageing. *J Cachexia Sarcopenia Muscle*. 2018;9(1):3-19. doi:10.1002/jcsm.12238
5. Manini TM, Clark BC. Dynapenia and aging: An update. *Journals of Gerontology - Series A Biological Sciences and Medical Sciences*. 2012;67 A(1):28-40. doi:10.1093/gerona/glr010
6. Walston JD. Sarcopenia in older adults. *Curr Opin Rheumatol*. 2012;24(6):623-627. doi:10.1097/BOR.0b013e328358d59b
7. Clark BC, Manini TM. Sarcopenia is not dynapenia. *J Gerontol*. 2008;63(8):829-834. Accessed April 10, 2019. https://academic.oup.com/biomedgerontology/article-abstract/63/8/829/567368
8. Clark BC, Manini TM. What is dynapenia? *Nutrition*. Published online 2012. doi:10.1016/j.nut.2011.12.002
9. Faulkner JA, Larkin LM, Claflin DR, Brooks S V. Age-related changes in the structure and function of skeletal muscles. *Clin Exp Pharmacol Physiol*. 2007;34(11):1091-1096. doi:10.1111/j.1440-1681.2007.04752.x
10. Kamiya K, Osaki T, Nakao K, et al. Electrophysiological measurement of ion channels on plasma/organelle membranes using an on-chip lipid bilayer system. *Sci Rep*. 2018;8(1):2-10. doi:10.1038/s41598-018-35316-4
11. Lynch GS, Hinkle RT, Chamberlain JS, Brooks S V., Faulkner JA. Force and power output of fast and slow skeletal muscles from mdx mice 6-28 months old. *Journal of Physiology*. 2001;535(2):591-600. doi:10.1111/j.1469-7793.2001.00591.x
12. Bauer JM, Sieber CC. Sarcopenia and frailty: A clinician's controversial point of view. *Exp Gerontol*. 2008;43(7):674-678. doi:10.1016/j.exger.2008.03.007
13. Waltz M, Fisher JA, Lyerly AD, Walker RL. Evaluating the National Institutes of Health's Sex as a Biological Variable Policy: Conflicting Accounts from the Front Lines of Animal Research. *J Womens Health*. 2021;30(3):348. doi:10.1089/JWH.2020.8674
14. NOT-OD-15-102: Consideration of Sex as a Biological Variable in NIH-funded Research. Accessed August 6, 2022. https://grants.nih.gov/grants/guide/notice-files/not-od-15-102.html
15. Phillips BE, Smith K, Atherton PJ, Williams JP, Greenhaff PL. Physiological adaptations to resistance exercise as a

function of age C L I N I C A L M E D I C I N E Physiological adaptations to resistance exercise as a function of age. doi:10.1172/jci.insight.95581
16. Kane AE, Bisset ES, Keller KM, Ghimire A, Pyle WG, Howlett SE. Age, Sex and Overall Health, Measured As Frailty, Modify Myofilament Proteins in Hearts From Naturally Aging Mice. *Sci Rep*. 2020;10(1):1-15. doi:10.1038/s41598-020-66903-z
17. Moran AL, Warren GL, Lowe DA. Soleus and EDL muscle contractility across the lifespan of female C57BL/6 mice. *Exp Gerontol*. 2005;40(12):966-975. doi:10.1016/j.exger.2005.09.005
18. Moran AL, Warren GL, Lowe DA. Removal of ovarian hormones from mature mice detrimentally affects muscle contractile function and myosin structural distribution. *J Appl Physiol*. 2006;100(2):548-554. doi:10.1152/japplphysiol.01029.2005
19. Kosir AM, Mader TL, Greising AG, Novotny SA, Baltgalvis KA, Lowe DA. Influence of ovarian hormones on strength loss in healthy and dystrophic female mice. *Med Sci Sports Exerc*. Published online 2015. doi:10.1249/MSS.0000000000000531
20. Le G, Novotny SA, Mader TL, et al. A Moderate Estradiol Level Enhances Neutrophil Number and Activity in Muscle after Traumatic Injury but Strength Recovery Is Accelerated. doi:10.1113/JP276432
21. Larson AA, Baumann CW, Kyba M, Lowe DA. Oestradiol affects skeletal muscle mass, strength and satellite cells following repeated injuries. *Exp Physiol*. 2020;105(10):1700-1707. doi:10.1113/EP088827
22. Skelton DA, Phillips SK, Bruce SA, Naylor CH, Woledge RC. Hormone replacement therapy increases isometric muscle strength of adductor pollicis in post-menopausal women. *Clin Sci*. 1999;96(4):357. doi:10.1042/cs19980318
23. Moran AL, Nelson SA, Landisch RM, Warren GL, Lowe DA. Estradiol replacement reverses ovariectomy-induced muscle contractile and myosin dysfunction in mature female mice. *J Appl Physiol*. 2007;102(4):1387-1393. doi:10.1152/japplphysiol.01305.2006
24. Tiidus PM, Lowe DA, Brown M. Estrogen replacement and skeletal muscle: mechanisms and population health. *J Appl Physiol*. Published online 2013. doi:10.1152/japplphysiol.00629.2013
25. Finni T, Kovanen V, Ronkainen PHA, et al. Combination of hormone replacement therapy and high physical activity is associated with differences in Achilles tendon size in monozygotic female twin pairs. *J Appl Physiol*. Published online 2009. doi:10.1152/japplphysiol.91439.2008
26. Pöllänen E, Kangas R, Horttanainen M, et al. Intramuscular sex steroid hormones are associated with skeletal muscle strength and power in women with different hormonal status. *Aging Cell*. 2015;14(2):236-248. doi:10.1111/acel.12309
27. Sipilä S, Narici M, Kjaer M, et al. Sex hormones and skeletal muscle weakness. *Biogerontology*. 2013;14(3):231-245. doi:10.1007/s10522-013-9425-8

28. Driska SP, Aksoy MO, Murphy RA. Myosin light chain phosphorylation associated with contraction in arterial smooth muscle. *Am J Physiol*. 1981;240(5). doi:10.1152/AJPCELL.1981.240.5.C222
29. Sweeney HL, Stull JT. Alteration of cross-bridge kinetics by myosin light chain phosphorylation in rabbit skeletal muscle: implications for regulation of actin-myosin interaction. *Proc Natl Acad Sci U S A*. 1990;87(1):414-418. doi:10.1073/PNAS.87.1.414
30. Campbell KS. Super-relaxation helps muscles work more efficiently. *Journal of Physiology*. 2017;595(4):1007-1008. doi:10.1113/JP273629
31. Mello RN, Laden A, Harris R, Anderson LJ, Thomas DD. Myosin Crosslinking and EPR Capture the Start of Force Generation in Muscle Fibers. *Biophys J*. 2010;98(3):347a. doi:10.1016/j.bpj.2009.12.1878
32. Lai S, Collins BC, Colson BA, Kararigas G, Lowe DA. Estradiol modulates myosin regulatory light chain phosphorylation and contractility in skeletal muscle of female mice. *American Journal of Physiology-Endocrinology and Metabolism*. 2016;310(9):E724-E733. doi:10.1152/ajpendo.00439.2015
33. Phung LA, Karvinen SM, Colson BA, Thomas DD, Lowe DA. Age affects myosin relaxation states in skeletal muscle fibers of female but not male mice. *PLoS One*. 2018;13(9):1-15. doi:10.1371/journal.pone.0199062
34. Miller MS, Bedrin NG, Callahan DM, et al. Age-related slowing of myosin actin cross-bridge kinetics is sex specific and predicts decrements in whole skeletal muscle performance in humans. *J Appl Physiol*. Published online 2013. doi:10.1152/japplphysiol.00563.2013
35. Lieber RL, Roberts TJ, Blemker SS, Lee SSM, Herzog W. Skeletal muscle mechanics, energetics and plasticity. *J Neuroeng Rehabil*. 2017;14(1). doi:10.1186/s12984-017-0318-y
36. Pette D, Staron RS. Myosin isoforms, muscle fiber types, and transitions. *Microsc Res Tech*. 2000;50(6):500-509. doi:10.1002/1097-0029(20000915)50:6<500::AID-JEMT7>3.0.CO;2-7
37. Cooper GM. Actin, Myosin, and Cell Movement. Published online 2000.
38. Fitts RH. The cross-bridge cycle and skeletal muscle fatigue. *J Appl Physiol*. 2008;104(2):551-558. doi:10.1152/JAPPLPHYSIOL.01200.2007/ASSET/IMAGES/LARGE/ZDG00030877640003.JPEG
39. Nag S, Trivedi D V. To lie or not to lie: Super-relaxing with myosins. *Elife*. 2021;10. doi:10.7554/elife.63703
40. Yadav L, Tamene F, Göös H, et al. Systematic Analysis of Human Protein Phosphatase Interactions and Dynamics. *Cell Syst*. 2017;4(4):430-444.e5. doi:10.1016/j.cels.2017.02.011
41. Kast D, Blakely SE, Svensson B, et al. *Measuring Myosin Light Chain Domain Orientation in the Pre-Power Stroke AlF 4 States with a Bifunctional Spin Label in Skinned Muscle Fibers Probing The Divalent Cation-Binding Region Of The*

Myosin Regulatory Light Chain During Muscle Contraction Using EP.; 2009.
42. Stewart MA, Franks-Skiba K, Chen S, Cooke R. Myosin ATP turnover rate is a mechanism involved in thermogenesis in resting skeletal muscle fibers. *Proc Natl Acad Sci U S A*. 2010;107(1):430-435. doi:10.1073/pnas.0909468107
43. Zhao FQ, Craig R, Woodhead JL. Head-head interaction characterizes the relaxed state of Limulus muscle myosin filaments. *J Mol Biol*. 2009;385(2):423-431. doi:10.1016/J.JMB.2008.10.038
44. Woodhead JL, Zhao FQ, Craig R. Structural basis of the relaxed state of a Ca2+-regulated myosin filament and its evolutionary implications. *Proc Natl Acad Sci U S A*. 2013;110(21):8561-8566. doi:10.1073/pnas.1218462110
45. Colson BA, Petersen KJ, Collins BC, Lowe DA, Thomas DD. The myosin super-relaxed state is disrupted by estradiol deficiency. *Biochem Biophys Res Commun*. Published online 2015. doi:10.1016/j.bbrc.2014.11.050
46. Fillion M, Tiidus PM, Vandenboom R. Lack of influence of estrogen on myosin phosphorylation and post-tetanic potentiation in muscles from young adult c57bl mice. *Can J Physiol Pharmacol*. 2019;97(8):729-737. doi:10.1139/cjpp-2018-0575
47. Volpi E, Nazemi R, Fujita S. Muscle tissue changes with aging. *Curr Opin Clin Nutr Metab Care*. 2004;7(4):405. doi:10.1097/01.MCO.0000134362.76653.B2
48. Yu SCY, Khow KSF, Jadczak AD, Visvanathan R. Clinical Screening Tools for Sarcopenia and Its Management. *Curr Gerontol Geriatr Res*. 2016;2016. doi:10.1155/2016/5978523
49. Lang T, Streeper T, Cawthon P, Baldwin K, Taaffe DR, Harris TB. Sarcopenia: Etiology, clinical consequences, intervention, and assessment. *Osteoporosis International*. 2010;21(4):543-559. doi:10.1007/s00198-009-1059-y
50. Narici M V., Maffulli N. Sarcopenia: Characteristics, mechanisms and functional significance. *Br Med Bull*. 2010;95(1):139-159. doi:10.1093/bmb/ldq008
51. Janssen I, Heymsfield SB, Wang ZM, Ross R. Skeletal muscle mass and distribution in 468 men and women aged 18-88 yr. *J Appl Physiol*. 2000;89(1):81-88. doi:10.1152/jappl.2000.89.1.81
52. Kawakami Y, Akima H, Kubo K, et al. Changes in muscle size, architecture, and neural activation after 20 days of bed rest with and without resistance exercise. *Eur J Appl Physiol*. 2001;84(1-2):7-12. doi:10.1007/s004210000330
53. Vang P, Vasdev A, Zhan WZ, Gransee HM, Sieck GC, Mantilla CB. Diaphragm muscle sarcopenia into very old age in mice. *Physiol Rep*. 2020;8(1). doi:10.14814/phy2.14305
54. Mitchell WK, Williams J, Atherton P, Larvin M, Lund J, Narici M. Sarcopenia, dynapenia, and the impact of advancing age on human skeletal muscle size and strength; a quantitative review. *Front Physiol*. Published online 2012. doi:10.3389/fphys.2012.00260

55. Carter EE, Thomas MM, Murynka T, et al. Slow twitch soleus muscle is not protected from sarcopenia in senescent rats. *Exp Gerontol*. 2010;45(9):662-670. doi:10.1016/j.exger.2010.04.001
56. Miller MS, Callahan DM, Toth MJ. Skeletal muscle myofilament adaptations to aging, disease and disuse and their effects on whole muscle performance in older adult humans. *Front Physiol*. Published online 2014. doi:10.3389/fphys.2014.00369
57. Nilwik R, Snijders T, Leenders M, et al. The decline in skeletal muscle mass with aging is mainly attributed to a reduction in type II muscle fiber size. *Exp Gerontol*. 2013;48(5):492-498. doi:10.1016/j.exger.2013.02.012
58. Agostini D, Zeppa SD, Lucertini F, et al. Muscle and bone health in postmenopausal women: Role of protein and vitamin d supplementation combined with exercise training. *Nutrients*. 2018;10(8). doi:10.3390/nu10081103
59. Goodpaster BH, Park SW, Harris TB, et al. The Loss of Skeletal Muscle Strength, Mass, and Quality in Older Adults: The Health, Aging and Body Composition Study. *J Gerontol A Biol Sci Med Sci*. 2011;61(10):1059-1064. doi:10.1093/gerona/61.10.1059
60. Samson MM, Meeuwsen IBAE, Crowe A, Dessens JAG, Duursma SA, Verhaar HJJ. Relationships between physical performance measures, age, height and body weight in healthy adults. *Age Ageing*. 2000;29(3):235-242. doi:10.1093/ageing/29.3.235
61. Haynes E, Neubauer N, Cornett K, BP O, Jones G, Jakobi J. Age and Sex-Related Decline of Muscle Strength Across the Adult Lifespan: A scoping review of aggregated data. :1-41.
62. Miller MS, Farman GP, Braddock JM, et al. Regulatory light chain phosphorylation and N-terminal extension increase cross-bridge binding and power output in Drosophila at in vivo myofilament lattice spacing. *Biophys J*. 2011;100(7):1737-1746. doi:10.1016/j.bpj.2011.02.028
63. Gregorich ZR, Peng Y, Cai W, et al. Top-down targeted proteomics reveals decrease in myosin regulatory light-chain phosphorylation that contributes to sarcopenic muscle dysfunction. *J Proteome Res*. 2016;15(8):2706-2716. doi:10.1021/acs.jproteome.6b00244
64. Thompson L V. Age-related muscle dysfunction. *Exp Gerontol*. 2008;44:106-111. doi:10.1016/j.exger.2008.05.003
65. Waldman S, Terzic A. *Pharmacology and Therapeutics - 1st Edition*.; 2008.
66. Cheskis BJ, Greger JG, Nagpal S, Freedman LP. Signaling by estrogens. *J Cell Physiol*. 2007;213(3):610-617. doi:10.1002/jcp.21253
67. Prossnitz ER, Barton M. The G-protein-coupled estrogen receptor GPER in health and disease. *Nat Rev Endocrinol*. 2011;7(12):715-726. doi:10.1038/nrendo.2011.122
68. Vrtačnik P, Ostanek B, Mencej-Bedrač S, Marc J. The many faces of estrogen signaling. *Biochem Med (Zagreb)*. 2014;24(3):329-342. doi:10.11613/BM.2014.035

69. Cui J, Shen Y, Li R. Estrogen synthesis and signaling pathways during aging: From periphery to brain. *Trends Mol Med*. 2013;19(3):197-209. doi:10.1016/j.molmed.2012.12.007
70. Kuhl H. Pharmacology of estrogens and progestogens: Influence of different routes of administration. *Climacteric*. 2005;8(SUPPL. 1):3-63. doi:10.1080/13697130500148875
71. Prossnitz ER, Arterburn JB, Sklar LA. *GPR30: A G Protein-Coupled Receptor for Estrogen*.
72. Simpson ER. Sources of estrogen and their importance. In: *Journal of Steroid Biochemistry and Molecular Biology*. Vol 86. Elsevier Ltd; 2003:225-230. doi:10.1016/S0960-0760(03)00360-1
73. Nelson JF, Felicio LS, Osterburg HH, Finch CE. Altered Profiles of Estradiol and Progesterone Associated with Prolonged Estrous Cycles and Persistent Vaginal Cornification in Aging C578L/6J Mice1. *Biol Reprod*. Published online 1981. doi:10.1095/biolreprod24.4.784
74. Ajayi AF, Akhigbe RE. Staging of the estrous cycle and induction of estrus in experimental rodents: an update. *Fertil Res Pract*. 2020;6(1). doi:10.1186/s40738-020-00074-3
75. Lab J. Biology of the Laboratory Mouse. *Arch Intern Med*. 1941;68(2):373. doi:10.1001/archinte.1941.00200080195019
76. Koebele S V., Bimonte-Nelson HA. Modeling menopause: The utility of rodents in translational behavioral endocrinology research. *Maturitas*. 2016;87:5-17. doi:10.1016/j.maturitas.2016.01.015
77. Buckler H. The menopause transition: Endocrine changes and clinical symptoms. *Journal of the British Menopause Society*. 2005;11(2):61-65. doi:10.1258/136218005775544525
78. Burger HG. Hormonal Changes in the Menopause Transition. *Recent Prog Horm Res*. Published online 2002. doi:10.1210/rp.57.1.257
79. Brinton RD. Minireview: Translational animal models of human menopause: Challenges and emerging opportunities. *Endocrinology*. 2012;153(8):3571-3578. doi:10.1210/en.2012-1340
80. Marczell I, Balogh P, Nyiro G, et al. Membrane-bound estrogen receptor alpha initiated signaling is dynamin dependent in breast cancer cells. *Eur J Med Res*. 2018;23(1). doi:10.1186/s40001-018-0328-7
81. Amenyogbe E, Chen G, Wang Z, Lu X, Lin M, Lin AY. A Review on Sex Steroid Hormone Estrogen Receptors in Mammals and Fish. *Int J Endocrinol*. 2020;2020. doi:10.1155/2020/5386193
82. Enns DL, Tiidus PM. *The Influence of Estrogen on Skeletal Muscle Sex Matters*.
83. Collins BC, Laakkonen EK, Lowe DA. Aging of the musculoskeletal system: How the loss of estrogen impacts muscle strength. *Bone*. 2019;123:137-144. doi:10.1016/j.bone.2019.03.033
84. Greising SM. Beneficial Effects of Estradiol on Murine Skeletal Muscle Function. 2011;(January).

85. Enns DL, Tiidus PM. The influence of estrogen on skeletal muscle: Sex matters. *Sports Medicine*. 2010;40(1):41-58. doi:10.2165/11319760-000000000-00000
86. Molina JR, Barton DL, Loprinzi CL. Chemotherapy-induced ovarian failure: Manifestations and management. *Drug Saf*. 2005;28(5):401-416. doi:10.2165/00002018-200528050-00004
87. Siddle N, Sarrel P, Whitehead M. The effect of hysterectomy on the age at ovarian failure, identification of a subgroup of women with premature loss of ovarian function and literature review. *Fertil Steril*. 1987;47(1):94-100. doi:10.1016/S0015-0282(16)49942-5
88. Nelson LM. Primary ovarian insufficiency. *New England Journal of Medicine*. 2009;360(6):606. doi:10.1056/nejmcp0808697
89. Maltais ML, Desroches J, Dionne IJ. Changes in muscle mass and tissue subcharacteristics after menopause. *J Musculoskelet Neuronal Interact*. 2009;9(October):186-197. doi:10.1130/SPE252-p29
90. Jubrias SA, Odderson IR, Esselman PC, Conley KE. Decline in isokinetic force with age: Muscle cross-sectional area and specific force. *Pflugers Arch*. 1997;434(3):246-253. doi:10.1007/s004240050392
91. Asikainen TM, Kukkonen-Harjula K, Miilunpalo S. Exercise for Health for Early Postmenopausal Women. *Sports Medicine*. 2004;34(11):753-778. doi:10.2165/00007256-200434110-00004
92. Phillips SK, Rook KM, Siddle NC, Bruce SA, Woledge RC. Muscle weakness in women occurs at an earlier age than in men, but strength is preserved by hormone replacement therapy. *Clin Sci*. 1993;84(1):95-98. doi:10.1042/cs0840095
93. Meeuwsen IB, Samson MM, Verhaar HJ. Evaluation of the applicability of HRT as a preservative of muscle strength in women. *Maturitas*. 2000;36(1):49-61. doi:10.1016/S0378-5122(00)00132-8
94. Phillips SK, Rook KM, Siddle NC, Bruce SA, Woledge RC. Muscle weakness in women occurs at an earlier age than in men, but strength is preserved by hormone replacement therapy. *Clin Sci*. 1993;84(1):95-98. doi:10.1042/cs0840095
95. Greising SM, Baltgalvis KA, Lowe DA, Warren GL. Hormone therapy and skeletal muscle strength: A meta-analysis. *Journals of Gerontology - Series A Biological Sciences and Medical Sciences*. 2009;64(10):1071-1081. doi:10.1093/gerona/glp082
96. Hart GW, Ball LE. Post-translational modifications: A major focus for the future of proteomics. *Molecular and Cellular Proteomics*. 2013;12(12):3443. doi:10.1074/mcp.E113.036491
97. Conibear AC. Deciphering protein post-translational modifications using chemical biology tools. *Nat Rev Chem*. 2020;4(12):674-695. doi:10.1038/s41570-020-00223-8
98. Chen BJ, Lam TC, Liu LQ, To CH. Post-translational modifications and their applications in eye research (review). *Mol Med Rep*. 2017;15(6):3923-3935. doi:10.3892/mmr.2017.6529

99. Ubersax JA, Ferrell JE. Mechanisms of specificity in protein phosphorylation. *Nat Rev Mol Cell Biol*. 2007;8(7):530-541. doi:10.1038/nrm2203
100. Mann M, Jensen ON. *Proteomic Analysis of Post-Translational Modifications*.; 2003. http://www.nature.com/naturebiotechnology
101. Cohen P. The role of protein phosphorylation in human health and disease: Delivered on June 30th 2001 at the FEBS meeting in Lisbon. *Eur J Biochem*. 2001;268(19):5001-5010. doi:10.1046/j.0014-2956.2001.02473.x
102. Lemeer S, Heck AJ. The phosphoproteomics data explosion. *Curr Opin Chem Biol*. 2009;13(4):414-420. doi:10.1016/j.cbpa.2009.06.022
103. Pan N, Liu P, Cui W, Tang B, Shi J, Chen H. Highly efficient ionization of phosphopeptides at low pH by desorption electrospray ionization mass spectrometry. *Analyst*. 2013;138(5):1321-1324. doi:10.1039/c3an36737a
104. Tsiatsiani L, Heck AJR. Proteomics beyond trypsin. *FEBS Journal*. 2015;282(14):2612-2626. doi:10.1111/febs.13287
105. Jedrychowski MP, Huttlin EL, Haas W, Sowa ME, Rad R, Gygi SP. Evaluation of HCD- and CID-type fragmentation within their respective detection platforms for murine phosphoproteomics. *Molecular and Cellular Proteomics*. 2011;10(12). doi:10.1074/mcp.M111.009910
106. Nagaraj N, D'Souza RCJ, Cox J, Olsen J V., Mann M. Feasibility of large-scale phosphoproteomics with higher energy collisional dissociation fragmentation. *J Proteome Res*. 2010;9(12):6786-6794. doi:10.1021/pr100637q
107. Gannon J, Staunton L, O'Connell K, Doran P, Ohlendieck K. Phosphoproteomic analysis of aged skeletal muscle. *Int J Mol Med*. 2008;22(1):33-42. doi:10.3892/ijmm.22.1.33
108. Højlund K, Bowen BP, Hwang H, et al. In vivo phosphoproteome of human skeletal muscle revealed by phosphopeptide enrichment and HPLC-ESI-MS/MS. *J Proteome Res*. 2009;8(11):4954-4965. doi:10.1021/pr9007267
109. Miller MS, Bedrin NG, Callahan DM, et al. Age-related slowing of myosin actin cross-bridge kinetics is sex specific and predicts decrements in whole skeletal muscle performance in humans. *J Appl Physiol*. 2013;115:1004-1014. doi:10.1152/japplphysiol.00563.2013.-We
110. Gregorich ZR, Peng Y, Cai W, et al. Top-down targeted proteomics reveals decrease in myosin regulatory light-chain phosphorylation that contributes to sarcopenic muscle dysfunction. *J Proteome Res*. 2016;15(8):2706-2716. doi:10.1021/acs.jproteome.6b00244
111. Kalyani RR, Corriere M, Ferrucci L. Age-related and disease-related muscle loss: the effect of diabetes, obesity, and other diseases. *Lancet Diabetes Endocrinol*. 2014;2(10):819. doi:10.1016/S2213-8587(14)70034-8
112. Cruz-Jentoft AJ, Bahat G, Bauer J, et al. Sarcopenia: Revised European consensus on definition and diagnosis. *Age Ageing*. 2019;48(1):16-31. doi:10.1093/ageing/afy169

113. Santilli V, Bernetti A, Mangone M, Paoloni M. Clinical definition of sarcopenia. *Clinical Cases in Mineral and Bone Metabolism*. 2014;11(3):177-180. doi:10.11138/ccmbm/2014.11.3.177
114. Haynes E, Neubauer N, Cornett K, BP O, Jones G, Jakobi J. Age and Sex-Related Decline of Muscle Strength Across the Adult Lifespan: A scoping review of aggregated data. :1-41.
115. Wattanapermpool J, Reiser PJ. Differential effects of ovariectomy on calcium activation of cardiac and soleus myofilaments. *Am J Physiol Heart Circ Physiol*. 1999;277(2 46-2):467-473. doi:10.1152/ajpheart.1999.277.2.h467
116. Qaisar R, Renaud G, Hedstrom Y, et al. Hormone replacement therapy improves contractile function and myonuclear organization of single muscle fibres from postmenopausal monozygotic female twin pairs. *Journal of Physiology*. Published online 2013. doi:10.1113/jphysiol.2012.250092
117. Xu M, Chen X, Chen D, Yu B, Huang Z. FoxO1: a novel insight into its molecular mechanisms in the regulation of skeletal muscle differentiation and fiber type specification. *Oncotarget*. 2017;8(6):10662. doi:10.18632/ONCOTARGET.12891
118. Schiaffino S, Mammucari C. Regulation of skeletal muscle growth by the IGF1-Akt/PKB pathway: Insights from genetic models. *Skelet Muscle*. 2011;1(1):1-14. doi:10.1186/2044-5040-1-4/FIGURES/4
119. Pallafacchina G, Calabria E, Serrano AL, Kalhovde JM, Schiaffino S. A protein kinase B-dependent and rapamycin-sensitive pathway controls skeletal muscle growth but not fiber type specification. *Proceedings of the National Academy of Sciences*. 2002;99(14):9213-9218. doi:10.1073/PNAS.142166599
120. Glass DJ. PI3 Kinase Regulation of Skeletal Muscle Hypertrophy and Atrophy. Published online 2010:267-278. doi:10.1007/82_2010_78
121. Silveira WA, Gonçalves DA, Machado J, et al. cAMP-dependent protein kinase inhibits FoxO activity and regulates skeletal muscle plasticity in mice. *The FASEB Journal*. 2020;34(9):12946-12962. doi:10.1096/FJ.201902102RR
122. Baruffaldi F, Montarras D, Basile V, et al. Dynamic Phosphorylation of the Myocyte Enhancer Factor 2Cα1 Splice Variant Promotes Skeletal Muscle Regeneration and Hypertrophy. *Stem Cells*. 2017;35(3):725-738. doi:10.1002/STEM.2495
123. Ramila KC, Jong CJ, Pastukh V, Ito T, Azuma J, Schaffer SW. Role of protein phosphorylation in excitation-contraction coupling in taurine deficient hearts. *https://doi.org/101152/ajpheart004972014*. 2015;308(3):H232-H239. doi:10.1152/AJPHEART.00497.2014
124. Vandenboom R. Modulation of skeletal muscle contraction by myosin phosphorylation. *Compr Physiol*. 2017;7(1):171-212. doi:10.1002/cphy.c150044
125. Szczesna D, Zhao J, Jones M, et al. Phosphorylation of the regulatory light chains of myosin affects Ca 2 sensitivity

of skeletal muscle contraction. *J Appl Physiol*. 2002;92:1661-1670. doi:10.1152/japplphysiol.00858.2001.-The
126. Ryder JW, Lau KS, Kamm KE, Stull JT. Enhanced Skeletal Muscle Contraction with Myosin Light Chain Phosphorylation by a Calmodulin-sensing Kinase. *Journal of Biological Chemistry*. 2007;282(28):20447-20454. doi:10.1074/JBC.M702927200
127. Kararigas G, Bito V, Tinel H, et al. Transcriptome characterization of estrogen-treated human myocardium identifies myosin regulatory light chain interacting protein as a sex-specific element influencing contractile function. *J Am Coll Cardiol*. 2012;59(4):410-417. doi:10.1016/j.jacc.2011.09.054
128. Duft K, Schanz M, Pham H, et al. 17β-Estradiol-induced interaction of estrogen receptor α and human atrial essential myosin light chain modulates cardiac contractile function. *Basic Res Cardiol*. 2017;112(1). doi:10.1007/s00395-016-0590-1
129. Gregorevic P, Plant DR, Stupka N, Lynch GS. Changes in contractile activation characteristics of rat fast and slow skeletal muscle fibres during regeneration. *Journal of Physiology*. 2004;558(2):549-560. doi:10.1113/jphysiol.2004.066217
130. Miller MS, Bedrin NG, Callahan DM, et al. Age-related slowing of myosin actin cross-bridge kinetics is sex specific and predicts decrements in whole skeletal muscle performance in humans. *J Appl Physiol*. 2013;115(7):1004-1014. doi:10.1152/japplphysiol.00563.2013
131. Ingalls CR, Warren GL, Lowe DA, Boorstein DB, Armstrong RB. Differential effects of anesthetics on in vivo skeletal muscle contractile function in the mouse. *J Appl Physiol (1985)*. 1996;80(1):332-340. doi:10.1152/JAPPL.1996.80.1.332
132. Rappsilber J, Ishihama Y, Mann M. Stop and Go Extraction Tips for Matrix-Assisted Laser Desorption/Ionization, Nanoelectrospray, and LC/MS Sample Pretreatment in Proteomics. *Anal Chem*. 2002;75(3):663-670. doi:10.1021/AC026117I
133. Wu T, Hu E, Xu S, et al. clusterProfiler 4.0: A universal enrichment tool for interpreting omics data. *The Innovation*. 2021;2:100141. doi:10.1016/j.xinn.2021.100141
134. Yu G, Wang LG, Han Y, He QY. ClusterProfiler: An R package for comparing biological themes among gene clusters. *OMICS*. 2012;16(5):284-287. doi:10.1089/OMI.2011.0118
135. Yu G, He QY. ReactomePA: an R/Bioconductor package for reactome pathway analysis and visualization. *Mol Biosyst*. 2016;12(2):477-479. doi:10.1039/C5MB00663E
136. Ardito F, Giuliani M, Perrone D, Troiano G, Muzio L lo. The crucial role of protein phosphorylation in cell signalingand its use as targeted therapy (Review). *Int J Mol Med*. 2017;40(2):271-280. doi:10.3892/ijmm.2017.3036
137. Potts GK, McNally RM, Blanco R, et al. A map of the phosphoproteomic alterations that occur after a bout of

maximal-intensity contractions. *Journal of Physiology*. 2017;595(15):5209-5226. doi:10.1113/JP273904
138. Deshmukh AS, Murgia M, Nagaraj N, Treebak JT, Cox J, Mann M. Deep proteomics of mouse skeletal muscle enables quantitation of protein isoforms, metabolic pathways, and transcription factors. *Molecular and Cellular Proteomics*. 2015;14(4):841-853. doi:10.1074/mcp.M114.044222
139. Yuen M, Cooper ST, Marston SB, et al. Muscle weakness in TPM3-myopathy is due to reduced Ca2+-sensitivity and impaired acto-myosin cross-bridge cycling in slow fibres. *Hum Mol Genet*. 2015;24(22):6278. doi:10.1093/HMG/DDV334
140. Marttila M, Lehtokari VL, Marston S, et al. Mutation Update and Genotype-Phenotype Correlations of Novel and Previously Described Mutations in TPM2 and TPM3 Causing Congenital Myopathies. *Hum Mutat*. 2014;35(7):779-790. doi:10.1002/humu.22554
141. Weisleder N, Ma J. Altered Ca2+ sparks in aging skeletal and cardiac muscle. *Ageing Res Rev*. 2008;7(3):177. doi:10.1016/J.ARR.2007.12.003
142. Renganathan M, Messi ML, Delbono O. Dihydropyridine receptor-ryanodine receptor uncoupling in aged skeletal muscle. *J Membr Biol*. 1997;157(3):247-253. doi:10.1007/S002329900233
143. Fodor J, Al-Gaadi D, Czirják T, et al. Improved Calcium Homeostasis and Force by Selenium Treatment and Training in Aged Mouse Skeletal Muscle. *Scientific Reports 2020 10:1*. 2020;10(1):1-14. doi:10.1038/s41598-020-58500-x
144. Herraiz-Martínez A, Álvarez-García J, Llach A, et al. Ageing is associated with deterioration of calcium homeostasis in isolated human right atrial myocytes. *Cardiovasc Res*. 2015;106(1):76. doi:10.1093/CVR/CVV046
145. Demion M, Gueffier M, Thireau J, et al. Ageing causes a progressive loss of L-type calcium current and a depression of the SR calcium content linked to lower SERCA2 and calsequestrin-2 expression in human atrial myocytes. *Eur Heart J*. 2013;34(suppl_1):P5018-P5018. doi:10.1093/EURHEARTJ/EHT310.P5018
146. Law ML, Cohen H, Martin AA, Angulski ABB, Metzger JM. Dysregulation of Calcium Handling in Duchenne Muscular Dystrophy-Associated Dilated Cardiomyopathy: Mechanisms and Experimental Therapeutic Strategies. *Journal of Clinical Medicine 2020, Vol 9, Page 520*. 2020;9(2):520. doi:10.3390/JCM9020520
147. Fares E, Pyle WG, Ray G, et al. The Impact of Ovariectomy on Calcium Homeostasis and Myofilament Calcium Sensitivity in the Aging Mouse Heart. *PLoS One*. 2013;8(9):e74719. doi:10.1371/JOURNAL.PONE.0074719
148. Zügel M, Wehrstein F, Qiu S, Diel P, Steinacker JM, Schumann U. Moderate intensity continuous training reverses the detrimental effects of ovariectomy on RyR1 phosphorylation in rat skeletal muscle. *Mol Cell Endocrinol*. 2019;481:1-7. doi:10.1016/J.MCE.2018.11.003

149. Li X, Fan L, Zhu M, Jiang H, Bai W, Kang J. Combined intervention of 17β-estradiol and treadmill training ameliorates energy metabolism in skeletal muscle of female ovariectomized mice. *Climacteric*. 2020;23(2):192-200. doi:10.1080/13697137.2019.1660639
150. Beckett T, Tchernof A, Toth MJ. Effect of ovariectomy and estradiol replacement on skeletal muscle enzyme activity in female rats. *Metabolism*. 2002;51(11):1397-1401. doi:10.1053/META.2002.35592
151. Sutham W, Sripetchwandee J, Minta W, et al. Ovariectomy and obesity have equal impact in causing mitochondrial dysfunction and impaired skeletal muscle contraction in rats. *Menopause*. 2018;25(12):1448-1458. doi:10.1097/GME.0000000000001149
152. Capllonch-Amer G, Sbert-Roig M, Galmés-Pascual BM, et al. Estradiol stimulates mitochondrial biogenesis and adiponectin expression in skeletal muscle. *Journal of Endocrinology*. 2014;221(3):391-403. doi:10.1530/JOE-14-0008
153. Cavalcanti-De-Albuquerque JPA, Salvador IC, Martins EL, et al. Role of estrogen on skeletal muscle mitochondrial function in ovariectomized rats: A time course study in different fiber types. *J Appl Physiol*. 2014;116(7):779-789. doi:10.1152/JAPPLPHYSIOL.00121.2013/ASSET/IMAGES/LARGE/ZDG00061409870009.JPEG
154. Jackson KC, Wohlers LM, Lovering RM, et al. Ectopic lipid deposition and the metabolic profile of skeletal muscle in ovariectomized mice. *Am J Physiol Regul Integr Comp Physiol*. 2013;304(3). doi:10.1152/AJPREGU.00428.2012
155. Imai K, Hao F, Fujita N, et al. Atg9A trafficking through the recycling endosomes is required for autophagosome formation. *J Cell Sci*. 2016;129(20):3781-3791. doi:10.1242/JCS.196196/265252/AM/ATG9A-TRAFFICKING-THROUGH-THE-RECYCLING-ENDOSOMES
156. Masiero E, Agatea L, Mammucari C, et al. Autophagy is required to maintain muscle mass. *Cell Metab*. 2009;10(6):507-515. doi:10.1016/J.CMET.2009.10.008
157. Masiero E, Sandri M. Autophagy inhibition induces atrophy and myopathy in adult skeletal muscles. *Autophagy*. 2010;6(2):307-309. doi:10.4161/auto.6.2.11137
158. Greising SM, Carey RS, Blackford JE, Dalton LE, Kosir AM, Lowe DA. Estradiol treatment, physical activity, and muscle function in ovarian-senescent mice. *Exp Gerontol*. 2011;46(8):685-693. doi:10.1016/j.exger.2011.04.006
159. Vang P, Baumann CW, Barok R, Larson AA, Dougherty BJ, Lowe DA. Impact of estrogen deficiency on diaphragm and leg muscle contractile function in female mdx mice. Wiche G, ed. *PLoS One*. 2021;16(3):e0249472. doi:10.1371/journal.pone.0249472
160. Sotiriadou S, Kyparos A, Albani M, et al. Soleus muscle force following downhill running in ovariectomized rats treated with estrogen. *Applied Physiology, Nutrition and Metabolism*. 2006;31(4):449-459. doi:10.1139/H06-008

161. Kitajima Y, Ono Y. Estrogens maintain skeletal muscle and satellite cell functions. *Journal of Endocrinology*. 2016;229(3):267-275. doi:10.1530/joe-15-0476
162. Gayi E, Ismail H, Neff L, et al. Lack of estrogens impairs motor function and muscle structure in dystrophic mice. *Neuromuscular Disorders*. 2016;26(2016):S130. doi:10.1016/j.nmd.2016.06.162
163. Wohlers LM, Sweeney SM, Ward CW, Lovering RM, Spangenburg EE. Changes in contraction-induced phosphorylation of AMP-activated protein kinase and mitogen-activated protein kinases in skeletal muscle after ovariectomy. *J Cell Biochem*. 2009;107(1):171-178. doi:10.1002/jcb.22113
164. Judson RN, Gray SR, Walker C, et al. Constitutive Expression of Yes-Associated Protein (Yap) in Adult Skeletal Muscle Fibres Induces Muscle Atrophy and Myopathy. *PLoS One*. 2013;8(3):e59622. doi:10.1371/JOURNAL.PONE.0059622
165. Watt KI, Turner BJ, Hagg A, et al. The Hippo pathway effector YAP is a critical regulator of skeletal muscle fibre size. *Nature Communications 2015 6:1*. 2015;6(1):1-13. doi:10.1038/ncomms7048
166. Goodman CA, Dietz JM, Jacobs BL, McNally RM, You JS, Hornberger TA. Yes-associated protein is up-regulated by mechanical overload and is sufficient to induce skeletal muscle hypertrophy. *FEBS Lett*. 2015;589(13):1491. doi:10.1016/J.FEBSLET.2015.04.047
167. Dupont S, Morsut L, Aragona M, et al. Role of YAP/TAZ in mechanotransduction. *Nature 2011 474:7350*. 2011;474(7350):179-183. doi:10.1038/nature10137
168. Fischer M, Rikeit P, Knaus P, Coirault C. YAP-Mediated Mechanotransduction in Skeletal Muscle. *Front Physiol*. 2016;7(FEB):41. doi:10.3389/FPHYS.2016.00041
169. Muttukrishna S, Sharma S, Barlow DH, Ledger W, Groome N, Sathanandan M. Serum inhibins, estradiol, progesterone and FSH in surgical menopause: a demonstration of ovarian pituitary feedback loop in women. *Human Reproduction*. 2002;17(10):2535-2539. Accessed July 31, 2022. https://academic.oup.com/humrep/article/17/10/2535/607722
170. Czieselsky K, Prescott M, Porteous R, et al. Pulse and Surge Profiles of Luteinizing Hormone Secretion in the Mouse. *Endocrinology*. 2016;157(12):4794-4802. doi:10.1210/EN.2016-1351
171. Kotsopoulos J, Shafrir AL, Rice M, et al. The Relationship Between Bilateral Oophorectomy and Plasma Hormone Levels in Postmenopausal Women. *Horm Cancer*. 2015;6(1):54-63. doi:10.1007/S12672-014-0209-7/TABLES/3
172. Flores A, Gallegos AI, Velasco J, et al. The acute effects of bilateral ovariectomy or adrenalectomy on progesterone, testosterone and estradiol serum levels depend on the surgical approach and the day of the estrous cycle when they are performed. *Reproductive Biology and Endocrinology*. 2008;6(1):1-7. doi:10.1186/1477-7827-6-48/FIGURES/3

173. Hendrix SL. Bilateral oophorectomy and premature menopause. *Am J Med*. 2005;118(12):131-135. doi:10.1016/J.AMJMED.2005.09.056
174. Wise PM, Rainer A. Effect of ovariectomy on plasma LH, FSH, estradiol, and progesterone and medial basal hypothalamic LHRH concentrations old and young rats. *Neuroendocrinology*. 1980;30(1):15-19. doi:10.1159/000122968
175. Haynes EMK, Neubauer N, Cornett KM, O'Connor BP, Jones GR, Jakobi JM. Age and Sex-Related Decline of Muscle Strength Across the Adult Lifespan: A scoping review of aggregated data. *Applied Physiology, Nutrition, and Metabolism*. Published online June 29, 2020:apnm-2020-0081. doi:10.1139/apnm-2020-0081
176. Asikainen TM, Kukkonen-Harjula K, Miilunpalo S. Exercise for health for early postmenopausal women: A systematic review of randomised controlled trials. *Sports Medicine*. 2004;34(11):753-778. doi:10.2165/00007256-200434110-00004
177. Shapiro M. Menopause practice: A clinician's guide, 4th edition. *Canadian Family Physician*. 2012;58(9):989. Accessed April 3, 2021. /pmc/articles/PMC3440278/
178. Arias E, Xu J. *National Vital Statistics Reports Volume 69, Number 12 November 17, 2020 United States Life Tables, 2018*. Vol 69.; 2020. Accessed March 29, 2021. https://www.cdc.gov/nchs/products/index.htm.
179. Sklar CA, Constine LS. Chronic neuroendocrinological sequelae of radiation therapy. *Int J Radiat Oncol Biol Phys*. 1995;31(5):1113-1121. doi:10.1016/0360-3016(94)00427-M
180. Shufelt CL, Torbati T, Dutra E. Hypothalamic Amenorrhea and the Long-Term Health Consequences. *Semin Reprod Med*. 2017;35(3):256-262. doi:10.1055/s-0037-1603581
181. Chan S, Head SI. Age- and Gender-Related Changes in Contractile Properties of Non-Atrophied EDL Muscle. *PLoS One*. 2010;5(8):e12345. doi:10.1371/JOURNAL.PONE.0012345
182. Sipilä S, Finni T, Kovanen V. Estrogen Influences on Neuromuscular Function in Postmenopausal Women. *Behav Genet*. 2015;45(2):222-233. doi:10.1007/s00223-014-9924-x
183. Rader EP, Faulkner JA. Effect of aging on the recovery following contraction-induced injury in muscles of female mice. *J Appl Physiol*. 2006;101(3):887-892. doi:10.1152/japplphysiol.00380.2006
184. Rutherford OM, Jones DA. The relationship of muscle and bone loss and activity levels with age in women. *Age Ageing*. 1992;21(4):286-293. doi:10.1093/ageing/21.4.286
185. Finni T, Noorkoiv M, Pöllänen E, et al. Muscle function in monozygotic female twin pairs discordant for hormone replacement therapy. *Muscle Nerve*. 2011;44(5):769-775. doi:10.1002/mus.22162
186. McClung JM, Davis JM, Wilson MA, Goldsmith EC, Carson JA. Estrogen status and skeletal muscle recovery from disuse atrophy. *J Appl Physiol*. 2006;100(6):2012-2023. doi:10.1152/japplphysiol.01583.2005
187. Le G, Novotny SA, Mader TL, et al. A moderate oestradiol level enhances neutrophil number and activity in muscle

after traumatic injury but strength recovery is accelerated. *Journal of Physiology*. 2018;596(19):4665-4680. doi:10.1113/JP276432
188. Mangan G, Bombardier E, Mitchell AS, Quadrilatero J, Tiidus PM. Oestrogen-dependent satellite cell activation and proliferation following a running exercise occurs via the PI3K signalling pathway and not IGF-1. *Acta Physiologica*. Published online 2014. doi:10.1111/apha.12317
189. Steinert ND, Potts GK, Wilson GM, et al. Mapping of the contraction-induced phosphoproteome identifies TRIM28 as a significant regulator of skeletal muscle size and function. *Cell Rep*. 2021;34(9):108796. doi:10.1016/J.CELREP.2021.108796
190. Potts GK, McNally RM, Blanco R, et al. A map of the phosphoproteomic alterations that occur after a bout of maximal-intensity contractions. *Journal of Physiology*. 2017;595(15):5209-5226. doi:10.1113/JP273904
191. Nelson JF, Felicio LS, Randall PK, Sims C, Finch CE. A longitudinal study of estrous cyclicity in aging C57BL/6J mice: I. Cycle frequency, length and vaginal cytology. *Biol Reprod*. 1982;27(2):327-339. doi:10.1095/biolreprod27.2.327
192. Ardito F, Giuliani M, Perrone D, Troiano G, Muzio L lo. The crucial role of protein phosphorylation in cell signaling and its use as targeted therapy (Review). *Int J Mol Med*. 2017;40(2):271-280. doi:10.3892/IJMM.2017.3036
193. Krä Mer A, Green J, Pollard J, Tugendreich S. Systems biology Causal analysis approaches in Ingenuity Pathway Analysis. 2014;30(4):523-530. doi:10.1093/bioinformatics/btt703
194. Du M, Li X, Zhang D, et al. Phosphorylation plays positive roles in regulating the inhibitory ability of calpastatin to calpain. *Int J Food Sci Technol*. 2022;57(1):370-378. doi:10.1111/IJFS.15437
195. di Lisa F, de Tullio R, Salamino F, et al. Specific degradation of troponin T and I by μ-calpain and its modulation by substrate phosphorylation. *Biochemical Journal*. 1995;308(1):57-61. doi:10.1042/BJ3080057
196. Goll DE, Neti G, Mares SW, Thompson VF. Myofibrillar protein turnover: The proteasome and the calpains,. *J Anim Sci*. 2008;86(suppl_14):E19-E35. doi:10.2527/JAS.2007-0395
197. Kedia N, Arhzaouy K, Pittman SK, et al. Desmin forms toxic, seeding-competent amyloid aggregates that persist in muscle fibers. doi:10.1073/pnas.1908263116
198. Fernando R, Drescher C, Nowotny K, Grune T, Castro JP. Impaired proteostasis during skeletal muscle aging. *Free Radic Biol Med*. 2019;132:58-66. doi:10.1016/J.FREERADBIOMED.2018.08.037
199. Wohlers LM, Sweeney SM, Ward CW, Lovering RM, Spangenburg EE. Changes in contraction-induced phosphorylation of AMP-activated protein kinase and mitogen-activated protein kinases in skeletal muscle after ovariectomy. *J Cell Biochem*. 2009;107(1):171-178. doi:10.1002/JCB.22113

200. Williamson D, Gallagher P, Harber M, Hollon C, Trappe S. Mitogen-activated protein kinase (MAPK) pathway activation: effects of age and acute exercise on human skeletal muscle. *J Physiol*. 2003;547(Pt 3):977. doi:10.1113/JPHYSIOL.2002.036673
201. Ronda AC, Vasconsuelo A, Boland R. Extracellular-regulated kinase and p38 mitogen-activated protein kinases are involved in the antiapoptotic action of 17β-estradiol in skeletal muscle cells. *Journal of Endocrinology*. 2010;206(2):235-246. doi:10.1677/JOE-09-0429
202. Silveira WA, Gonçalves DA, Machado J, et al. cAMP-dependent protein kinase inhibits FoxO activity and regulates skeletal muscle plasticity in mice. *FASEB Journal*. 2020;34(9):12946-12962. doi:10.1096/FJ.201902102RR
203. Privett GE, Needham KW, Ricci AW, Mongold SJ, Callahan DM. Protein Kinase A Modifies Skeletal Muscle Contractile Function Via Modification Of Mybp-C. *Med Sci Sports Exerc*. 2021;53(8S):121-121. doi:10.1249/01.MSS.0000760548.30406.A9
204. Kim SS, Lee EH, Lee K, Jo SH, Seo SR. PKA regulates calcineurin function through the phosphorylation of RCAN1: identification of a novel phosphorylation site. *Biochem Biophys Res Commun*. 2015;459(4):604-609. doi:10.1016/J.BBRC.2015.02.155
205. Sakuma K, Nishikawa J, Nakao R, et al. Calcineurin is a potent regulator for skeletal muscle regeneration by association with NFATc1 and GATA-2. *Acta Neuropathol*. 2003;105(3):271-280. doi:10.1007/S00401-002-0647-0/FIGURES/5
206. Yang Q, Chan P. Skeletal Muscle Metabolic Alternation Develops Sarcopenia. *Aging Dis*. 2022;13(3):801. doi:10.14336/AD.2021.1107
207. Sartori R, Romanello V, Sandri M. Mechanisms of muscle atrophy and hypertrophy: implications in health and disease. *Nature Communications 2021 12:1*. 2021;12(1):1-12. doi:10.1038/s41467-020-20123-1
208. Hudson MB, Price SR. Calcineurin: A Poorly Understood Regulator of Muscle Mass. *Int J Biochem Cell Biol*. 2013;45(10):2173. doi:10.1016/J.BIOCEL.2013.06.029
209. Berdeaux R, Stewart R. cAMP signaling in skeletal muscle adaptation: Hypertrophy, metabolism, and regeneration. *Am J Physiol Endocrinol Metab*. 2012;303(1):1-17. doi:10.1152/AJPENDO.00555.2011/ASSET/IMAGES/LARGE/ZH10091265220005.JPEG
210. Sakuma K, Yamaguchi A. The functional role of calcineurin in hypertrophy, regeneration, and disorders of skeletal muscle. *J Biomed Biotechnol*. 2010;2010. doi:10.1155/2010/721219
211. Olson EN, Williams RS. Calcineurin Signaling and Muscle Remodeling. *Cell*. 2000;101(7):689-692. doi:10.1016/S0092-8674(00)80880-6

APPENDIX

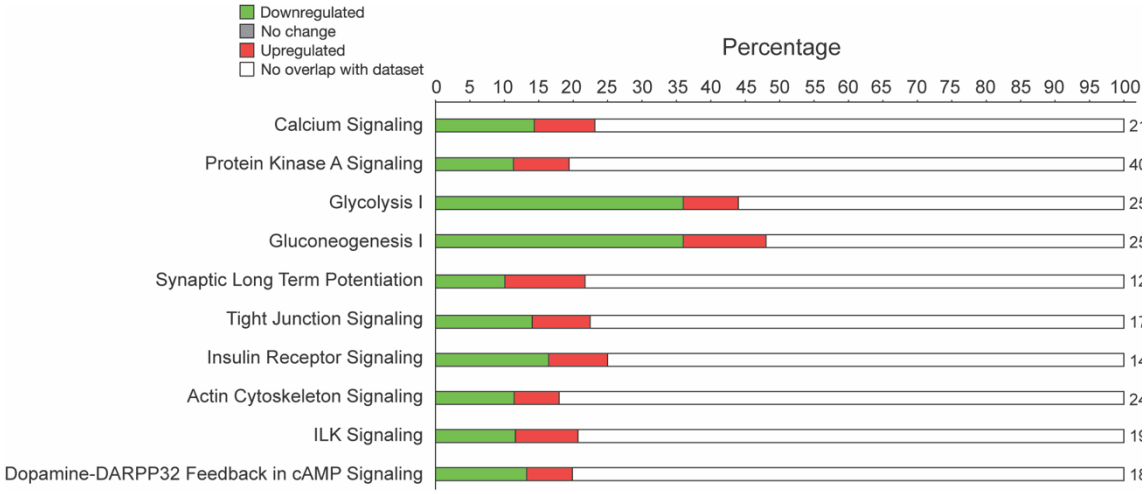

Supplementary Figure 3.1 Distribution of up- and down-regulated molecules that map to IPA's canonical pathways The number of downregulated and upregulated phosphoproteins observed from the dataset were mapped to IPA's annotated canonical pathways. The top 10 canonical pathways are shown. The total number of molecules annotated to the pathway from IPA's Knowledge Base are listed at the end of the stacked bar graph. The green and red bar represents down- or upregulated molecules in Ovx relative to Sham muscle observed in our phosphoproteomics dataset.

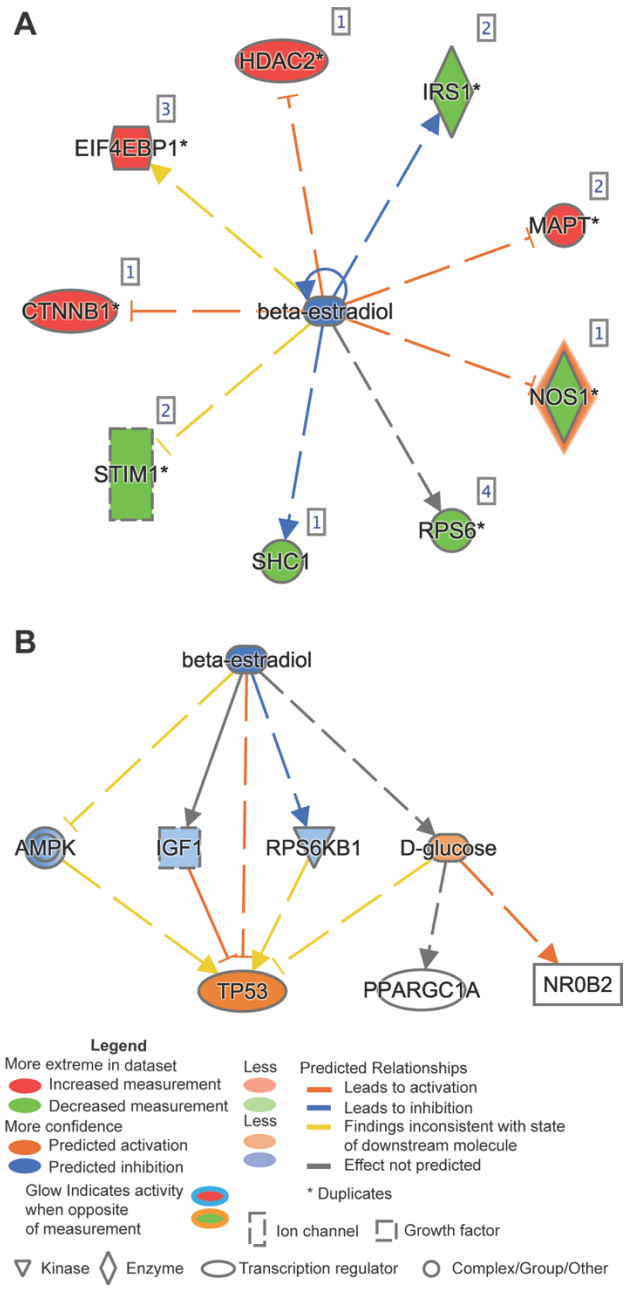

Supplementary Figure 3.2 E2 targets and interactions with upstream regulators. Based on the phosphorylation alterations in the dataset, IPA's prediction algorithm was used to predict the activation state of E2 as an upstream regulator. The number in the upper right box next to the molecule denotes the number of phosphopeptides observed in the dataset for the molecule. (A) E2 targets measured in our dataset that supports the predicted inhibition of E2 are shown. (B) E2 relationship with other predicted upstream regulators that describe the alterations seen in the dataset are plotted. See Figure 5 for explanation of color scheme, edges, and nodes.

Supplemental Table 4.1 Estrogen-deficiency associated phosphoproteins in Ovx and Old mice

Uniprot ID	Protein description	Phosphosite (Score): Ovx/Sham	Phosphosite (Score): Old/Young
Q60876	Eukaryotic translation initiation factor 4E-binding protein 1	T40(88.2); T45(90.8); T69(100)	T36(94.4); T45(99.8)
A0A494B9J0	Ankyrin repeat domain-containing protein 2	S72(99.4); S321(100); T325(100)	S56(100); S72(99.2); S321(100); T325(98.2)
Q5EBG6	Heat shock protein beta-6	S16(100); S157(100)	S16(100)
Q00PI9	Heterogeneous nuclear ribonucleoprotein U-like protein 2	S159(100); S226(98.4)	S159(100); S183(100); S186(100); S191(100); S226(94.1)

			T218(100); S225(100); T257(99.4); T258(99.2); T381(100); Y413(100); T415(100); T444(100); T619(99); S650(98.9); T667(100); S735(100); S745(100); T761(100); T793(100); T944(100); T967(100); T995(100); T1000(100); T1026(100); S1044(100); S1095(100); S1135(100); S1147(100); S1165(100); T1195(100); S1206(100); S1240(100); T1244(100); S1268(100); T1282(99.2);
G3UW82	Myosin heavy chain 2, MCG140437	T257(100); T258(100); T381(100); Y413(100); T415(100); T444(100); S649(99); T667(100); T687(100); S745(100); T761(100); T793(100); T918(100); T986(100); T1000(100); T1026(100); T1028(100); S1044(100); S1095(100); S1135(100); S1147(100); S1165(100); T1198(100); S1206(100); S1240(100); S1268(100); T1282(99.3); S1306(100); S1309(100); T1316(100); S1373(100); Y1382(100); T1390(100); Y1467(99.3); S1483(100); S1498(100); T1504(100); T1520(100); S1577(100); S1603(99.3); T1607(100); S1614(100); T1653(100); S1717(100); T1725(100); T1733(100); T1739(100); S1742(100);	; T1289(100); S1306(100); S1309(100); T1316(100); S1369(100); S1373(100); T1380(100); T1384(100); T1390(100); S1483(100); T1486(100); S1498(100); T1504(100); S1517(100); T1520(100); S1577(100); S1614(100); S1639(100); T1653(100); S1717(100); T1733(100);

		T1767(100); T1782(100); T1796(100); S1835(100); T1858(100); T1861(100); S1901(100); S1922(100)	S1742(100); T1767(100); S1835(100); T1861(100); S1901(100); S1922(100)
Q9CYR6	Phosphoacetylglucosamine mutase	S64(100)	S64(100)
P16015	Carbonic anhydrase 3	S9(100); S50(100); S85(100); Y114(100); T129(100); T216(99.2); S219(99); S227(100)	S48(100); S50(100); T73(100); S85(100); Y114(100); T129(100); S219(99.2)
Q91YE8	Synaptopodin-2	S543(100); S546(98.7); S596(99.2); S618(100); S629(97.8); T744(100); S767(91.5); S813(100); S895(100); S899(100)	S220(100); S543(99.2); S563(100); S566(100); S596(99); S618(100); S629(97.6); S704(100); T744(100); S813(100); S895(100); S899(100); S903(100)
P17751	Triosephosphate isomerase	T121(100); S156(100); T228(100); S245(100); S273(100)	T121(100); S245(100); S254(99.4); S273(100)
D3YVS1	Smoothelin	S132(99); S313(100)	S132(98.8); S313(100)

G3UWY3	Protein cordon-bleu	S40(98.4); S228(100); S253(100); S265(100); S302(98.6); S310(100); S325(100); S339(100); S342(99.6); S365(100)	S40(100); S43(100); S205(100); S228(100); S253(100); S265(100); S300(95.8); S325(100); S339(100); S342(99)
D3Z1D3	Cardiac-enriched FHL2-interacting protein	S221(100); S252(100); S328(100); S473(100); S518(100); S677(100); S813(100); S876(98.7); S954(100); S1176(100); S1384(100)	S221(100); S252(100); S328(100); S471(99.9); S473(100); S518(100); S677(98.3); S813(100); S876(99.2); S954(100); S1347(100); S1384(100)
A0A0R4J1B1	Troponin T	S2(100); S138(100); S146(100); S182(100)	S2(100); T6(100); S146(100); S182(100)
A0A0G2JDV6	Ubiquitin associated protein 2-like	S462(94.8); S477(100); S609(100)	S477(100); S604(98.2); S609(100)
D3YUT2	Alpha-protein kinase 3	S23(100); S229(100); T545(100); S1153(100); S1165(100); S1169(100); T1184(100); S1628(100); S1638(100)	S23(100); S229(100); S361(98.9); T545(100); S1006(100); S1165(100); S1169(100); S1181(100); S1628(100); S1638(100)

Q8CE04	Calpastatin	S82(100); S136(100)	S82(100); S136(100); T396(100)
Q03265	ATP synthase subunit alpha, mitochondrial	S53(99.2); S521(100)	S53(100); S65(100); S521(100)
A0A1D5RLD8	Glyceraldehyde-3-phosphate dehydrogenase	T81(100); T180(100); T182(99); S208(99.2); T209(98.9); S264(100); Y316(100); S319(100); S331(100)	T81(100); T182(98.9); S208(99); S264(100); S319(100); S331(100)

G5E8J6	Histidine rich calcium binding protein	S81(100); S104(100); S129(100); S139(100); S141(100); S150(100); S199(100); S201(100); S219(100); S228(100); S249(100); S253(100); S272(100); S305(98.5); S324(100); S332(100); Y339(100); S354(100); S376(100); S385(100); S390(100); S402(100); S421(100); S449(100); S466(100); S474(100); S483(100); S516(98.4); S520(100); S527(100); S528(100); S542(100); S565(100); S569(100); S591(100); S595(100); S640(100); S641(100)	S81(100); S104(100); S129(100); S141(99.5); S150(100); S151(100); S219(100); S228(99.2); S249(100); S253(100); S272(100); S324(100); S332(100); S354(100); S390(100); S402(98.8); T403(98.8); S421(100); S466(100); S474(100); S483(100); S516(98.1); S517(98.9); S520(100); S527(100); S528(100); S542(100); S565(100); S569(100); S591(100); S595(100); S640(100); S641(100)
O54724	Caveolae-associated protein 1 OS=Mus musculus OX=10090 GN=Cavin1 PE=1 SV=1	S42(99.1); S169(100); S302(99.4)	T34(99.8); S38(100); S42(100); S120(100); S169(100); S302(100)

O88990	Alpha-actinin-3	T63(100); S115(100); S153(100); T243(100); S297(100); S320(100); S375(100); S417(100); S437(100); S439(100); S455(100); S484(100); T607(100); S610(100); S626(100); S696(100); S736(100); T750(100); S757(100); Y850(100)	T63(100); S115(100); S153(100); T184(99); T220(100); S297(100); S320(100); S375(100); S417(100); S437(100); S439(100); S601(100); T607(100); S609(100); S610(100); S626(100); T630(100); S696(100); S711(100); S722(98.4); T735(99.1); S736(98.8); T750(100); S757(100); Y850(99.2)
P31001	Desmin	S28(100); S68(100); S81(99.8); S343(100)	S25(96.8); S28(100); S48(100); S60(100); S68(100)
P48678	Prelamin-A/C	S22(99.2); S390(100); S392(100); S637(100)	S22(99.3); S390(100); S392(100); S637(100)
P70302	Stromal interaction molecule 1	S519(100); S521(100); S575(100); S602(75); S660(100)	S512(100); S521(100); S567(100); S575(100); S660(100)

P70670	Nascent polypeptide-associated complex subunit alpha, muscle-specific form	S257(100); S565(100); T590(100); S765(100); S822(100); S929(100); T946(98); S947(97.4); S951(98); S1039(100); S1177(100); S1208(98.7); S1285(100); S1303(100); S1400(100); S1492(100); S1579(100); S1583(100); S1715(100); S1727(98.7); S2138(100)	S249(100); S257(100); S442(100); S519(99.9); S565(100); T590(100); S822(100); S843(99.9); S929(100); S947(97.6); S951(99.9); S1039(100); S1120(100); S1174(100); S1177(100); S1285(100); S1303(100); T1398(99.9); S1400(100); T1405(96.9); S1478(100); S1489(100); S1492(99.1); S1579(100); S1583(100); S1627(98.9); S1715(100); S1727(98.8); S1744(100); T2131(96.2); S2138(100)
Q148W8	Inactive dual specificity phosphatase 27	S555(100); S562(100)	S305(100); S555(100); S966(100); T1009(91.4); S1016(99.8); T1025(100); S1029(100); S1034(100)

Q14BI5	Myomesin 2	S19(100); S76(100); S78(99.1); S95(100); S106(100); S145(100); Y209(100); S239(98.8); T294(100); T296(100); Y317(100); S535(100); S555(100); T563(100); S613(100); T626(100); S737(100); S762(100); S763(99.2); T776(100); S828(100); S863(100); T1015(100); Y1024(100); Y1265(100); S1272(100); S1274(100); S1311(100); S1315(100); S1319(100); S1446(100)	S76(100); S78(100); S106(100); S145(100); S162(100); Y209(100); T294(100); T296(100); Y317(100); T445(100); S472(100); S535(100); S555(100); Y570(100); T626(100); T676(98.8); S737(100); S740(99.1); S762(100); S763(100); T776(100); S828(100); S839(100); S863(100); Y1024(100); S1046(100); S1057(100); S1102(100); Y1265(100); S1274(100); S1311(100); S1315(100); Y1400(100); S1446(100)
Q64347	Chloride channel protein 1	S682(100)	S704(100); S892(100)
Q80WJ7	Protein LYRIC	S297(100); S423(100); S565(100)	S297(98.8); S565(100)
Q9CT10	Ran-binding protein 3	S58(100); S146(100)	S58(100); T458(99.9)
Q9ET54	Palladin	S901(100); S1141(98.8); S1146(100)	S194(100); S1129(100); S1131(100); S1141(100); S1143(100); S1146(100)

Q9QVP4	Myosin regulatory light chain 2	S23(98.7)	S23(98.8)
A2A542	Voltage-dependent L-type calcium channel subunit beta-1	S26(100); S139(100); S146(99); T158(100); T201(95.5); S454(100)	S21(90.3); S23(100); S26(100); S136(90.7); S139(100); S143(100); S145(100); S146(99); S197(96.3); S198(96.2); T201(98.4); S454(100)
A0A087WQ94	Tensin 1	S621(99.2); S885(100); S949(100); T1174(100); S1177(100); S1194(100); S1228(97.9); S1230(97.5); S1254(100); S1282(100); S1299(100); S1366(100); S1378(100); S1385(100)	S623(98.9); S667(100); S675(95.8); S730(99); S753(100); S844(97); S885(100); S949(97.3); T1174(100); S1177(100); S1194(100); S1228(98.2); S1292(100); S1299(100); S1366(100); S1385(100)
A0A087WR45	Proline-rich basic protein 1	S234(100); S376(100); S396(100); S398(100); S440(100); S494(100); S576(100); S772(98.7); S848(100)	S234(100); S396(100); S398(100); S440(95.1); T449(100); S451(100); S494(100); S576(100); S772(98.6); S848(100)

A0A087WRY3	Nuclear ubiquitous casein and cyclin-dependent kinase substrate 1	S19(100); S58(100); S61(100); S75(100); S79(100); S180(100); S213(100)	S19(100); S54(100); S58(100); S61(100); S75(100); S79(100); S180(100); S213(100)
A0A3Q4EBK4	Myc box-dependent-interacting protein 1	S267(100); S273(100); T277(100); S293(100)	S267(100); S273(100); T277(100); S293(100); S303(97.9); S305(98.1)
A0A571BF58	Nebulin	S84(100); S128(100); S420(100); S513(100); Y549(100); S608(100); S667(100); Y796(100); S855(100); S1099(100); Y1325(100); S1343(100); S1587(100); S1723(100); T1753(99.1); Y1813(100); S1831(100); Y2057(100); S2075(100); Y2544(99.2); S2596(100); S2839(100); Y3030(100); S3082(100); Y3273(100); S3325(100); Y3516(100); Y3759(100); S3811(100); Y4002(100); S4020(100); T4185(98); Y4245(99.2); S4263(100); Y4730(100);	S40(96.3); S84(100); S219(100); S362(100); S513(100); Y549(100); S584(100); S608(100); Y796(100); S831(100); S855(100); S971(100); S990(100); S1000(98.9); S1099(100); S1205(100); Y1325(100); S1723(100); T1753(99.3); Y1813(100); T1862(97.9); S2026(100); Y2057(100); S2177(100); S2420(100); Y2544(100); S2667(98); S2943(100); Y3030(100); S3186(100); Y3273(100); S3429(100);

		S4913(100); S5015(100); T5151(100); S5445(98.9); S5480(100); Y5702(100); S5894(100); S6423(100); S6459(100); S6528(100); S6918(100); T7050(100); T7143(100); T7174(100); T7200(100); T7231(100); T7236(100)	Y3516(100); Y3759(100); Y4002(100); S4020(100); Y4245(100); S4611(100); Y4730(100); T5151(100); S5445(98.8); S5645(100); Y5702(100); S5888(100); S5894(100); T5972(100); S6423(100); S6459(100); S6462(100); S6528(100); S6811(100); S6852(99)

			T7050(100); T7143(100); T7174(100); T7231(100); T7236(100); S7257(100); T7346(100); S7359(100); S7374(100); S7390(100); S7392(100); S7397(100); S7399(97.8); S7405(100); S7408(100); S7416(98.1); S7419(100); S7447(89.7); S7456(100); S7457(100); S7460(100); S7463(96.4); T7464(98.3); S7484(100)
		S7257(100); T7317(100); T7346(100); S7359(100); S7374(100); S7397(100); S7405(100); S7408(100); S7419(100); S7457(100); S7460(100); T7464(98.3)	

E9QLJ0	Cardiomyopathy-associated protein 5	S52(100); S142(100); S155(100); S289(100); S313(98.9); S705(100); S786(100); S794(98.7); S1019(100); S1797(100); S1924(97.9); S2072(98.8); S2129(100); S2144(100); S2186(99); S2348(100); S2444(100); S2842(100); S3067(100)	S142(100); S155(100); S174(100); S199(98.4); S289(100); S705(100); S708(100); S786(99.9); S951(100); S1019(100); S1022(96.9); T1023(97.2); S1030(98.3); S1160(96.5); T1163(100); S1692(100); S1794(97.8); S1797(100); S2072(100); S2129(100); S2144(100); S2186(100); S2348(100); S2680(100); S2688(98.7); T2689(98.4); S2767(100); S2842(100); S3067(96.9); S3087(100)

			S19(100); S316(100); S375(100); T379(100); S394(100); S423(100); S439(100); T453(100); S457(100); S463(100); S490(100); S511(97.5); S518(100); S531(100); S542(100); T546(98.7); S554(100); S860(100); S865(99.9); S1177(100); S1993(98.1); S2004(100); S2019(100); S2020(100); S2042(100); S2052(100); S2099(100); S2114(100); S2135(100); S2171(98.4); S2182(100); S2204(96.4); S2288(100); T2303(100); S2327(97.1); S2361(100); S2396(100); S2413(100); S2442(97.8); S2446(95.6); S2447(95.6); S2451(100); S2461(100); S2462(99.2); S2476(100);
E9QQ25	Striated muscle-specific serine/threonine-protein kinase	S19(100); S316(100); S375(100); T379(100); S385(97.2); S423(100); S439(100); S463(100); S481(100); S493(100); S511(100); S518(100); T546(99.4); S554(100); S578(100); S860(100); S1177(100); S2004(100); S2019(100); S2020(100); S2042(100); S2052(100); S2114(100); S2135(100); S2171(100); S2182(98.2); S2204(96.6); S2288(100); T2303(100); S2327(100); S2347(100); S2359(100); S2361(100); S2396(100); S2413(100); S2451(100); S2461(100); S2462(99.2); S2487(99); T2488(100); S2499(100); S2562(95.2); S2777(100); T2847(100); S2936(100)	

			T2488(100); S2499(100); S2503(100); S2527(96.8); S2530(96.8); S2777(100); T2847(100); S2936(100); S2944(98.4)
P07310	Creatine kinase M-type	S24(100); T35(100); T103(100); S128(99.3); T166(100); S178(100); T180(98.6); T313(100); T322(100); S372(100)	S24(100); T35(100); Y125(100); S128(99.3); T166(100); Y174(99.7); T313(100); T322(100); S372(100)
P52480	Pyruvate kinase PKM	T41(100); S57(100); S67(100); S77(100); S97(98.4); S127(99.4); Y148(100); S202(100)	T41(100); S57(100); S67(100); S77(100); Y175(100); S202(100); Y370(100)

P58774	Tropomyosin beta chain	S61(100); S63(99.3); T79(100); S87(100); T108(100); Y162(100); S179(100); S206(100); T252(100); Y267(100)	S61(100); S63(99.2); T79(100); S87(100); T108(100); Y162(100); S215(99.3); T237(100); S245(100); T252(100); Y267(100); S283(99)
P97457	Myosin regulatory light chain 2	S16(99.2)	S15(100); S16(99.1); T25(96.7); T35(100)
Q5SX40	Myosin-1	T64(100); T257(100); T258(100); T381(100); Y389(100); Y413(100); T415(100); T444(100); T619(100); S625(100); S649(99); T667(100); T687(100); S745(100); T761(100); T793(100); S904(100); T918(100); T986(100); T1000(100); T1026(100); T1028(100); S1044(100); S1072(99.2); S1095(100); S1135(100); S1147(100); S1165(100); T1198(100); S1206(100); S1246(100); S1264(100); T1281(100); S1291(100); S1303(100);	T64(99.1); T68(100); T218(100); S225(100); T257(99.4); T258(99.2); T381(100); Y389(100); T415(100); T444(100); T619(100); S625(100); S635(100); S650(98.9); T667(100); S745(100); T761(100); T793(100); S900(100); S904(100); T944(100); T967(100); T995(100); T1000(100); T1026(100); S1044(100); S1072(100); S1095(100); S1135(100); S1147(100); S1165(100); T1195(100); S1206(100); S1229(100); S1246(100);

		S1309(100); T1316(100); S1334(100); Y1354(100); S1373(100); Y1382(100); T1390(100); Y1467(99.3); S1483(100); S1485(100); S1498(98.9); T1504(100); T1520(100); S1557(100); S1577(100); S1603(99.3); T1607(100);	S1248(100); S1264(100); T1289(100); S1303(100); S1309(100); T1316(100); S1334(100); Y1354(100); S1369(100); S1373(100); T1380(100); T1384(100); T1390(100); S1483(100); S1485(100); Y1495(100); T1504(100);

		S1614(100); T1653(100); S1717(100); T1725(100); T1733(100); T1739(100); S1742(100); T1767(100); T1782(100); T1858(100); T1861(100); S1880(100); S1896(100); S1922(100)	S1517(100); T1520(100); S1557(100); S1577(100); S1614(100); S1639(100); T1653(100); S1717(100); T1733(100); S1742(100); T1767(100); T1861(100); S1880(100); S1896(100); S1922(100)
Q5XKE0	Myosin-binding protein C	T26(100); S40(100); S56(100); S105(97.8); S163(100); S172(100); S295(100); S404(100); S476(100); S482(100); S548(100); T583(100)	T26(100); S40(100); S105(100); S156(100); S160(100); S163(100); S172(100); S295(100); S404(100); S476(100); S482(100); S548(100); T564(100); T583(99.3); S900(98.9)

Q70IV5	Synemin	S172(100); T430(100); T464(100); S780(100); S1044(100); S1049(100); S1075(100); S1077(100); S1502(100)	S172(100); S404(100); S405(98.5); S780(100); T811(100); S1043(97.6); S1049(100); S1075(100); S1077(100); S1087(100)
Q7TQ48	Sarcalumenin	S228(94.5); T229(86.5); T234(95.5); T302(98.2); S304(100); S432(100); S442(100); S464(100); S491(100); T503(100); Y558(100); S592(100); Y816(100); S848(100); T873(100); S882(100)	T222(97.9); S224(97); S228(94.3); S244(100); S304(100); S317(98.1); S432(97.4); S442(100); S464(100); Y490(98.9); S491(100); T503(100); Y558(100); S569(100); S592(100); Y816(100); S848(100); S878(100); S882(100)
Q8CI12	Smoothelin-like protein 2	S98(100); S124(99.1); S126(99.4); S131(100); S250(99.2); S265(100); T270(100); S274(100); S339(100)	S4(100); T96(100); S98(100); T122(100); S124(100); S131(100); S138(100); S250(100); S252(100); S265(100); T270(100); S274(100); S339(100)

Q922J3	CAP-Gly domain-containing linker protein 1	S146(98.4); S199(100); S203(100); S311(100); S347(100)	S146(97.6); S194(100); S199(100); S203(100); S311(100); S347(100); S1317(100)
Q99JB8	Protein kinase C and casein kinase II substrate protein 3	S319(100); S354(100); S383(100)	S276(100); S354(100); S383(100)
Q9DCL8	Protein phosphatase inhibitor 2	S122(100); S123(100)	S122(100); S123(100)
Q9JI91	Alpha-actinin-2	T57(100); S147(100); S201(100); S291(100); S411(99.1); S431(100); S449(100); S574(100); S590(100); S594(100); S624(100); S840(100)	T57(100); S147(100); T237(100); S291(100); T308(100); S369(100); S411(99.1); T412(99); T435(100); S574(100); S590(100); S594(100); S595(97.3); T744(100); S840(100)
Q9JK37	Myozenin-1	S16(99.3); T23(100); S30(100); S57(100); S80(98.5); S82(98.8); S83(100); S118(98.5); S121(100); S134(100); S141(100); S164(100)	S15(100); S16(99.2); T23(100); S57(99.2); S80(100); S82(98.8); S83(100); S118(98.5); S121(100); S134(100); S164(100); S183(100)

Q9QXS1	Plectin	S728(100); S927(100); S1443(100); T1740(100); S3448(100); T4037(100); S4389(100); S4393(100); S4396(98); S4629(100); S4633(100); S4649(100)	S728(100); S927(100); S1443(100); T1740(100); S3448(100); T4037(100); S4392(100); S4393(100); S4396(100); S4398(98.1); S4625(100); S4627(89.1); S4629(100); S4633(98.9); S4637(98); S4649(100)
Q9WUB3	Glycogen phosphorylase, muscle form	S26(100); Y186(100); Y204(100); S430(100); Y473(100); S524(100)	S26(100); Y186(100); Y204(100); S430(100); Y473(100); S514(100); S524(100); Y732(100); Y733(100); S748(99); S831(100)
Q9Z1E4	Glycogen [starch] synthase, muscle	Y44(99.1); S412(100); S641(100); S645(100); S652(100); S653(100); S657(100); S672(100); S711(98.5)	Y44(99.1); S412(100); S641(100); S645(100); S649(98.5); S653(100); S657(100); S672(100); S711(98.2); S728(99.9)

V9GWW6	Muscular LMNA-interacting protein	S61(100); S387(100); S511(93.3)	S61(100); S387(100)
A0A0G2JEX1	Nexilin	S80(100); S360(100); S500(100); S559(100)	S80(100); S86(100); S87(100); S345(100); S352(100); S360(100); S500(100); S559(100); T566(96.3)
A2AUD5	Tumor protein D54	S166(100); S175(100); S189(100)	S166(100); S171(99.1); S189(100)
Q8R429	Sarcoplasmic/endoplasmic reticulum calcium ATPase 1	S186(100); T191(100); S229(99.2); T242(100); T441(100); T533(100); S547(100); T569(100); S581(100); S643(100)	S186(100); T191(100); T242(100); T441(100); S488(100); T533(98.6); S547(100); T554(100); T569(100); S581(100); S643(100); S693(90.9)
Q91VK2	Eef1d protein	S128(100); S157(100)	T58(96.3); S128(100); T142(100); S157(100)

Q9ET78	Junctophilin-2	S162(98.8); S228(100); S231(100); S234(100); T453(100); S462(100); T470(96.3); T483(100); S514(99.9); S527(100); S533(100); S613(100)	S228(100); T230(100); S231(100); S234(100); S440(99); T453(100); S462(100); T470(100); S479(95.4); T483(100); S514(100); T518(98); S520(97.9); S527(100); S533(100); S593(100); S597(100); S613(100); T621(100)
Q9ET80	Junctophilin-1	S162(98.9); S165(100); S186(100); S216(100); S220(100); S238(100); S241(100); S448(100); S452(100); T461(98.1); S465(100); S469(98.1); S475(100); S480(98.8); S490(100); S496(100); S501(100); S527(100); S593(99.2)	S171(91.8); S174(99.6); T190(98.8); S216(100); S220(100); S413(100); S448(100); S452(100); T460(98.4); T461(98.2); S465(100); S468(100); S469(98.4); S475(100); S490(100); S496(100); S501(100); S532(100)

F8WIS9	Calcium/calmodulin-dependent protein kinase type II subunit alpha	S333(98.9); S344(98.6)	S333(96.6); S344(100)
A0A0A0MQC7	Microtubule-associated protein	S188(100); S494(100); S506(100); S688(100); S696(98.6); S708(98.6)	S188(100); S491(100); S494(100); S506(100); T523(100); S529(98.9); S688(100); S692(100); S696(100)